The Pennsylvania State University

The Graduate School

College of Engineering

LAYERED SURFACE ACOUSTIC WAVE DEVICES FOR FILM CHARACTERIZATION AND SENSOR APPLICATIONS

A Thesis in

Engineering Science and Mechanics

by

Michael K. Pedrick

Submitted in Partial Fulfillment
of the Requirements
for the Degree of

Doctor of Philosophy

May 2007

The thesis of Michael K. Pedrick was reviewed and approved* by the following:

Bernhard R. Tittmann
Schell Professor of Engineering Science and Mechanics
Thesis Adviser
Chair of Committee

Joseph L. Rose
Paul Morrow Professor of Engineering Science and Mechanics

Mark W. Horn
Associate Professor of Engineering Science and Mechanics

Samia A. Suliman
Assistant Professor of Engineering Science and Mechanics
Special Member

James P. Runt
Professor of Polymer Science

Judith A. Todd
Professor of Engineering Science and Mechanics
P.B. Breneman Department Head of Engineering Science and Mechanics

*Signatures are on file in the Graduate School.

ABSTRACT

This work has introduced novel applications for Layered Surface Acoustic Wave (SAW) devices along with concepts for enhanced sensitivity via refined modeling techniques. The derivation of Love Wave and Rayleigh wave propagation pertinent to SAW substrates with thin film overlayers was explored. Novel aspects were presented for Finite Element analysis of Layered SAW sensors. This included coordinate transformations of model geometries to coincide with crystallographic orientations known to generate Surface Skimming Bulk Waves (SSBW) and various Rayleigh wave types of propagation in ST Quartz, 90^0 rotated ST Quartz, and 77^0 Y rotated Lithium Tantalate. This work has shown for the first time, FEM prediction of SSBW, Generalized SAW and High Velocity SAW waves. Rayleigh damping properties were extended to develop a Finite element model capable of predicting Layered SAW response to glass transition in a polymer film.

The ability to monitor localized mechanical behavior in a PMMA film was explored with Love Waves generated by 90^0 rotated ST Quartz and Shear Vertical (SV)-SAWs generated by 77^0 Y rotated Lithium Tantalate. Similar trends were found experimentally as compared to the Finite element models. The capability of Love Wave devices for monitoring polymer film curing behavior was investigated. The ability to qualitatively asses the bond quality between film and substrate was also demonstrated based on the characteristics of the transmitted frequency response. The results of these developments have laid the ground work for developing diagnostic tools to better characterize film behavior in practical applications

Several sensor applications for Layered SAW devices were discussed. The Shear Horizontal displacement of the Love Wave device was exploited to demonstrate the capability of such a sensor for ice detection. A clear distinction between air, water, and ice loading was found with Love Waves whereas SV-SAWs were unable to distinguish between liquid and ice loading. The concept of a Layered SAW radiation sensor based on ion modification of a polymer film was presented for the first time. A Finite element model based on published experimental modification data was presented and validated experimentally with the UV cross-linking of an SU-8 photoresist film. Frequency changes on the order of parts in 10^4 were demonstrated for apparent Elastic Modulus changes of 1-2 GPa.

TABLE OF CONTENTS

LIST OF FIGURES

LIST OF SYMBOLS

Abbreviations

APM	Acoustic Plate Mode
CAPA	Coupled Acoustic Piezoelectric Analysis
CL	Cross Linking
CS	Chain Scissioning
FEM	Finite Element Model
FFT	Fast Fourier Transform
FPM	Flexural Plate Mode
GSAW	Generalized Surface Acoustic Wave
HVPSAW	High Velocity Pseudo Surface Acoustic Wave
HVSAW	High Velocity Surface Acoustic Wave
IDT	Inter Digital Transducer
L	Longitudinal
PMMA	Poly Methyl Methacrylate
QCM	Quartz Crystal Microbalance
SAW	Surface Acoustic Wave
SH	Shear Horizontal
SSBW	Surface Skimming Bulk Wave
ST	Stable Temperature (referring to a crystallographic cut in Quartz)
SV	Shear Vertical
UV	Ultraviolet

Mathematical Conventions

∇^2	Laplacian
dn/dm	Derivative of n with respect to m
i	imaginary unit

Symbols

A,B,D	Arbitrary Constants
[C]	Elasticity Matrix, Structural Damping Matrix
c,c_p	Phase Velocity
c_g	Group Velocity
c_L	Longitudinal or Compressional Velocity
c_T	Transverse or Shear Velocity
d	Layer thickness
{D}	Electric Flux Density vector
[e]	Piezoelectric Stress Matrix
{E}	Electric Field Vector
E	Elastic Modulus, Young's Modulus

E'	Storage Modulus
E''	Loss Modulus
f	Frequency
f_0	Centerline Frequency
$\{F^a\}$	Applied Load Force Vector
k	Wavenumber
k_{TS}	Transverse Wavenumber
$[K]$	Structural Stiffness Matrix
$[M]$	Structural Mass Matrix
n	Iteration step unit
N_p	Number of finger pairs
$\underline{r}$	Wave vector
R	Reflection Coefficient
$\{S\}$	Strain Vector
S_{21}	Transmitted Frequency Response
S_ω	Mass Sensitivity factor in terms of frequency
t	Time Step
T	Transmission Coefficient
$\{T\}$	Stress Vector
$u,\dot{u},\ddot{u}$	Nodal Displacement, Velocity, and Accelarations, respectively
$\mathbf{v}$	Velocity vector
V_s	Shear Velocity in Layer
V'_s	Shear Velocity in Substrate
$x_{1,2,3}$	Cartesian Coordinates
x,y,z	Cartesian Coordinates
Z	Shear Wave Acoustic Impedance
α'_{TS}	Transverse Decay Constant in the Substrate
α,β	Rayleigh Damping Parameters
α,δ	Newmark Integration Parameters
β	Phase Component
$[\varepsilon]$	Dielectric Matrix
λ	Wavelength
η,ζ	Rayleigh Wave Equation Ratio
ϕ	Scalar Potential
$\underline{\Psi}$	Vector Potential
σ	Surface Density
ρ	Density
μ	Bulk/Shear Modulus
θ_s	Reflected Angle
θ'_s	Refracted Angle
$\tan\delta$	Loss Tangent
ξ	Critical Damping Ratio

ACKNOWLEDGEMENTS

My deepest gratitude goes out to my wife, Allison, and my family for all of their tremendous support and patience throughout this and all of my endeavors. I am forever indebted to my advisor Dr. Bernie Tittmann without whose guidance I could not have completed this work. He will always have my utmost respect as a scientist, a mentor, and a friend. To my lab colleagues and friends, I will always cherish our camaraderie and greatly appreciate your help and support throughout this work. If it takes a village to raise a child, it takes an entire lab to raise a Ph.D. I would also like to thank my committee for their commitment of time and effort in evaluating this work. Their suggestions and guidance have provided much improvement to this thesis. A portion of this work was supported by the Pennsylvania State University Materials Research Institute Nano Fabrication Network and the National Science Foundation Cooperative Agreement No. 0335765, National Nanotechnology Infrastructure Network, with Cornell University. Thanks also to Paul Roach and Dr. Michael Newton of Nottingham Trent University for supplying many of the SAW devices used in this thesis. Finally, I would like to thank all those who have assisted me over the past several years in making my path throughout all levels of education a rewarding and enjoyable one.

Chapter 1 Introduction

1.1 Background

The development of Surface Acoustic Wave (SAW) devices has forever changed both the telecommunications and sensor industries. Fabrication via microlithography allows for the construction of devices operating at frequencies into the GHz range. The advance of this technology allows for both the improvement of current sensor performance along with the development of novel applications. The challenge of today's sensor research is determining the best configurations, wave propagation modes, and materials to optimize the sensitivity for a particular application. A deeper understanding of wave propagation phenomena can lead to the development of new applications for a particular device.

SAW devices typically have three configurations: resonators, one-, and two-port delay lines. Schematics of these devices are shown in figure 1.1. Resonators consist of transmitting/receiving inter-digital transducers (IDTs) with periodically spaced reflectors. Typically, the spacing between the reflectors matches that of the IDTs, thus producing a standing wave resonance in the device. The frequency is dictated by the wave speed in the substrate and the wavelength determined by the IDT and reflector spacing. A one-port delay line operates much like pulse-echo mode in traditional ultrasonics where the IDTs act as both the transmitting and receiving transducer. A reflector is typically used in a one-port delay line to provide a fixed path length. The substrate edge may also act as the reflector. In a two-port delay line, separate

IDT sets are used for transmitting and receiving transducers.

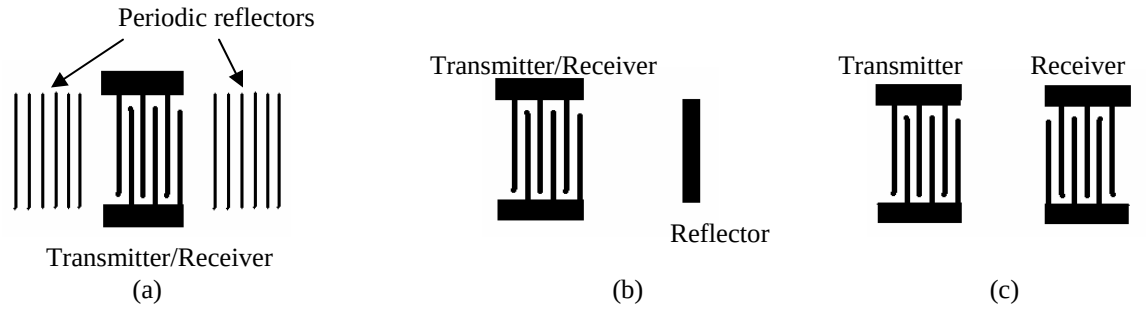

Figure 1.1. Typical configurations of SAW devices including (a) resonator, (b) one-port delay line and (c) two-port delay line.

There are several piezoelectric substrates commonly used for SAW devices including various cuts of Quartz, $LiNbO_3$, and $LiTaO_3$. Two common wave propagation modes found in these devices are Rayleigh type SAW Waves with elliptical wave motions consisting of longitudinal and shear vertical displacements and Surface Skimming Bulk waves (SSBW), which have a dominant shear horizontal displacement. Of particular interest is the behavior of these waves when the surface is coated with a film. In the presence of a film, the free boundary condition necessary for Rayleigh Wave propagation is no longer present. Although wave propagation still occurs with characteristics similar to a Rayleigh wave, it is strictly speaking not a Rayleigh Wave. In order to maintain this distinction, waves with elliptical, shear vertical displacements in the presence of a film will be referred to as SV-SAW or shear vertical surface acoustic waves. Surface Skimming Bulk waves convert into Love Waves in the presence of a film. Love Waves are defined as shear-horizontally polarized waves in a layer on an elastic half-space. In this work, an emphasis is placed on Love Waves while comparing their sensitivities to SV-SAW wave counterparts.

1.2 Literature Survey

1.2.1 A Historical Perspective

In 1911, A.E.H. Love derived dispersion relations for “Transverse waves in a Superficial Layer” to describe the shear displacement of the earth’s crust present in shock wave propagation [Love, 1911]. This work came on the heels of the mathematical description of surface wave propagation described by Rayleigh [Rayleigh, 1887]. The concept of Shear-Horizontally (SH) polarized waves traveling in a thin layer on an elastic half-space have since been coined “Love Waves”. In his derivation, Love discovered two necessary conditions for real solutions to exist that is to say, for wave propagation to be significantly confined in the layer with minimal penetration deep into the subjacent material. These conditions are that the transverse (shear) velocity of the layer material be less than that of the substrate and that the layer thickness is significantly small with respect to that of the substrate.

Love’s derivation encompassed the boundary value problem based on the two dimensional wave equation for transverse wave propagation with appropriate stress and displacement boundary conditions. This methodology has since been followed under the generalization of wave propagation in solids by Ewing [Ewing, 1957], Brekhovskikh [Brekhovskikh, 1960], Viktorov [Viktorov, 1969], Achenbach [Achenbach, 1984], and Rose [Rose, 1999]. Auld derived the Love Wave dispersion relation by applying the transverse resonance principle of acoustic velocity fields to determine the transmission and reflection

conditions at the boundaries for the layer and the substrate [Auld, 1990]. Although the derivation methodologies differ slightly, the resulting relationships have held since Love's original treatise on the topic.

The practical application of such wave propagation in the context of acoustic sensors has relied on the development of Surface Acoustic Wave (SAW) technology. Morgan has provided an excellent description of the historical perspectives of this technology [Morgan, 1998], from which, some key components are mentioned here. In the first half of the 20th century, the introduction of surface acoustic waves in a material was realized with a wedge or a comb transducer. One of the largest contributions to SAW devices as they are known today is the introduction of the inter-digital transducer (IDT) in 1965. White and Voltmer constructed a SAW transmitter and receiver with "spatially periodic electrodes on plane surface of piezoelectric plate" [White, 1965].

In the late 1960s and into the 1970s, several researchers began to find that different orientations of a piezoelectric crystal with respect to the IDT placement yields different wave displacement types. Two papers were published by independent authors, Jeffrey Bleustein [Bleustein, 1968] and Juri Gulyaev [Gulyaev, 1969] on the theoretical existence of SH-wave generation in hexagonal crystals. Another theoretical treatment of such a wave along with its experimental validation was published by Ohta, Nakamura, and Shimizu [Ohta, 1969]. These findings would prove essential in the development of SH-wave based devices for practical applications. For further review on the historical perspectives of SH-wave discoveries and contributions, see the review article by Hickernell [Hickernell, 2005].

The early motivation for innovations in SAW device technology was for communications and RADAR particularly for military applications. These devices include filters, convolvers, delay lines, and so on. Love wave devices for these applications have been reported on a limited basis [Josse, 1982; Parker, 1979; Josse, 1984]. The advent of Love wave-based sensors has been a recent one, the last two decades in particular. This development was based on limited theoretical treatment of Love Wave liquid-based sensors and biosensors [Josse, 1988; Josse, 1989]. The details and progression of Love Wave acoustic sensors are detailed in the following section.

1.2.2 Operating Principles

The allure of Love Wave devices for sensing applications stems from their high sensitivity to small changes in viscosity, chemical composition, density, and elastic properties of the overlayer. These devices also have the added benefit of low insertion losses in liquid environments. This makes Love Wave sensors ideal for the detection of chemical, biological, and mechanical effects under a variety of different conditions.

In 1990, Caliendo *et. al*. presented the development of a Love Wave-based sensor for the detection of K^+ concentrations in liquid [Caliendo, 1990]. The practical application of liquid loaded sensors had until that point been limited to SH propagation near the surface of a solid or the use of the first antisymmetric Lamb mode at a very low frequency/thickness combination. The researchers built a device where IDTs where fabricated on ST-Quartz which was then coated

with a PVC-Valinomycin layer, effective in the sorption of K^+ ions. The introduction of K^+ enriched solution on the surface of the device caused a reduction in the optimal frequency response due to the mass loading associated with the sorption of the ions. It was also determined that this response was reversible by rinsing the device with deionized water.

Gizeli and researchers published work in 1991 showing a signal gain associated with the introduction of an overlayer of SiO_2 on Y-Cut Quartz [Gizeli, 1991]. Signal gains up to 10 dB were reported for overlayer thickness of 2 μm. Similar results were obtained with Poly (Methyl Methacylate) (PMMA) showing signal gains of 8 dB for layer thicknesses between 1.5 and 2 μm. Finally, these researchers showed characteristic phase changes associated with the sorption of glycerols of varying viscosities.

As a result of this early work, researchers began studying the propagation characteristics of Love waves in relevant materials. The insertion loss and frequency shifts associated with the viscoelasticity of the overlayer were of particular concern [Kovacs, 1994; Kielczynski, 1996]. This is particularly important since a fair amount of work on Love Waves is based on polymer overlayers. The results of these derivations showed a direct relationship between the attenuation coefficient and the shear viscosity of the overlayer. Experimental results for viscosity sensors were obtained shortly after these studies [Jacoby, 1998] along with viscoelastic effects as they pertain to Love Wave biosensors [Jacoby, 1998; Weiss, 1998; Gizeli, 1997; Hermann, 1999].

A majority of research concerned with Love Wave devices is the optimization of device sensitivity for particular applications. Many references can be found on this topic but in the

interest of being concise, some of the more critical features are highlighted here for the sensing applications found to date. An overlayer of relatively small thickness, with respect to the acoustic wavelength, is required for the generation and propagation of Love waves. In light of that, a natural parameter to consider for device optimization is the overlayer thickness.

In order to unify the results of different setups, most researchers define the properties of a Love Wave sensor in terms of a normalized layer thickness. This is usually done by dividing the thickness by the acoustic wavelength (h/λ). The highest mass sensitivity for Love Wave devices is typically found in the region of h/λ between 0.1 and 0.2 for the fundamental mode [Knoll, 1993; Kielczynski, 1996; Jakoby, 1997; McHale, 2001]. This sensitivity has been attributed to the minimum insertion loss and highest ratio between phase and group velocities at these inspection points [McHale, 2002]. Although there has been some work on the insertion loss and sensitivity of higher order modes [Newton, 2002], the practicality of sensors based on these modes remains limited. The correlation of sensitivity to guided wave velocity ratios has been studied and has confirmed the earlier suppositions [Herrmann, 2001].

A majority of the publications found on Love Wave sensors discuss the mass sensitivity of the associated device. Experimental studies have been conducted on SiO_2/ST Quartz systems showing maximum mass sensitivity around 5-6 μm layer thickness, consistent with the earlier predicted result of h/λ between 0.1 and 0.2 [Du, 1997]. Similar results have been obtained for systems using a PMMA overlayer [Harding, 1997]. It is important to note that the optimum layer thickness of PMMA is 2 or 3 times lower than SiO_2. The practicality of PMMA layers much thicker than several microns is minimal since the insertion losses associated with those

thicknesses are too great to overcome. Although PMMA and SiO_2 are the traditional layer materials, similar studies have been conducted on Silicon-Oxy-Fluoride [Harding, 2001] and Zinc Oxide [Kalantar-Zadeh, 2001].

Following the perturbation methods of Auld [Auld, 1990], attempts have been made to theoretically predict the sensitivity to mass loading by accounting for the critical features and properties of the device [Wang, 1996]. The results of such predictions show the same trends in data and are fairly close to predicting the optimum normalized layer thickness. Recently, some general treatments have been given for Love Wave Acoustic sensors. McHale, Newton, and group have derived a generalized dispersion relation which characterizes the propagation of both SH-Acoustic Plate Modes (APM) and Love Waves in their respective regimes [McHale, 2001; McHale, 2003]. The descriptions of these works truly help illuminate the behavior of Love Wave sensors and are highly recommended.

1.2.3 Sensor Applications

A majority of SAW sensor development is concerned with applications in analytical chemistry [Thompson, 1997]. The main mechanism is the detection of mass loading associated with the binding of a particular analyte to a film deposited with a selective affinity for that analyte. The ultimate goal is the detection of a variety of analytes by a single device. This has spawned research in the area of the "electronic nose" [Gardner, 1992, Staples, 1999, Yang, 2000], where chemical analytes in a gaseous medium are detected according to pattern recognition techniques of an array of SAW components with characteristic sensing elements.

Similar sensors in liquid medium have been coined “smart tongues” with research seeking to separate responses from different liquid loads according to their effects on the permittivity and conductivity of the sensing element [Cole, 2002; Jacesko, 2005].

A natural analog of the chemical sensor is its biological counterpart. Chemical analyte-selective films can be replaced with films whose ligands bond to particular molecules or biological components. Love Wave devices of this type have been studied for PMMA layers covered with thin gold films which attract a particular molecule [Gizeli, 1997; Schlensog, 2004]. These principles have been applied in the detection of numerous biological agents including: Bacillus Anthracis [Branch, 2004], Staphylococcal Entrerotoxin B [Jin, 2003], Bacteriophage [Tamarin, 2003], and various protein bindings [Gizeli, 2004; Gizeli, 2003].

Another “classic” application of Love Wave sensors is the monitoring and characterization of thin film properties [Thompson, 1997; Ballantine, 1997]. In particular, Love Wave devices are ideal for monitoring the storage modulus, G’, analogous to the elastic shear modulus in the glassy state as well as the loss modulus, G’’, which accounts for the viscoelastic behavior and dominates in the rubbery state of a polymer film. One can think of the overall shear modulus to be the sum of contributions from the storage and loss modulus. Most researchers are concerned with the transition from glassy to rubbery behavior[1]. This can be measured by the drastic increase in insertion loss of a Love Wave sensor [Sterling, 1992; Razan, 2005].

The dependence of Love Wave propagation on the physical characteristics of the

[1] The temperature at which this transition occurs, T_g, is termed the glass transition temperature [73]

overlayer film make this type of sensor ideal to characterize/monitor film deposition techniques as it pertains to film quality. These types of studies have been conducted on films including: ZnO [Chang, 2006; Carlotti, 1990], InSe and GaSe [Panella, 1999], along with numerous types of polymers that have been previously discussed in this review. The dependence of elastic and viscoelastic properties on the phase of the loading medium has become the critical feature for such Love Wave devices as humidity sensors [Cheeke, 1996] and ice detectors [Vellekoop, 1999].

1.3 Thesis Impact and Scope

In order to build an effective sensor, the operating principles and propagation characteristics of Love Waves must be further understood. This presents a prime opportunity for applying the Finite Element Method (FEM). An overall view on the effectiveness of FEM for modeling Ultrasonic Guided Wave behavior has been discussed [Rose, 2004]. Researchers have studied the dispersion characteristics and wave interference phenomena in plates [Moser, 1999; Greve, 2005; El-Kettani, 2004], hollow cylinders/pipes [Zhu, 2005; Hayashi, 2004; Cho, 2004], along with more arbitrary geometries such as rails [Hayashi, 2003; Sanderson, 2002; Hayashi, 2006]. These principles have also been extended to studying guided waves at interfaces [Clatot, 2003; McLean, 2003]. Although Surface Acoustic Waves have been studied via FEM [Endoh, 1995; Hasegawa, 2003], a more common analysis technique is the Equivalent Circuit. Some studies have utilized FEM techniques to study displacement profiles and electrical shorting

effects of layered SAW devices [Ippolito, 2003], along with the potential for hydrogen sensing [Atashbar, 2004]. Although these works demonstrate the feasibility of FEM analysis in Love-type devices, the scope of the work was somewhat narrow.

Although theoretical predictions of guided wave propagation can be extremely effective, they are typically based on *a priori* knowledge of mode selection. It is difficult to determine one's inspection point on the Love Wave dispersion curve knowing only the Inter-digital Transducer spacing and material properties. The benefit of this work is that the successful FEM analysis of SAW devices allows for the prediction of frequency and velocities to provide greater information on dispersion curve location.

The first aim of this work is to determine the ability of an FEM-based model to characterize the dispersion principles of Love Waves and predict the sensing mechanisms of this type of Acoustic Wave device. The limitations of the technique in predicting the behavior of Love waves and Love Wave devices will be investigated. The results of an FEM model will be compared to analytical results as well as, experimental data found in the literature. This will help to shed light on the operating principles and behavior of this type of wave propagation along with, validate the FEM analysis for these types of sensors.

Once the capabilities and limitations of such a model are explored, extensions to solid-state radiation sensing can be inferred, given the large amount of data in the literature on polymer modification via energetic ions. The effect of ion modification of polymers on the propagation of Love Waves can be explored both analytically and through Finite Elements. A

determination of changes in group velocity, insertion loss, and frequency shifts can aid in an initial determination of the potential effectiveness of such a device.

Despite the ion modification data in the literature, the exact sensing mechanisms must be tested in the lab from a more fundamental viewpoint. Toward this end, Nanoindentation tests will be conducted on thin (~2μm) polymer films to determine the relationship of Elastic Modulus and polymer chain cross-linking. These property tests represent the critical mechanical components that will effect the propagation of Love Waves in the current proposed system as well as, provide information on the potential performance of the device.

Finally, experimental validation of the proposed sensing mechanisms must be achieved. Sensors will be tested with various thickness films. Measurements of the group velocity, insertion loss, and frequency shifts associated with polymer cross-linking will be made in the hopes of validating the prediction laid forth in the aforementioned studies proposed.

The benefit of such work relies on the versatility of the study. Although a major thrust of this work is in the development of new sensing applications for Love Wave acoustic devices, improvements on existing sensing techniques will always be warranted. By extending FEM models to study Love Wave devices, the actual guided wave phenomena and sensing mechanisms can be further understood and more efficiently exploited. Mode selection and isolation is a critical component of building a high quality sensor. The proposed study will help to provide some insight toward that end. Improvements in film characterization can also be obtained from studies like the one proposed. The dependence of Love Wave propagation on

properties such as: Elastic Modulus, Shear Modulus, density, Poisson's ratio, and Viscoelastic behavior can all be used to classify films either in situ or in an evaluation type of environment. A better understanding of the fabrication techniques and costs along with potential issues in implementation will provide fruitful information on the practical applications of these devices along with their limitations. Provided are principles for which little information can be found in literature.

By addressing these research goals several milestones have been reached with this work. In summary, this work has for the first time:

- Refined Finite Element techniques to investigate wave propagation phenomena in Layered Surface Acoustic Wave devices taking into account the crystallographic orientation of the substrate
- Demonstrated the capability to model both guided wave propagation and sensor behavior as a function of parameters key to a practical device
- Developed a Finite Element model to predict Layered SAW response to glass transition and localized change in mechanical behavior in a polymer film
- Compared the sensitivities of SV-SAW Wave and Love Wave devices and gain fundamental understanding of the benefits of one device over the other
- Applied these principles to an experimental verification of Layered SAW devices for polymer film characterization
- Evaluated/Demonstrated the potential for Love and SV-SAW wave devices for existing and novel sensing applications such as Ice detection and Radiation sensing

In particular, the finite element method as an analysis tool for SAW delay lines/sensors

has been enhanced by introducing transformation and mapping techniques to account for the crystallographic axis of the piezoelectric substrate. Since wave propagation modes are strictly dependent on substrate orientation, this technique opened the door for modeling both Love Waves and Rayleigh waves in several piezoelectric substrates. The capability of such models to predict the sensitivity of these devices in particular applications was also demonstrated. Given the high cost associated with small scale fabrication of research type devices, this analysis tool can dramatically reduce costs associated with prototype development.

The sensor response of Love Wave delay lines was traced back to fundamental principles of the guided wave behavior of such a device. Appropriate mode selection for Love Wave propagation was shown to greatly enhance the device sensitivity. This is associated with the isolation of energy in the film for modes operating at the dispersive portion of the curve. In general, Love Wave devices show a significantly greater sensitivity than SV-SAW wave counterparts. These results may save future researchers time and money in selecting an appropriate SAW device for a particular application.

Some novel applications of these SAW devices have also been presented. The capability of SAW devices to characterize the localized changes in mechanical behavior in polymer films has been demonstrated. Recommendations on advancing this capability to monitor films less than 100 nm have also been made. The ice detecting capabilities of Love Wave sensors has been explored and demonstrated. The lightweight, low-profile nature of these devices along with their wireless capability could make them excellent candidates for aerospace applications. Finally, a novel Radiation sensor was proposed based on the principles of polymer ion modification. The

concept was demonstrated with the finite element model and validated with an experimental investigation of UV cross-linking in a polymer film. These devices could provide a cost-effective diagnostic tool desirable for Power Generation, Environmental Safety, as well as Homeland Security applications.

1.4 Thesis Organization

The organization of this thesis is done in the following manor. After this introduction, Chapter 2 introduces the theoretical developments of wave propagation pertinent to Surface Acoustic Wave devices. This includes a derivation of Love Wave dispersion along with Rayleigh wave propagation in isotropic media. A discussion of Rayleigh wave propagation in anisotropic substrates is also discussed.

Chapter 3 introduces the Finite Element method and its application to modeling Surface Acoustic wave devices. A description of the coupled mechanical and piezoelectric governing equations is discussed and the finite element software ANSYS and CAPA are introduced. Basic models of SAW devices are shown and compared with experimental data.

Chapter 4 discusses the applicability of Layered SAW devices for polymer film characterization. A Finite Element procedure is introduced for modeling the glass transition behavior of a polymer film. Experimental results are shown and discussed for localized changes in mechanical behavior in a PMMA film along with curing experiments via the evaporation of

solvents in a polymer film.

Chapter 5 introduces two prominent applications for Layered SAW devices, ice detection and radiation sensing. Ice detection represents an existing application so this work is aimed at comparing capabilities of SV-SAW and Love Wave devices. Radiation sensing introduces a new application for Layered SAW devices which measures the change in wave propagation characteristics associated with the ion modification of a polymer film. A finite element model is used to show feasibility and experimental results from UV cross-linking are shown to validate the potential. Resolution and comparisons with existing devices in terms of efficiency and lifetime are also discussed.

Chapter 6 includes conclusions and discussion of the thesis work. The scope and accomplishments are reiterated and novel contributions are highlighted. Future directions for this research are also discussed including further modeling needs, novel applications, and more research to further understand the behavior of Layered SAW devices.

Several Appendices have been included to elaborate on some aspects discussed in the chapters described above. Appendix A gives a brief description of the Lift-Off microlithography process for patterning IDTs on piezoelectric substrates. Appendix B discusses the ANSYS/CAPA interface along with providing a process flow for utilizing this tool. Appendix C contains a short catalog of the written software used in the numerical work discussed in the thesis.

Chapter 2 Wave Propagation in Layered Surface Acoustic Wave Devices

2.1 Introduction

Descriptions of wave propagation in layered structures date back to the late 1800s. In 1887, Lord Rayleigh showed that a wave mode with longitudinal and shear vertical components can propagate along a traction free surface of a semi-infinite medium [Rayleigh, 1887]. The velocity of such a wave is independent of frequency and is therefore, non-dispersive. These theoretical predictions were confirmed through seismological data resulting from earthquake propagation. Later, A.E.H. Love showed the existence of shear-horizontally (SH) polarized waves in a thin layer on an elastic half-space [Love, 1911]. Although originally developed to help interpret seismological data, the description of these wave propagation modes has become prevalent over the last several decades in the realm of Surface Acoustic Wave devices.

This chapter aims to highlight some basic derivations for Rayleigh wave and Love wave propagation. The effect of anisotropy and piezoelectricity in the substrate is discussed. The illustration of the Transverse Resonance principle and its application to the derivation of Love Wave propagation is detailed. Guided wave phenomena and key elements of wave structure as pertaining to Love wave propagation are also reviewed.

2.2 Surface Acoustic Waves

2.2.1 Rayleigh Waves in an Isotropic Solid

The description of Rayleigh wave propagation in isotropic, homogeneous media can be treated through Helmholtz decomposition of Navier's Governing Wave equation [Rose, 1999]. This yields the following two equations in terms of the scalar potential, ϕ, representing longitudinal waves and vector potential, $\underline{\psi}$, representing shear waves:

$$\nabla^2\phi - \frac{1}{c_L^2}\ddot{\phi} = 0 \tag{2.1a}$$

and

$$\nabla^2\underline{\psi} - \frac{1}{c_T^2}\ddot{\underline{\psi}} = 0\,. \tag{2.1b}$$

In these equations, c_L represents the longitudinal velocity and c_T represents the shear velocity in the material. One can then assume a harmonic solution:

$$\phi = D_1(x_3)e^{i(kx_1-\omega t)} \tag{2.2a}$$

and

$$\underline{\psi} = D_2(x_3)e^{i(kx_1-\omega t)}\,, \tag{2.2b}$$

where D_1 and D_2 are arbitrary constants, ω is the angular frequency and k is the wavenumber defined by ω and the phase velocity, c_p as:

$$k = \frac{\omega}{c_p}. \tag{2.3}$$

This notation assumes x_1 is the propagation direction and x_3 is into the depth of the material. Surface waves, theoretically, are confined to the sagittal plane such that displacement in the x_2 direction is zero. Displacements can be written in terms of the above potentials and equations (2.2a and b) can be substituted into (2.1a and b) as shown in [Rose, 1999]. Solutions for the displacements u_1 and u_3 can then be determined. At this point, traction free boundary conditions can be applied on the surface yielding the following governing equation for Rayleigh wave velocity [Rose, 1999]:

$$\eta^6 - 8\eta^4 + 8\eta^2(3 - 2\zeta^2) + 16(\zeta^2 - 1) = 0 \tag{2.4}$$

where the terms η and ξ can be represented by:

$$\eta = \frac{c_p}{c_T} \tag{2.5a}$$

and

$$\zeta = \frac{c_T}{c_L}. \tag{2.5b}$$

One can see from equation (2.4) there is no dependence on frequency thus, Rayleigh surface waves are non-dispersive. It is important to note that equation (2.4) is cubic with respect to η^2 and thus has three roots. This equation has only one real root and so it is considered to be the only solution of importance. The equation also has two complex roots. From a practical standpoint, these represent waves that are "leaky", i.e., energy is carried away from the surface as they propagate. The importance of these solutions is discussed in the following section.

Rose has also shown that longitudinal, *u*, and shear vertical, *w*, displacements can be described by an equation representing an ellipse [Rose, 1999]. This demonstrates that Rayleigh waves travel with an elliptical displacement pattern which decays into the depth of the material. Significant displacement amplitude is typically found up to a depth of approximately one wavelength.

2.2.2 Rayleigh Waves in Anisotropic Piezoelectric Substrates

SAW propagation in anisotropic materials is a more cumbersome problem compared with the isotropic case discussed earlier. As mentioned, the complex solutions to equation (2.4) represent "leaky" waves. There exist two types of leaky surface waves represented by the complex conjugate solutions of equation (2.4). The first of these waves typically propagates at a velocity of 1.3-1.4 times that of the Rayleigh wave velocity whereas the second propagates at approximately twice the Rayleigh wave velocity [Kalantar-Zadeh, et al, 2003]. These waves are not often discussed as the high propagation losses limit their applicability. Leaky SAW waves can be found in certain orientations of Quartz, $LiNbO_3$, and $LiTaO_3$ [Kalantar-Zadeh, 2003].

In more general terms, these wave propagation types are referred to as pseudo SAW (PSAW) modes with the faster one being coined the High Velocity Pseudo SAW (HVPSAW) mode [da Cunha, 1995]. These researchers have also shown that for certain crystal orientations, the losses associated with the HVPSAW are fairly small making this wave of practical interest in SAW applications [Hickernell, 1997]. The HVPSAW will also be referred to as the HVSAW throughout this work.

2.3 Love Waves

Initially handled to describe the propagation of seismic shock waves, this problem has recently found application in Ultrasonic sensors. Love solved the boundary value problem associated with the appropriate differential wave equation for stress and displacement conditions of a SH polarized wave in a layer on an elastic half-space [Love, 1911]. This methodology was followed and extended by [Achenbach, 1984], [Ditri, 1997], and [Rose, 1999]. Auld handled this problem according to the reflection and transmission of the velocity fields in both the layer and the half-space (substrate) [Auld, 1990].

Auld solved the problem according to the Transverse Resonance Method. With this section, I aim to further illustrate the concept of the Transverse Resonance technique and its application to the derivation of Love Wave dispersion. Auld's derivation will be extended to a more practical form for numerical solutions given our current day computing power. Physical

interpretations of the results will be discussed in the context of potential Love Wave Acoustic Devices.

2.3.1 Transverse Resonance Method

Auld defines the Transverse Resonance principle as the superposition of partial waves. This formulation has been greatly used in electromagnetics and can be extremely beneficial in elastodynamic guided wave propagation problems. This method makes two critical assumptions about its application. The medium must be isotropic with planar geometry and the boundaries of the waveguides are lossless. This principle states that the waves propagating in the waveguide can be treated in two parts. The first portion consists of a standing wave resonance perpendicular to the boundaries and the second portion is a traveling wave along the waveguide axis. This concept is illustrated in figure 2.1. The underlying assumption of this wave partitioning is that the transverse standing waves must contain appropriate phase shifts and incident angles at the boundaries in order to achieve constructive interference and therefore, resonance. It will be shown in the derivation how this translates into an appropriate boundary condition for which solutions to certain waveguide problems can be achieved.

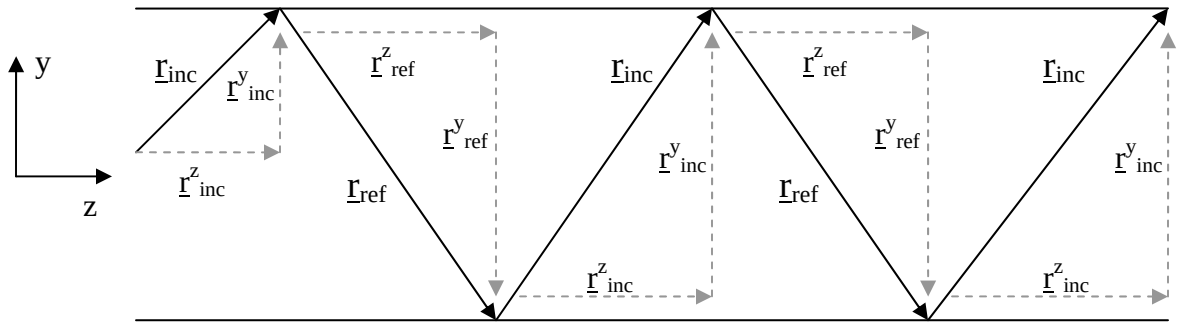

Figure 2.1. Illustration of the Transverse Resonance Principle. The incident and reflected vectors can be broken into components which sum to a standing wave transverse resonance and a traveling wave along the z-axis.

2.3.2 Derivation of Love Wave Dispersion Relation

As mentioned earlier, Love was interested in seismic shock wave propagation. Since the wavelengths associated with these shock waves are small with respect to the radius of the earth, the problem can be treated as a two dimensional plate problem. The earth, however, has different layers with very distinct elastic properties. For this reason, Love modeled the problem as a thin layer (Earth's crust) on an elastic half-space (Earth's mantle). Although very different scales, this model is valid for certain Ultrasonic sensors where one has a film deposited on a SH polarized Surface Acoustic Wave (SAW) Device. An illustration of the wave patterns for this problem is shown in figure 2.2.

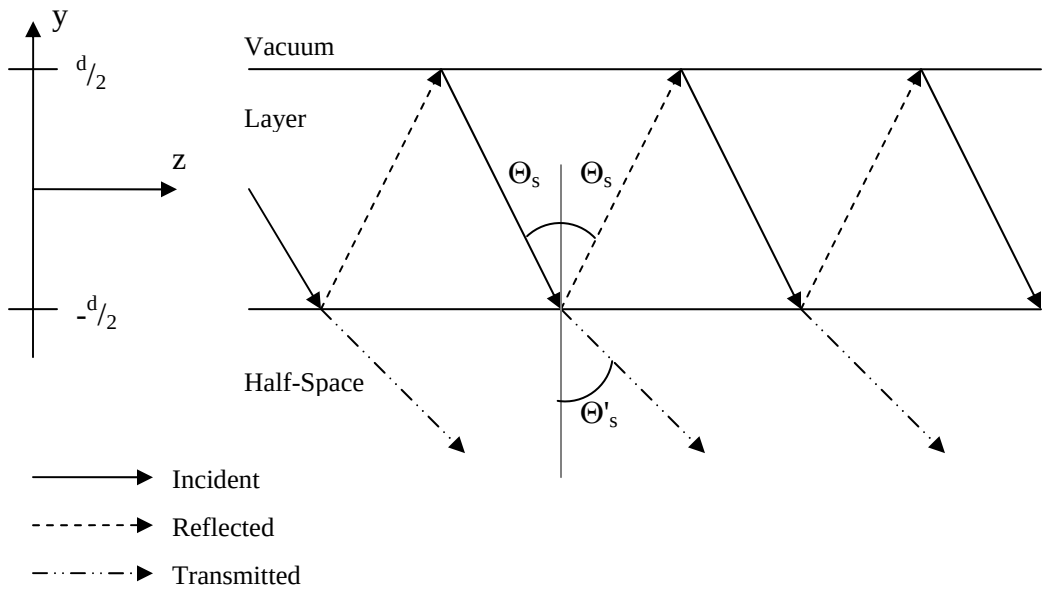

Figure 2.2. Schematic of notation and wave vectors for SH waves in a layer on an elastic half-space. Note that primes indicate properties of the half space (substrate) and unprimed symbols represent properties of the layer

One can express the particle velocity fields of the incident, reflected, and transmitted waves as:

$$v_x^I = Ae^{-i(-k_{ts}y+\beta z)}, \tag{2.6a}$$

$$v_x^R = Be^{-i(k_{ts}y+\beta z)}, \tag{2.6b}$$

and

$$v'^T_x = B'e^{-i(-k'_{ts}y+\beta z)}. \tag{2.6c}$$

The particle velocity fields are strictly in terms of x as a results of SH polarization according to the orthogonal axis indicated in Figure 2.2. k_{ts} represents the transverse wave number and β is the wave vector component often referred to as the phase component. Notice the signs inside the exponent expression indicate the direction of propagation. Again, the primes indicate properties in the substrate and unprimed symbols represent those associated with the layer.

The free boundary at $y=d/2$ requires a reflection coefficient of 1 at this interface. This can be expressed as:

$$R_1(\frac{d}{2}) = \frac{v_x^I}{v_x^R} = \frac{Ae^{ik_{ts}\frac{d}{2}}e^{\beta z}}{Be^{-ik_{ts}\frac{d}{2}}e^{\beta z}} = \frac{Ae^{ik_{ts}\frac{d}{2}}}{Be^{-ik_{ts}\frac{d}{2}}} = 1. \tag{2.7}$$

Since there is some admissibility at the lower interface, the reflection and transmission coefficients are not as clean. Let us first express a general relation for reflection and

transmission coefficients according to Snell's Law:

$$R = \frac{B}{A} = \frac{Z_s \cos\Theta_s - Z'_s \cos\Theta'_s}{Z_s \cos\Theta_s + Z'_s \cos\Theta'_s} \tag{2.8a}$$

$$T = \frac{B'}{A} = \frac{2Z_s \cos\Theta_s}{Z_s \cos\Theta_s + Z'_s \cos\Theta'_s} \tag{2.8b}$$

where Z_s and Z'_s represent the shear acoustic impedances in the layer and substrate, respectively. One defines the shear acoustic impedance as:

$$Z_s = \sqrt{\rho\mu} \tag{2.9}$$

where μ is the Bulk modulus in the material. According to these definitions, one can write expressions for the Reflection and Transmission coefficients at the lower boundary ($y=-d/2$):

$$R_2 = \frac{v_x^R}{v_x^I} = \frac{Be^{ik_{ts}\frac{d}{2}}}{Ae^{-ik_{ts}\frac{d}{2}}} = \frac{Z_s \cos\Theta_s - Z'_s \cos\Theta'_s}{Z_s \cos\Theta_s + Z'_s \cos\Theta'_s}, \tag{2.10a}$$

$$T_2 = \frac{v_x^T}{v_x^I} = \frac{B'e^{-ik'_{ts}\frac{d}{2}}}{Ae^{-ik_{ts}\frac{d}{2}}} = \frac{2Z_s \cos\Theta_s}{Z_s \cos\Theta_s + Z'_s \cos\Theta'_s}. \tag{2.10b}$$

At this point, one can see the power of the Transverse Resonance Method. Typically, other boundary conditions would have to be applied to proceed. According to the principles of the Transverse Resonance technique, we require that the boundary conditions of (2.7) and (2.10a

and b) be satisfied simultaneously. Therefore, we require $R_1=R_2$, such that:

$$\frac{e^{ik_{ts}d}}{e^{-ik_{ts}d}} = \frac{Z_s \cos\Theta_s - Z'_s \cos\Theta'_s}{Z_s \cos\Theta_s + Z'_s \cos\Theta'_s}. \tag{2.11}$$

One can then carry out some algebraic simplifications:

$$e^{ik_{ts}d}(Z_s \cos\Theta_s + Z_s \cos\Theta_s) = e^{-ik_{ts}d}(Z'_s \cos\Theta'_s - Z'_s \cos\Theta'_s),$$

$$Z_s \cos\Theta_s (e^{ik_{ts}d} - e^{-ik_{ts}d}) = -Z'_s \cos\Theta'_s (e^{ik_{ts}d} + e^{-ik_{ts}d}),$$

$$Z_s \cos\Theta_s [2i\sin(k_{ts}d)] = -Z'_s \cos\Theta'_s [2\cos(k_{ts}d)],$$

$$-i\tan(k_{ts}d) = \frac{Z'_s \cos\Theta'_s}{Z_s \cos\Theta_s}. \tag{2.12}$$

For ease in further derivation, we will express the cosines in terms of wave vector components which yield the following:

$$-i\tan(k_{ts}d) = \frac{Z'_s V'_s k'_{ts}}{Z_s V_s k_{ts}}. \tag{2.13}$$

At this point, we must employ some physical interpretation to continue. There are two distinct possibilities for k'_{ts}. When k'_{ts} is real, the transmitted wave carries energy away from the plate (the so-called leaky wave). On the other hand, if k'_{ts} is imaginary then actual wave propagation in the substrate is non-existent. Another way to visualize this is to say that imaginary values of k'_{ts} yield trapped energy in the plate and thus, guided wave propagation.

Since it is of greater practical interest, let us consider the case of an imaginary wave number in the substrate such that:

$$k'_{ts} = -i\alpha'_{ts}. \tag{2.14}$$

One can interpret α'_{ts} as the transverse decay constant in the substrate. Substituting this back into (2.13):

$$-i\tan(k_{ts}d) = \frac{Z'_s V'_s \alpha'_{ts}}{Z_s V_s k_{ts}}. \tag{2.15}$$

At this point we will stray slightly from Auld's derivation. Dispersion relations can be obtained from (2.15) graphically which was the typically analysis of the day. Given the advances in numerical techniques and the computing power available, it behooves us to develop a more intuitive dispersion relationship. Also, one can show how this derivation provides the same results as those obtained by other authors as mentioned in the introduction.

First, let us consider definitions for general dispersion and the phase component term. The general dispersion relation can be expressed as:

$$k_{ts}^2 = \left(\frac{\omega}{V_s}\right)^2 - \beta^2. \tag{2.16}$$

Recall that β is the phase component and can be defined as:

$$\beta^2 = \left(\frac{\omega}{c}\right)^2, \tag{2.17}$$

where *c* represents the phase velocity in the medium. One can now apply (2.16) and (2.17) to (2.15) and follow through some simplifications:

$$\tan\left[d\sqrt{\frac{\omega^2}{V_s^2}-\beta^2}\right]=\frac{V_s'Z_s'\sqrt{\beta^2-\left(\frac{\omega}{V_s'}\right)^2}}{V_sZ_s\sqrt{\left(\frac{\omega}{V_s}\right)^2-\beta^2}},$$

$$\tan\left(d\omega\sqrt{\frac{1}{V_s^2}-\frac{1}{c^2}}\right)=\frac{V_s'Z_s'\omega\sqrt{\frac{1}{c^2}-\frac{1}{V_s'^2}}}{V_sZ_s\omega\sqrt{\frac{1}{V_s^2}-\frac{1}{c^2}}}. \tag{2.18}$$

In order to express the equation in tangible parameters we utilize the following relation:

$$V_sZ_s=\sqrt{\frac{\mu}{\rho}}\sqrt{\frac{\mu}{\rho}}\rho=\mu. \tag{2.19}$$

Substituting (2.18) into (2.19) gives the final dispersion relationship:

$$\tan\left[d\omega\sqrt{\frac{1}{V_s^2}-\frac{1}{c^2}}\right]=\frac{\mu'\sqrt{\frac{1}{c^2}-\frac{1}{V_s'^2}}}{\mu\sqrt{\frac{1}{V_s^2}-\frac{1}{c^2}}}. \tag{2.20}$$

2.3.3 Group and Phase Velocity

The phase velocity relationships we have derived above represent the individual particle velocities in the lattice. Recall that these are simply oscillations in the x direction given the SH polarization of the wave propagation we are describing. Of greater interest is the actual energy transport velocity. In other words, we would like to know how fast the particle oscillations translate along the z-axis (propagation direction). Although the phase velocity derivation changes for different waveguide problems due to the changing boundary conditions, the concept of group velocity dispersion is more of a universal derivation. Here, we follow the expression as shown by [Rose, 1999] since it lends itself to physical interpretation:

$$c_g = c_p \left[c_p - \left(fd \frac{dc_p}{d(fd)} \right) \right]^{-1}, \tag{2.21}$$

where c_g represents the group velocity and c_p represents the phase velocity. The *fd* term is often referred to as the *fd* product and represents the wave frequency multiplied by the thickness of the propagation medium.

Equations (2.20) and (2.21) become excellent guidelines for experimental determination of optimum operating conditions. These baseline models can then be further adapted for a given model system. They are powerful in this context because we can easily realize the effects on wave propagation according to the material properties and/or boundary conditions of our specific problem. These are the most active areas of research in Ultrasonic Guided wave problems. By finding and predicting the wave scattering/interference phenomena associated with a given

problem, one can determine the potential effectiveness of an actual sensor.

An example of this is illustrated in figure 2.3. Here we see results for a Poly(methyl methacralate) layer (PMMA) of thickness 1.9 μm deposited on a Quartz substrate. The first thing we notice from equation 2.20 is that in order to have physically admissible Love Waves, the Shear velocity in the layer must be less than that of the substrate. If this is not the case, one obtains the square root of an imaginary number which is experimentally non-existent. In our case, the shear velocity of the PMMA is approximately 1.1 mm/μs and the shear velocity of the Quartz is approximately 5.05 mm/μs.

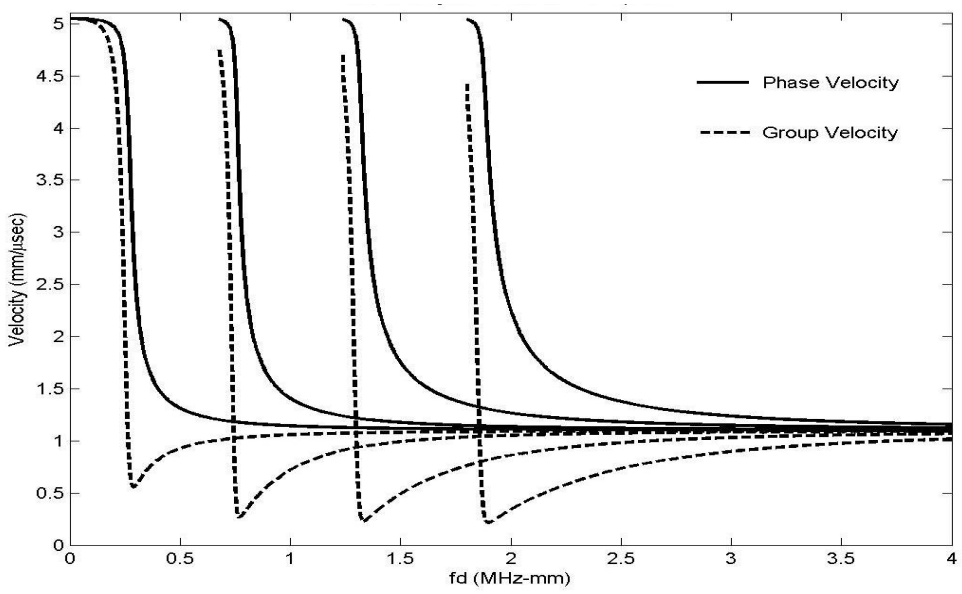

Figure 2.3. Dispersion Curves for a PMMA layer on a Quartz substrate

Areas of the curve where the slope is high represents areas of high dispersion. In these regions, long travel distance results in the spreading of waveforms in time yielding a general decrease in amplitude. Typically, a more non-dispersive or flat region of the curve is more

desirable for propagation over long distances. In this case, the wave packet can stay more compact in time and attenuation due to dispersion is much less of a problem. Typical SAW devices have smaller travel paths (10-100 λ). In this case, we are less concerned with dispersion issues. This provides the freedom of choosing inspection points on the curve that exhibit a high slope. These areas are often much more sensitive to smaller changes in the material properties.

2.3.4 Wave Structure

An important feature in analyzing guided wave behavior is the so-called wave structure of a mode at a particular frequency and thickness combination. The benefit of Guided waves for inspection is the multitude of possibilities given that different modes at different locations will be sensitive to different effects. The displacement profiles for Love Waves can be written as two expressions: one for the layer and one for the substrate. These can be written in the form of [Rose, 1999]:

$$u = D\cosh\left[\beta k(x+d)\right]e^{i(\omega t - kz)} \tag{2.22a}$$

and

$$u' = D\cosh\left(\beta kd\right)e^{-\beta' kx}e^{i(\omega t - kz)} \tag{2.22b}$$

for the layer and substrate, respectively. In this description, D is an arbitrary constant and β and β' represent

$$\beta = 1 - \frac{c^2}{c_T^2} \tag{2.23a}$$

and

$$\beta' = 1 - \frac{c^2}{c_T'^2}\,. \tag{2.23b}$$

Analytical results for the first mode at low and high fd products are shown in figure 2.4a while results for the second mode at low and high fd products are shown in figure 2.4b.

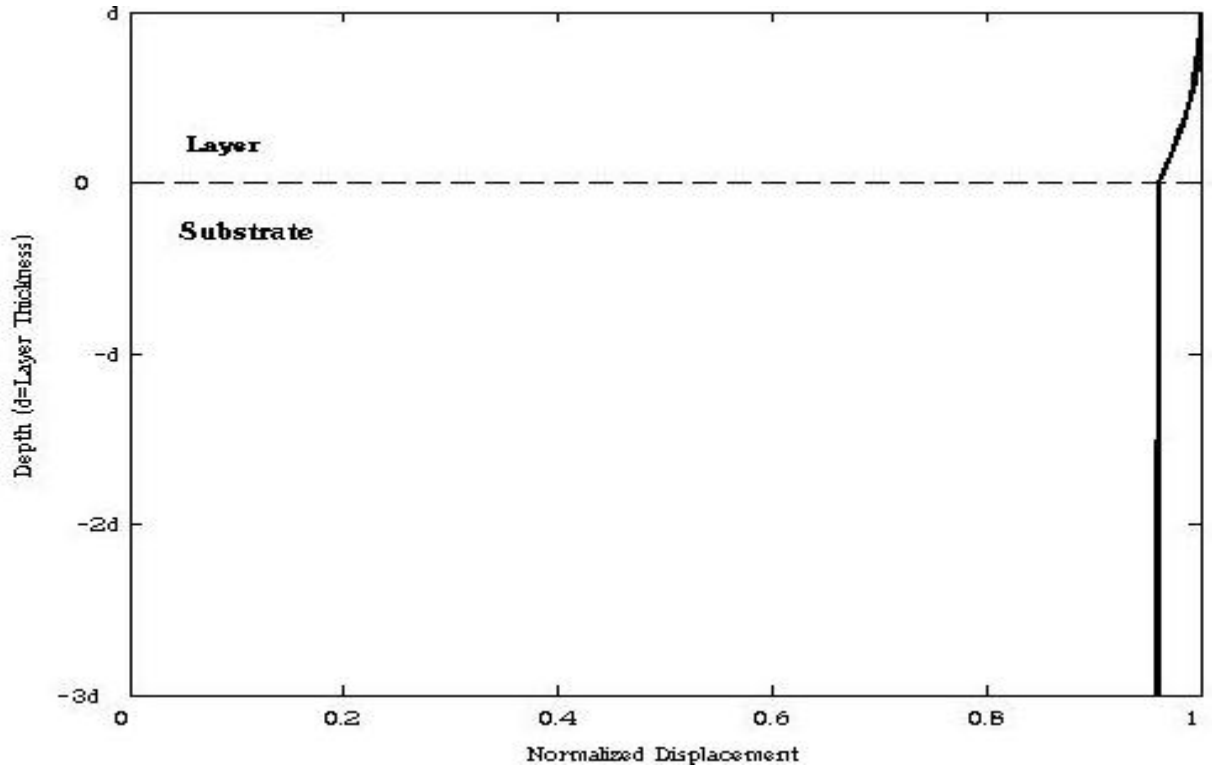

(a)

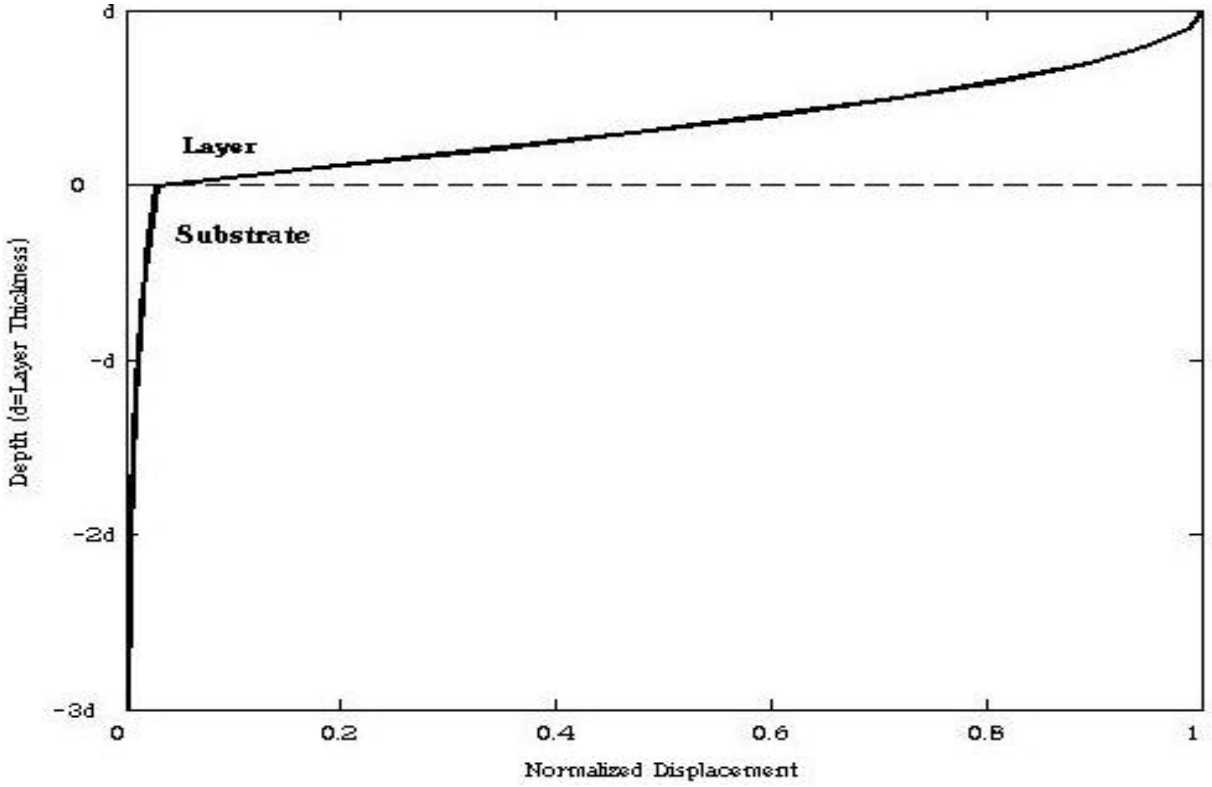
d
0
-d
-2d
-3d
Layer
Substrate
Depth (d=Layer Thickness)
0
0.2
0.4
0.6
0.8
1
Normalized Displacement

(b)

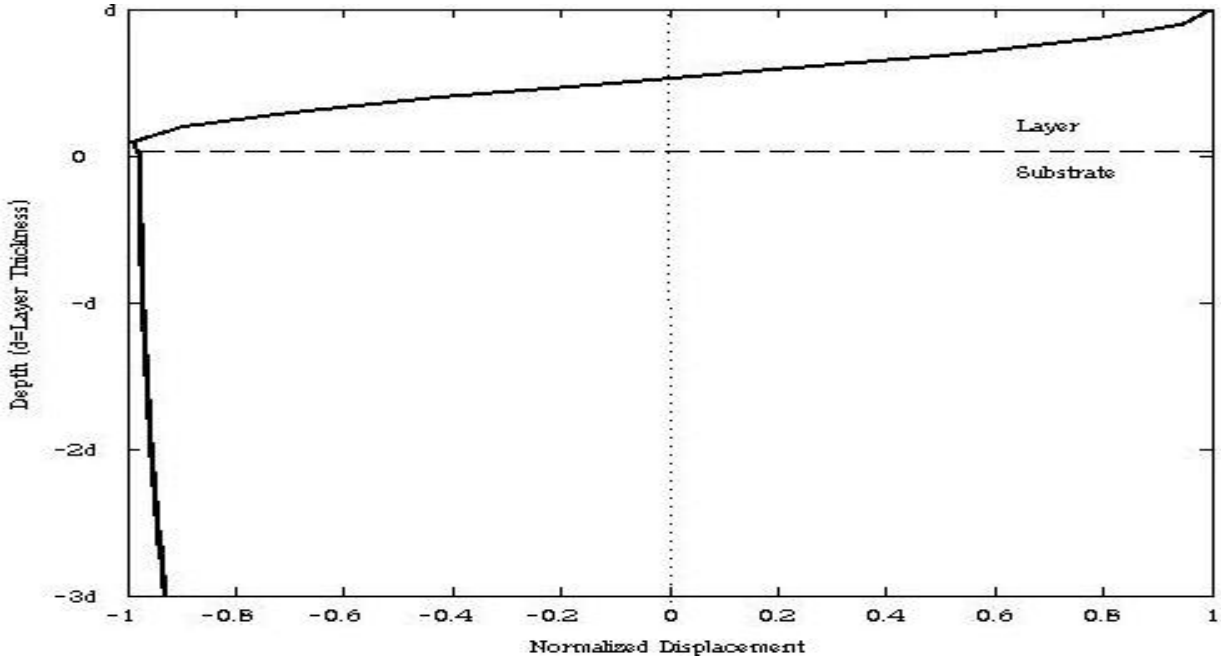
d
0
-d
-2d
-3d
Layer
Substrate
Depth (d=Layer Thickness)
-1
-0.8
-0.6
-0.4
-0.2
0
0.2
0.4
0.6
0.8
1
Normalized Displacement

(c)

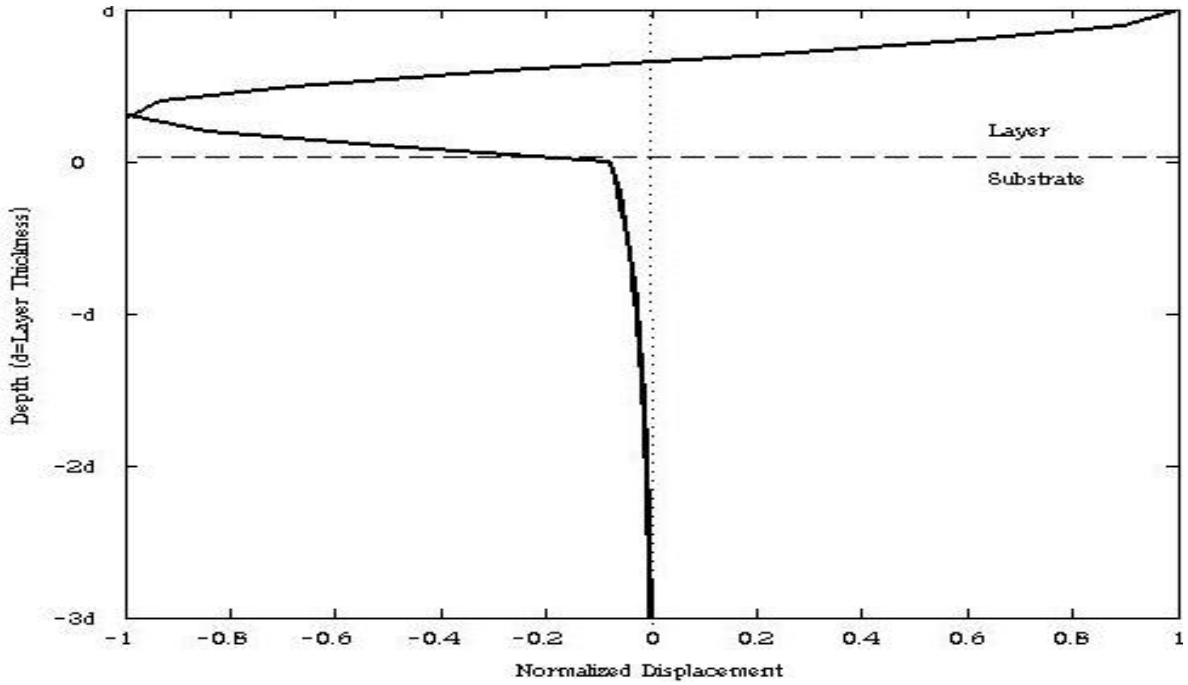

(d)

Figure 2.4. Analytical results of wave structure for (a) the 1st Mode at low fd and (b) the 1st Mode at high fd products along with (c) the 2nd Mode at low fd and (d) 2nd Mode at high fd products.

Chapter 3 Finite Element Modeling of Surface Acoustic Wave Devices

3.1 Introduction

The high fabrication cost of small quantities of SAW devices presents a need for effective modeling techniques to describe their behavior. Analytical descriptions of SAW devices, although adequate, provide limited insight into many factors affecting the actual behavior of wave propagation and frequency response. Several numerical techniques have been utilized for modeling of SAW devices. The most common method employed is the equivalent circuit. Equivalent circuit models allow for the modeling of frequency response and insertion loss (both magnitude and phase) along with the admittance. The benefit of such a technique is that the number of IDTs can be specified by coupling an equivalent circuit for each IDT pair. An overlayer or waveguide can also be added to the model by including a scattering matrix to account for its affect on the device response. This technique does not account for the geometry of the model and requires *a priori* knowledge of a scattering matrix to accurately describe an overlayer.

Applying the Finite Element method to such a problem has the benefit of taking device geometry into consideration. An FEM model can also provide more insight into the behavior of a SAW device by not only providing information on frequency response, but also including wave propagation characteristics such as: displacement profiles, beam steering, attenuation, along with stress and strain fields all at specific instances in time. This analysis technique allows for the

systematic study of many parameters that may affect the behavior of Surface Acoustic Wave device as well as, provide information as to how such a device would operate in a particular sensing environment.

Three-dimensional transient models are used in this work to model the generation and reception of Ultrasonic waves via IDTs. Various orientations of piezoelectric substrates are examined to determine wave propagation modes and behavior. These models are then extended to investigate the sensitivities of certain wave modes to particular sensing applications to determine optimal conditions for device operation.

3.2 Transient Models using the Finite Element Method

3.2.1 Basic Theory

In structural dynamics problems, loads and responses can be considered as a function of time. If the load duration is sufficiently short in time (i.e. an impact or impulse), wave propagation in the absence of rigid body motion can occur. From Newton's Second Law, the governing finite element equation can be obtained by applying Galerkin's Method or the Principle of Virtual Work [Chandrupatla, 2002]:

$$[M]\{\ddot{u}\} + [C]\{\dot{u}\} + [K]\{u\} = \{F^a\} \tag{3.1}$$

where [M] is the structural mass matrix, [C] is the structural damping matrix, and [K] is the

structural stiffness matrix. The $\{\ddot{u}\}, \{\dot{u}\}$, and $\{u\}$ represent the nodal acceleration, velocity and displacement vectors, respectively. $\{F_a\}$ is a vector representing the applied load. This equation can be solved transiently by finite difference expansions in the time domain. Solvers which use this idea are referred to as iterative. Many iterative solvers rely on the Newmark Integration Method which assumes [Bathe, 1996]:

$$\{\dot{u}_{n+1}\} = \{\dot{u}_n\} + [(1-\delta)\{\ddot{u}_n\} + \delta\{\ddot{u}_{n+1}\}]\Delta t \tag{3.2a}$$

$$\{u_{n+1}\} = \{u_n\} + \{\dot{u}_n\}\Delta t + \left[\left(\frac{1}{2} - \alpha\right)\{\ddot{u}_n\} + \alpha\{\ddot{u}_{n+1}\}\right]\Delta t^2, \tag{3.2b}$$

where α and δ are referred to as Newmark integration parameters and the indexes on the vectors represent the time step. The benefit of implicit solvers is their unconditionally stablity for the following combination of Newmark Integration parameters[2]:

$$\delta \geq 1/2 \tag{3.3a}$$

and

$$\alpha \geq 1/2\,\delta. \tag{3.3b}$$

The drawback of this method is its computational expense since it depends on both current (n+1) and historical data (n, n-1, n-2,…):

[2] Found in ANSYS Release Notes, version 7.1

$$\{u_{n+1}\} = f\left(\{\dot{u}_{n+1}\}, \{\ddot{u}_{n+1}\}, \{u_n\}, \{\dot{u}_n\}, \{\ddot{u}_n\}, \{u_{n-1}\}, \ldots\right). \tag{3.4}$$

The explicit solver, counterpart to the aforementioned implicit one, has the benefit of lower computational expense due to its dependence only on historical data. In that way, the solution for the current time step, n+1, can be solved via:

$$\{u_{n+1}\} = f\left(\{u_n\}, \{\dot{u}_n\}, \{\ddot{u}_n\}, \{u_{n-1}\}, \ldots\right). \tag{3.5}$$

The drawback of the explicit solver is its conditional stability. The stability of such a solver can be thought of intuitively in relation to wave propagation in a finite element-discretized system. Instability can arise when the discretization in time, (Δt), is large enough to allow displacements associated with the wave propagation to traverse across more than one element. For this reason, Δt is often prescribed by allowing for upwards of 30 times steps per period of the associated wave propagation. However, given complexities in geometry and meshing strategies, care must be given to the smallest distances between elements. For this reason, a Δt upwards of several hundred time steps per period may be necessary to achieve stability in the model.

3.2.2 Piezoelectric Coupled Field Modeling

Coupled Field finite element models take into account constitutive relations between multiple sets of governing equations. Coupled-field relations between electromagnetics and mechanics have been established and are readily available in most commercial finite element

software. The relationship between Hooke's Law and Maxwell's equations allows for the modeling of the piezoelectric and inverse piezoelectric effect. From a wave propagation perspective, this allows for modeling of transduction and reception, both electrically and mechanically, which can very much mimic real world scenarios.

Constitutive relations for piezoelectric analysis in finite elements can be derived from variational principles [Allik, 1970] and are typically described by:

$$\{T\} = [C]\{S\} - [e]\{E\} \tag{3.6a}$$

and

$$\{D\} = [e]^T \{S\} - [\varepsilon]\{E\}. \tag{3.6b}$$

The newly introduced symbols in equations (3.6a and b) are as follows:

$\{T\}$ = stress vector
$[C]$ = elasticity matrix
$\{S\}$ = strain vector
$[e]$ = piezoelectric stress matrix (T superscript denotes stress)
$\{E\}$ = electric field vector
$\{D\}$ = electric flux density vector
$[\varepsilon]$ = dielectric matrix

From equations (3.6a and b) one can see that the actual coupling between mechanical and electromagnetic quantities occurs through the piezoelectric stress matrix. This matrix is a material property and is typically available for common piezoelectric materials. This analysis does assume a constant value for elasticity matrix under constant electric field along with a dielectric matrix under constant strain. Although not exactly the case, this assumption is fairly good to a first approximation. As a result of the large sizes of SAW models in finite elements, a

direct explicit solver was used for this work. The benefit of smaller computational expense far outweighs the convenience of unconditional stability. As a result, later discussions detail the effect of discretization on the modeling results.

3.2.3 Temporal and Spatial Discretization

Great consideration must be given to the discretization of a finite element model in both time and space when one is modeling wave propagation. A suggested rule of thumb for spatial discretization is twenty elements per wavelength. This can become difficult as limited propagation paths can be modeled with strict finite elements as the model size becomes extremely large, especially for three dimensional models. The motivation for such a large mesh density is to avoid any effects from numerical dispersion.

The easiest way to consider this phenomenon is by the digital signal processing analogy of aliasing. When a digital signal is discretized with too coarse a time step, some information about the actual signal could be lost. This can result in higher frequency content being "aliased" or shifted downward so that the observed frequencies appear lower than expected. To coarse a mesh in finite elements can have the same effect on the frequency of acoustic wave propagation. Due to the large spacing between elements, wave velocities may also appear much higher than expected. In practice, it is best to investigate the effect of mesh density on the results of a particular model to ensure no numerical dispersion is being observed.

As discussed earlier, time discretization can play a critical role in the stability of an

explicit solution to a finite element problem. The time step Δt is typically associated directly with the level of spatial discretization for explicit solvers. As the mesh gets finer, the time step must also shrink to maintain stability. One must consider the trade-offs between model accuracy and solution time/size. Ideal scenarios may not often be feasible due to computational limitations so the evaluation of model accuracy is critical in finite element problems.

3.3 SAW Delay Line Models for Anisotropic Piezoelectrics

3.3.1 Modeling Inter-Digital Transducers (IDTs)

Surface Acoustic Wave devices are typically based on transmitting and receiving IDTs. The spacing and thickness of the IDTs control the wavelength of the generated acoustic wave. Although many variations have been studied, a traditional IDT design is shown in figure 3.1. IDTs are typically realized by depositing periodic structures of metal layers onto piezoelectric substrates.

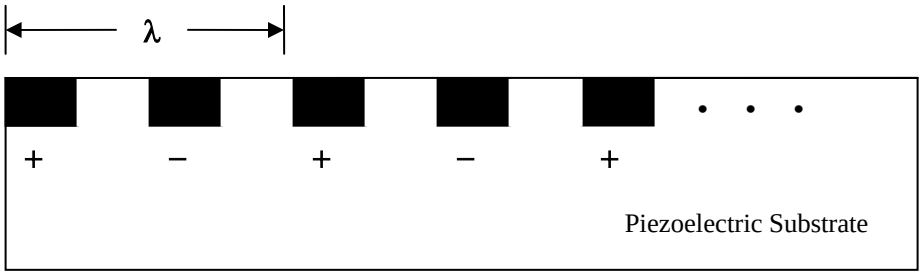

Figure 3.1. Schematic of periodic IDT structure and its associated wavelength.

IDTs can be modeled in several ways using finite elements. In this work, the metalized

layer associated with the IDT fingers are modeled as mass-less electrical contacts by simply applying appropriate boundary conditions to areas of the model (i.e., electrical potential is zero on ground (-) electrodes and electrical loads are applied to positive (+) electrodes). The assumption of this technique is the mass and dimension of the IDTs play little role in the characteristics of the generated waves.

One can easily simulate a two-port SAW device which contains an IDT set for transmission and a second set for reception. The boundary conditions for the receiving IDTs can be applied in the same manner. Ground electrodes are defined by setting the electrical potential to zero. Positive receiving electrodes are usually denoted with a constraint equation. This is a condition whereby the electrical potential of all nodes on the defined IDT surfaces are equivalent to that of the master node. This mimics a real situation where all positive IDT fingers are electrically connected to the same contact.

Wave propagation is initiated by applying a time dependant electrical load on the transmitting IDTs. Knowing the wave propagation speed of the substrate, c, and the wavelength prescribed by the IDT widths and spacing, λ, one can estimate the center-line frequency of the generated wave, f, according to:

$$c = f\lambda \, . \tag{3.7}$$

To characterize the frequency response of a two-port delay line, the electrical load should take the form of a pulse containing a spectrum of frequencies including the frequency of interest

according to equation (3.7). Given the earlier discussion on numerical dispersion, care should be taken to limit the higher frequency content of the signal. Since the wavelength of the generated waves is fixed according to the IDT definition, the numerical dispersion at higher frequencies becomes a concern for higher harmonics. In this fashion, the frequency associated with the third harmonic of the slowest propagating wave should be significantly attenuated so as to not confuse the results of the simulation.

The devices tested in this work have central frequencies around 100 MHz. An electrical input signal was then constructed in MatLab. The frequency content of this impulse signal was then examined to ensure significant attenuation at frequencies higher than 200 MHz where a third harmonic could potentially be generated. Figure 3.2 shows the input signal used for this study in both time and frequency domain.

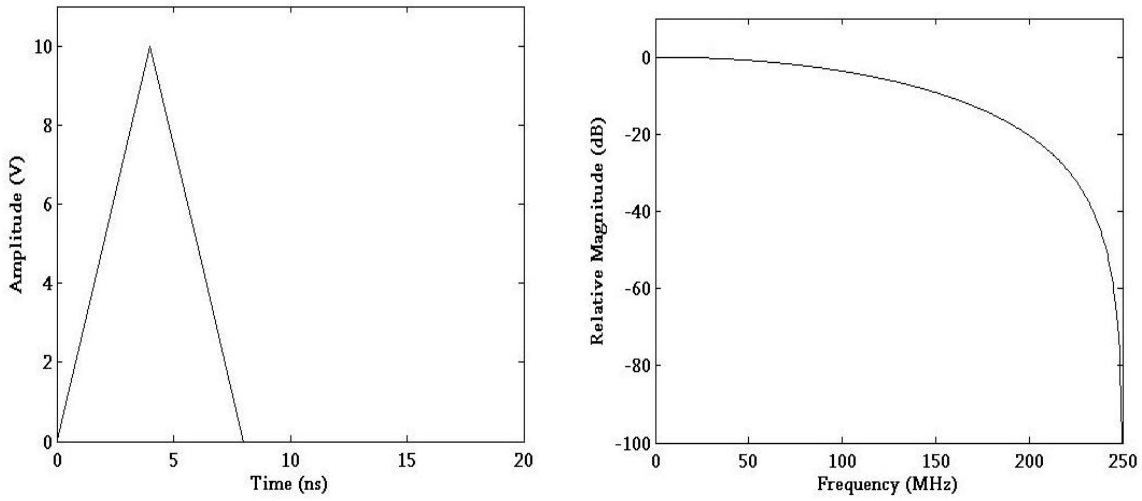

Figure 3.2. (a) Time domain and (b) Frequency domain impulse signal used to excite the IDTs ensuring significant attenuation above 200 MHz.

3.3.2 Piezoelectric Crystal Orientation

Most common piezoelectrics are anisotropic and surface acoustic wave devices are fabricated on particular orientations of piezoelectric substrates which support surface wave propagation. Material properties are defined in ANSYS/CAPA according to a Cartesian coordinate system. It is often the case that rotated orientations of piezoelectric substrates yield the desired wave propagation mode as is the case in Quartz, the piezoelectric substrate considered in this work. The so-called "ST cut" Quartz is a y-rotated, x propagating orientation that supports surface acoustic wave propagation. In a similar fashion, 90 degree rotated ST Quartz supports the generation of Surface skimming bulk waves (SSBW) which coupled with an overlayer, can produce Love Waves [Kalantar-Zedeh, 2003].

These orientations can be modeled with finite elements in one of two ways. The first is to rotate the material property data into an orthogonal coordinate system with normal components parallel to the surfaces of the model geometry (in the case of a rectangular model). In this work, the geometry itself was rotated with respect to the global coordinate system to represent the particular orientation as shown in figure 3.3 for ST-X Quartz.

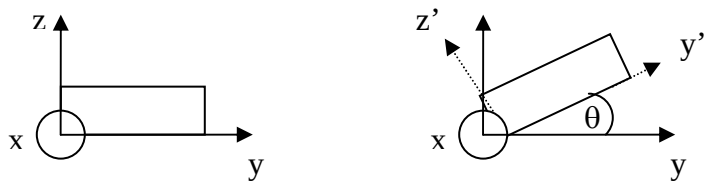

Figure 3.3. Shows the initial and rotated geometries for a Quartz rectangular structure. For ST-X Quartz, theta is 42.75^0 and propagation is in the x direction.

It is important to note that ANSYS/CAPA saves displacements in the global coordinate system. In order to obtain conventional (Shear-Horizontal, Shear-Vertical, and Longitudinal) displacements, the global values of dx, dy, and dz must be mapped into the rotated coordinate system.

3.3.3 Baseline Models

A baseline model for an ST Quartz delay line was developed to determine the effectiveness of an ANSYS/CAPA model in characterizing the behavior of a SAW device. The mesh density necessary for SAW devices are fairly large considering their high frequency. For this reason, full scale replications of actual SAW devices are often difficult while maintaining an appropriate meshing scheme. A miniaturized model was developed as shown in figure 3.4.

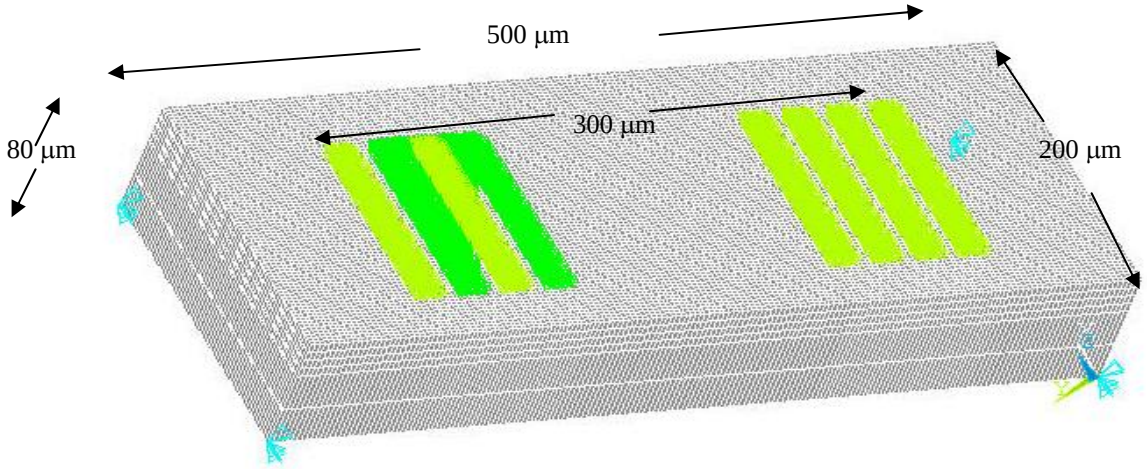

Figure 3.4. ANSYS/CAPA Model of Quartz Substrate with two pairs of transmitting and receiving IDTs. The yellow and green bars represent the individual IDTs/electrodes. An equipotential boundary condition was applied to the receiving electrodes such that the voltage read by a master node on one of the IDTs is mapped onto all the other nodes of the positive receiver IDTs. This condition is represented in green. The yellow represents electrodes where boundary conditions have been defined across the entire IDT (i.e. either grounded or excitation condition)

A mapped mesh was used in order to preserve the element shape throughout the model, and a finer mesh of at least 10 nodes per wavelength was maintained near the surface of the device since most of the wave energy dissipates after depths on the order of one wavelength. An investigation into the necessary time step, Δt, to ensure stability revealed that approximately 100 time steps per period consistently resulted in stable models throughout this investigation. Typical simulations were run for 100 nanoseconds which allowed enough time to visualize all wave propagation of interest without interference from the back and sidewalls.

A thorough knowledge of material properties is necessary for developing an accurate finite element simulation including: elastic properties, density, piezoelectric coupling coefficients, and dielectric properties. Piezoelectric alpha quartz has trigonal-trapezohedral crystal symmetry [Sossman, 1927] and can be defined according to the following elastic constant matrix:

$$[C]_{quartz} = \begin{bmatrix} c_{11} & c_{12} & c_{13} & c_{14} & 0 & 0 \\ & c_{11} & c_{13} & -c_{14} & 0 & 0 \\ & & c_{33} & 0 & 0 & 0 \\ & & & c_{44} & 0 & 0 \\ & & & & c_{44} & 0 \\ sym & & & & & \frac{1}{2}(c_{11}-c_{12}) \end{bmatrix}. \tag{3.8}$$

The piezoelectric coupling matrix for alpha quartz can be described by:

$$[e]_{quartz} = \begin{bmatrix} e_{11} & -e_{11} & 0 & -e_{14} & 0 & 0 \\ 0 & 0 & 0 & 0 & -e_{14} & -e_{11} \\ 0 & 0 & 0 & 0 & 0 & 0 \end{bmatrix} \tag{3.9}$$

Table I lists the material properties used for this analysis as taken/adapted from [Ward, 1992].

Table I. Material Property Data used for Finite Element Simulations of Alpha Quartz

Elastic Constants ($x10^{-9}$ N/m^2)	C_{11} = 86.74	C_{14} = -18.04
	C_{12} = 6.99	C_{33} = 107.2
	C_{13} = 11.91	C_{44} = 57.94
Density (kg/m^3)	2650	
Dielectric Constants ($x10^{12}$ F/m)	ε_{11} = 39.97	ε_{33} = 41.03
	ε_{22} = 39.97	
Piezoelectric Constants (C/m^2)	e_{11} = 0.171	e_{14} = .0403

The first model consisted of finger widths and spacings of 13 μm yielding a periodicity of 52 μm. The electrical potential was monitored as a function of time. The frequency content of the resulting signal was analyzed using the Fast Fourier Transform (FFT). Figure 3.5 shows a time trace for signals generated under this scheme where figure 3.6 shows the associated frequency response.

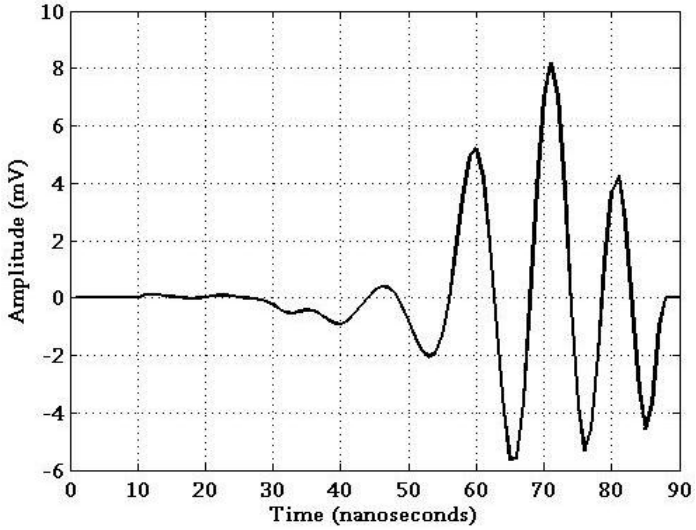

Figure 3.5. Time trace obtained from model of 90^0 rotated ST-Quartz, known to generate Surface Skimming Bulk Waves (SSBWs).

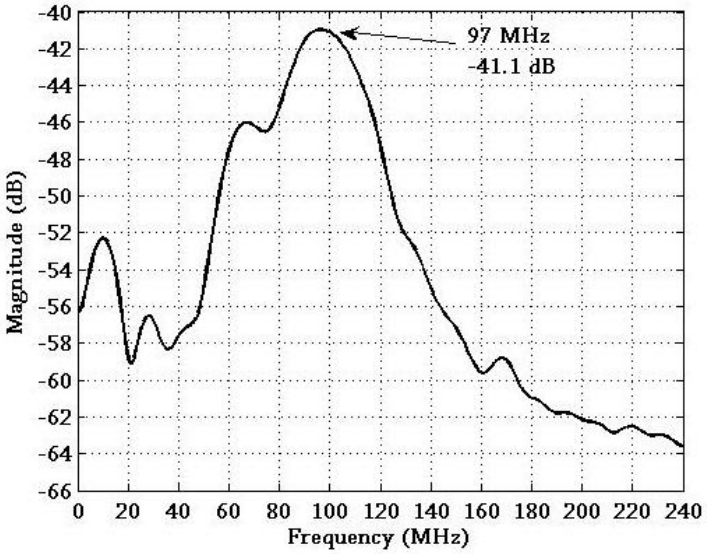

Figure 3.6. Frequency response of the signal in Figure 3.5 obtained via FFT.

Typically, SAW devices consist of 10-50 finger pairs for each IDT. From a FEM perspective, this is a challenging aspect to model as it requires a significantly larger scale resulting in an extremely large element matrix. One can argue that the only significant contribution from more finger pairs is a decreased bandwidth. More fingers result in a larger

number of cycles in the generated pulse. More cycles decrease the bandwidth as it transitions from a pulse to a toneburst and ultimately to a continuous wave.

A mathematical relationship accounting for bandwidth in terms of the number of IDT pairs has been introduced [Acoustic wave Sensors,]. The relationship can be described as:

$$\left|\phi^{+}(f)\right| = \left|\frac{\sin x}{x}\right|. \tag{3.10}$$

In this scenario, $\phi^{+}(f)$ represents the S_{21} parameter or transmitted frequency response and x can be described by:

$$x = \frac{N_p \pi (f - f_0)}{f_0} \tag{3.11}$$

where N_p represents the number of finger pairs and f_0 is the centerline frequency of the device. A comparison of the results of equation 3.10 using N_p=2 and f_0 = 97 MHz is overlayed on the FEM results for S_{21} in figure 3.7. The FEM model closely resembles the theoretical bandwidth predicted by equations 3.10 and 3.11. The overall differences in structure are attributed to the geometric constraints of the model (i.e. the aspect ratio of the fingers does not resemble a semi-infinite source as used in the derivation of equations 3.10 and 3.11).

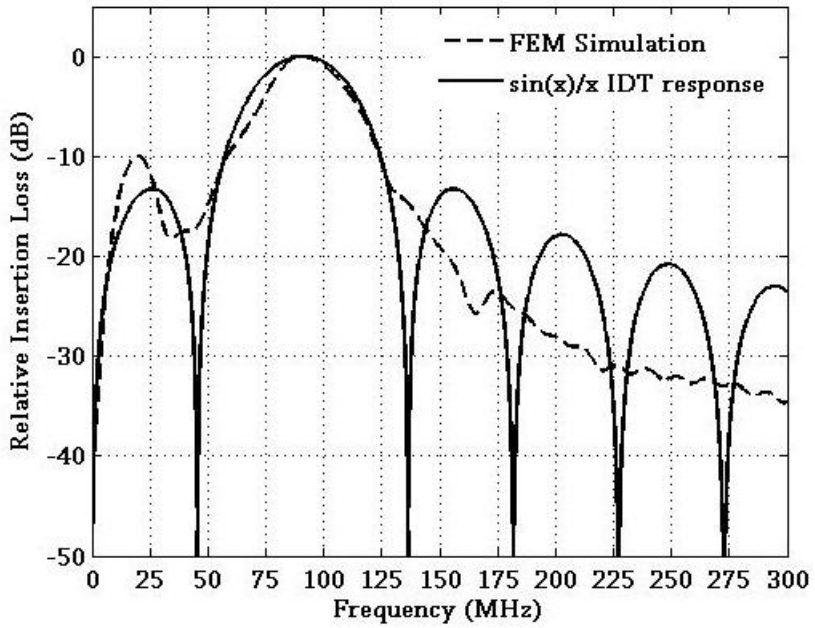

Figure 3.7. Comparison of FEM results for bandwidth of a transmitted signal on 90^0 rotated ST Quartz compared to a theoretical sin(x)/x bandwidth prediction for $N_p = 2$. The larger attenuation at frequencies higher than 150 MHz is attributed to Excitation signal which was designed to attenuate higher frequencies to eliminate effects from numerical dispersion. This was shown in figure 3.2.

The benefit of the FEM models of SAW delay lines is the ability to analyze both frequency and time domain aspects of the generated wave propagation. From a guided wave perspective, this is beneficial since the time delay, group delay, allows for the calculation of the energy transport or group velocity. Also, the frequency analysis allows for calculation of the phase velocity. In bulk wave ultrasonics these values are the same, however, in guided wave analysis these values will often vary with respect to one another.

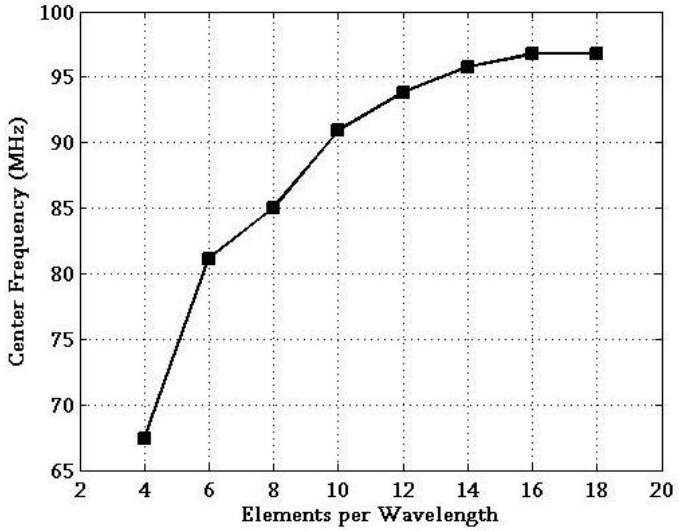

Figure 3.8. Effect of mesh density on accuracy of results. Convergence occurs at 16 elements per wavelength.

Since modeling high frequency delay lines requires an extremely large mesh density, computation times of these FEM models can be quite lengthy. Figure 3.8 shows the results for center line frequency as a function of mesh density for the model described above. With too coarse a mesh density one can see the effects of numeric dispersion. For example, the calculated frequency for 6 elements/wavelength results in an operating frequency of 82 MHz whereas 10 elements/wavelength results in 91 MHz. The goal is to find the minimum mesh density where the results converge. As shown in figure 3.8, the minimum mesh density is 16 elements/wavelength. This density was maintained for all models.

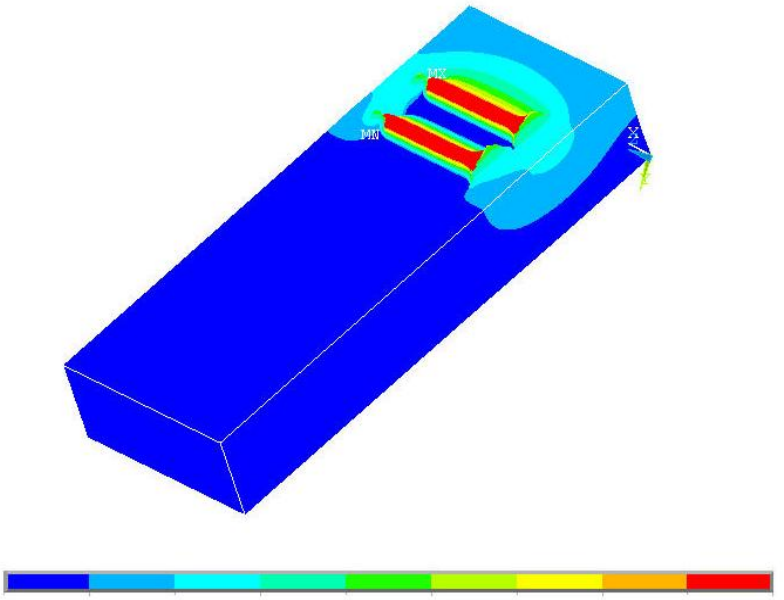

(a)

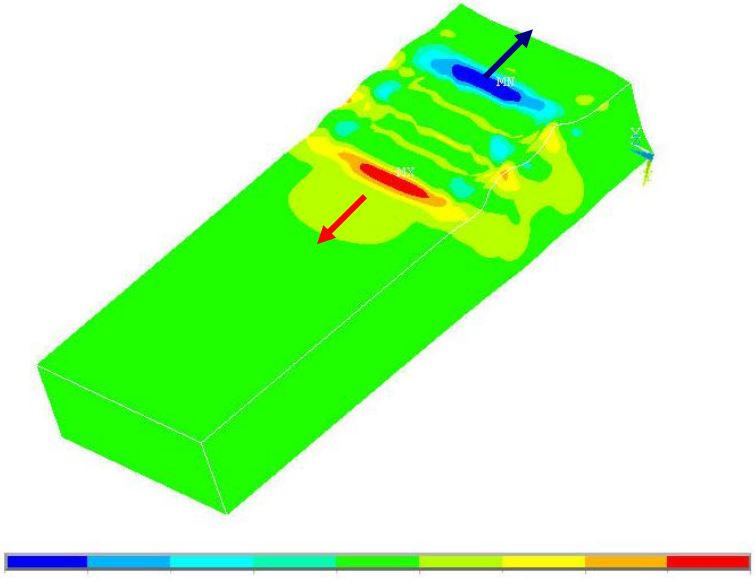

(b)

Figure 3.9. (a) Displacement field showing the excitation of the electrodes and (b) Displacement field for the forward (red) and backward (blue) traveling waves.

3.3.4 Layered SAW Sensitivity from FEM

A critical eye is necessary for evaluating the effectiveness of a Finite element model. A key component of this work is to determine the capability of this model to describe the guided wave phenomena associated with Love Waves. For this purpose, an isotropic layer was added to the model representing an elastic film. Figure 3.10 shows a closeup of the model where the film is red and the substrate gray. Notice that the model consists of two elements per thickness for the film. This was maintained throughout the analysis to avoid spurious results from having only one element to describe the film thickness. The yellow and green markings of the model are indications of the electrical boundary conditions associated with the model.

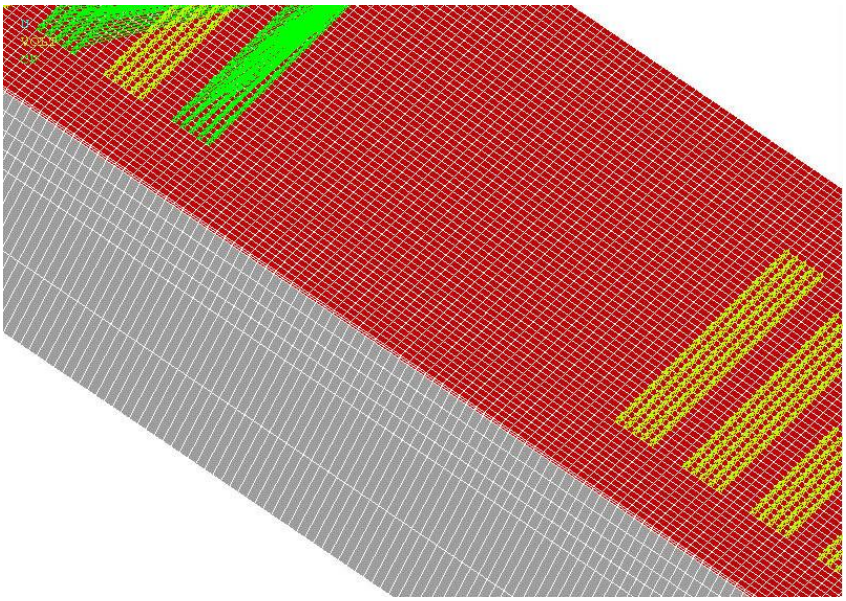

Figure 3.10. Closeup image of the FEM model representing an elastic, isotropic layer on an elastic, anisotropic, piezoelectric substrate. The yellow markers indicate the electrical boundary conditions associated with the IDTs. The green markers and lines represent the equi-potential boundary condition applied to the receiving IDTs.

The model was also rotated and to investigate both ST and 90^0 rotated ST Quartz known for generating Rayleigh and SSBW, respectively. Finally, a model was constructed based on 77^0 Y Rotated Lithium Tantalate, also known to generate Rayleigh type waves. These three devices became the comparison base for determining sensitivity and comparisions with experimental data.

A benefit of the FEM for Layered SAWs is the ability to investigate nodal displacements which provide a clear indication of wave structure. The discretized nature of the model allows for the investigation of such wave structure as a function of both time and space. By understanding the wave structure associated with a particular propagation mode, key characteristics and further understanding of the device's behavior are obtained. This capability was explored to investigate the wave structure associated with Love waves in 90^0 rotated ST Quartz and SV-SAW waves in 77^0 Y-rotated $LiTaO_3$.

The ANSYS/CAPA convention is to save displacements in the global coordinate system. In order to investigate the displacements in a rotated SAW model, displacement results must be mapped into the local coordinate system. Figure 3.11 shows the results for nodal displacements along a vertical line through the center of the model. The time step was chosen to maximize the acoustic energy along the line being investigated. Note the maximum Shear Horizontal displacement and the wave structure resembling those shown in Chapter 2. Note that although small, there are some displacement contributions from the longitudinal and shear vertical modes. These contributions are an indication of the Surface Skimming Bulk Wave (SSBW) excited by 90^0 Rotated ST Quartz. This illustrates another benefit of FEM analysis of SAW propagation.

One can investigate wave components more consistent with realistic scenarios in contrast to the idealized cases of pure theoretical developments.

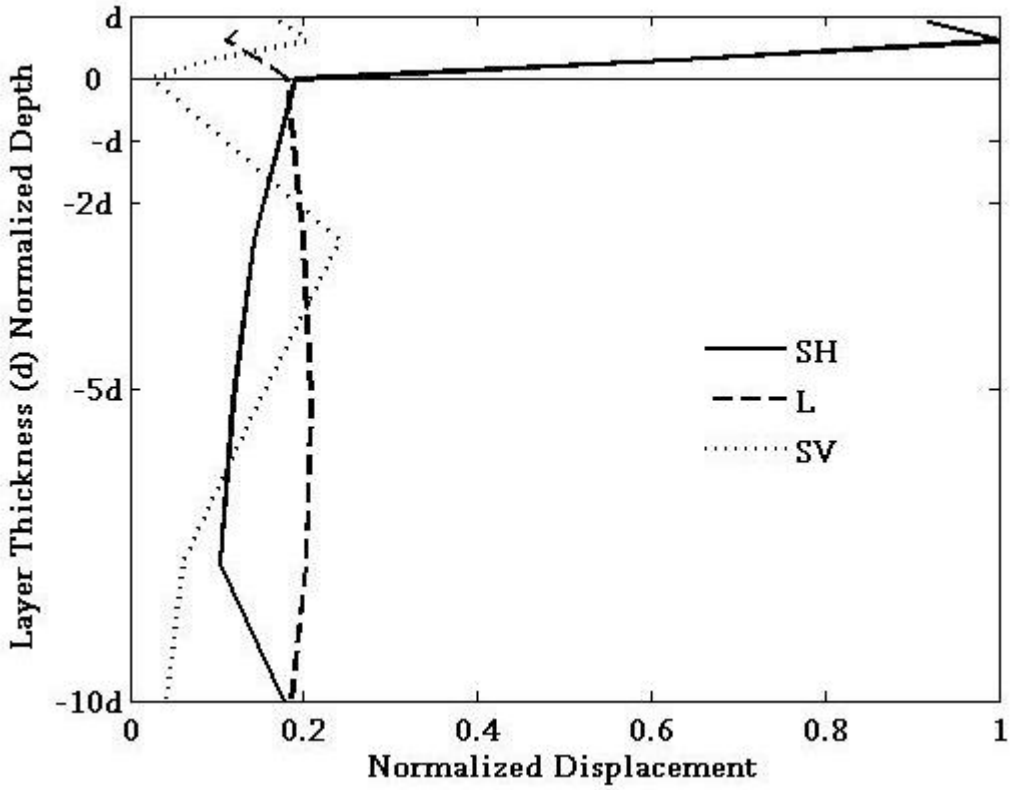

Figure 3.11. Normalized displacements through the depth of the device at time step t= 69 ns showing dominant Shear Horizontal displacement (SH) compared to Longitudinal (L) and Shear Vertical (SV).

Figure 3.12 shows the normalized displacements for 77^0 Y-Rotated $LiTaO_3$ generating SV-SAW waves. The longitudinal and shear vertical displacements dominate in the film and near the surface. A large portion of the wave energy in a SV-SAW is concentrated at the interface between film and substrate. However, compared to the Love Wave device, the SV-SAW wave device has a non-negligible contribution of displacement into the substrate. The displacement localization in the layer found in the Love Wave device makes these devices more

attractive for layered SAW applications.

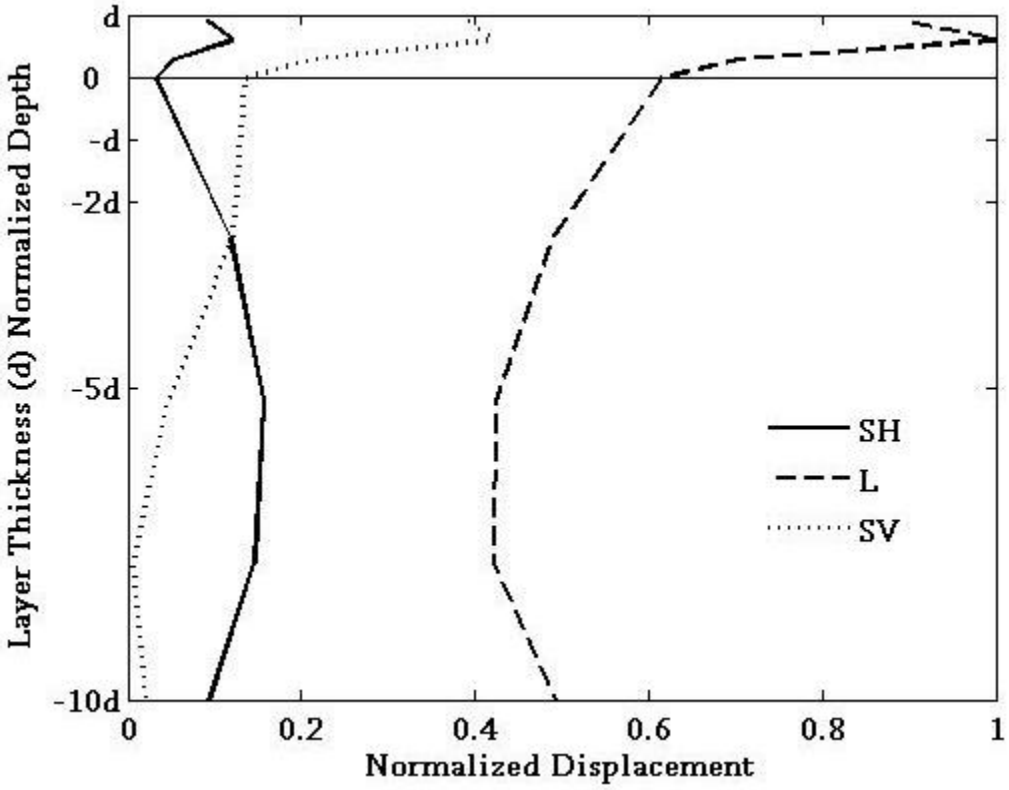

Figure 3.12. Normalized displacements through the depth of the device at time step t= 48 ns showing dominant Shear Vertical (SV) and Longitudinal (L) displacments compared to Shear Horizontal (SH).

The frequency response of each device configuration was tested as a function of overlayer thickness of a PMMA film. The purpose of this test was to investigate the wave propagation phenomena associated with the different modes. Figure 3.13 shows a comparison of results from ST Quartz and 90^0 rotated ST Quartz. The ST Quartz generates both HVSAW and GSAW as expected from experimental results found in literature [Hickernell, 1997]. The HVSAW and GSAW both show a downward trend in frequency of around 10-15 MHz as the film thickness increases to approximately 1.5-2 μm. This type of SAW dispersion agrees with

those shown in literature [da Cunha, 1995]. The Love Wave device, however, shows a more dramatic decrease in frequency of approximately 30 MHz up to a thickness of 3 μm.

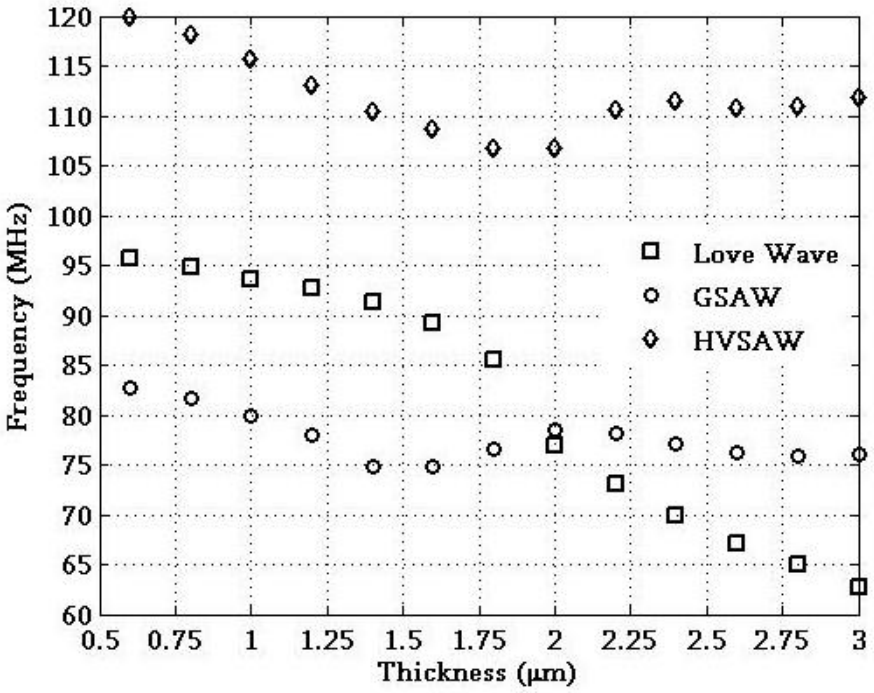

Figure 3.13. FEM results for centerline frequency of two-port delay lines based on 90^0 rotated ST Quartz generating Love Waves (squares) and ST Quartz generating GSAW (circles) and HVSAW (diamonds) as a function of PMMA film thickness. Recall the Generalized SAW (GSAW) represents the common SV-SAW type with velocity slightly less than the transverse velocity in the material. The High Velocity SAW (HVSAW) represents a "leaky" SV-SAW mode determined by the complex solution to the Rayleigh wave equation. The HVSAW typically has velocities on the order of 1.9 times that of the GSAW.

The larger frequency changes associated with the Love Wave device can be understood by reinvestigating the wave propagation phenomena. The Love Wave propagates with a majority of energy trapped in the film, as derived in the previous chapter and demonstrated by the FEM results on wave structure. Therefore, its propagation is much more dependant on the state of the film than the SV-SAW Wave counterpart. Recall that the derivation of Love Wave propagation consisted of the Transverse Resonance Principle where the thickness component of the displacement produces a standing wave resonance. This resonance is affected by the film

thickness much more than the SV-SAW wave propagation where the film merely represents a modification of the free boundary condition.

Another reason for the enhanced thickness dependence is the guided wave nature of Love Wave propagation. This can be investigated by mapping the FEM results from the thickness study into a relationship between group velocity and fd product. A comparison of the FEM results and the theoretical group velocity dispersion curve for the fundamental Love Wave mode is shown in figure 3.14. The group velocity as a function of fd product found in the FEM results trends fairly well with the theoretical curve for the first mode.

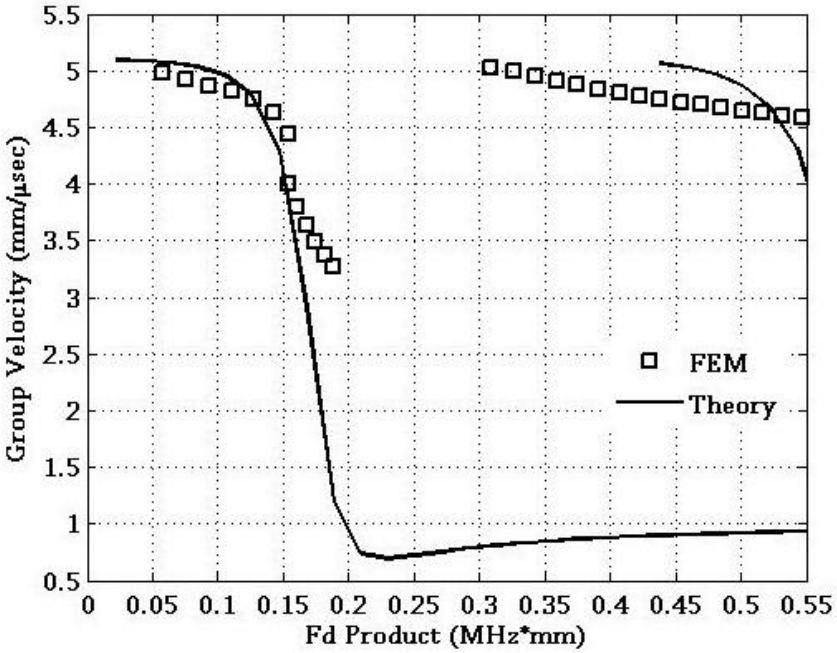

Figure 3.14. Comparison of Theoretical (lines) and FEM (squares) results for Love Waves in a PMMA layer on a Quartz substrate.

Although the model is able to predict a mode conversion from first to second mode, the trend of the second mode found in the FEM results only loosely resembles the theoretical trend

of the curve. This can be attributed to a numerical dispersion effect. Looking back at the wave structures of the previous chapter, one realizes that two displacement maxima exist in the film as opposed to one maximum for the fundamental mode. The wavelengths associated with the second mode are half that of the fundamental mode. This introduces a problem with the mesh density which was set at 16 elements per wavelength for the fundamental mode. This scenario represents only 8 elements per wavelength for the second mode which has been shown to be insufficient earlier in this chapter. Due to the large size of the existing model, increasing the mesh density to adequately model the second mode is extremely difficult with typical computing power. This illustrates a current limitation with the FEM model for Love Wave modeling.

A derivation of Love Wave device mass sensitivity can be found in the literature [Jacoby, 1997] and has been represented in terms of frequency as [Francis, 2005]:

$$S_{\omega} = \frac{1}{\omega}\frac{d\omega}{d\sigma} \tag{3.12}$$

where ω is the angular frequency and σ represents the surface density (i.e. density normalized by the layer thickness). This relationship was used to investigate the mass sensitivity of Layered SAW devices as a function of thickness. The results are shown in figure 3.15. Note the higher mass sensitivity in the Love Wave device which occurs at a different thickness compared to the HVSAW.

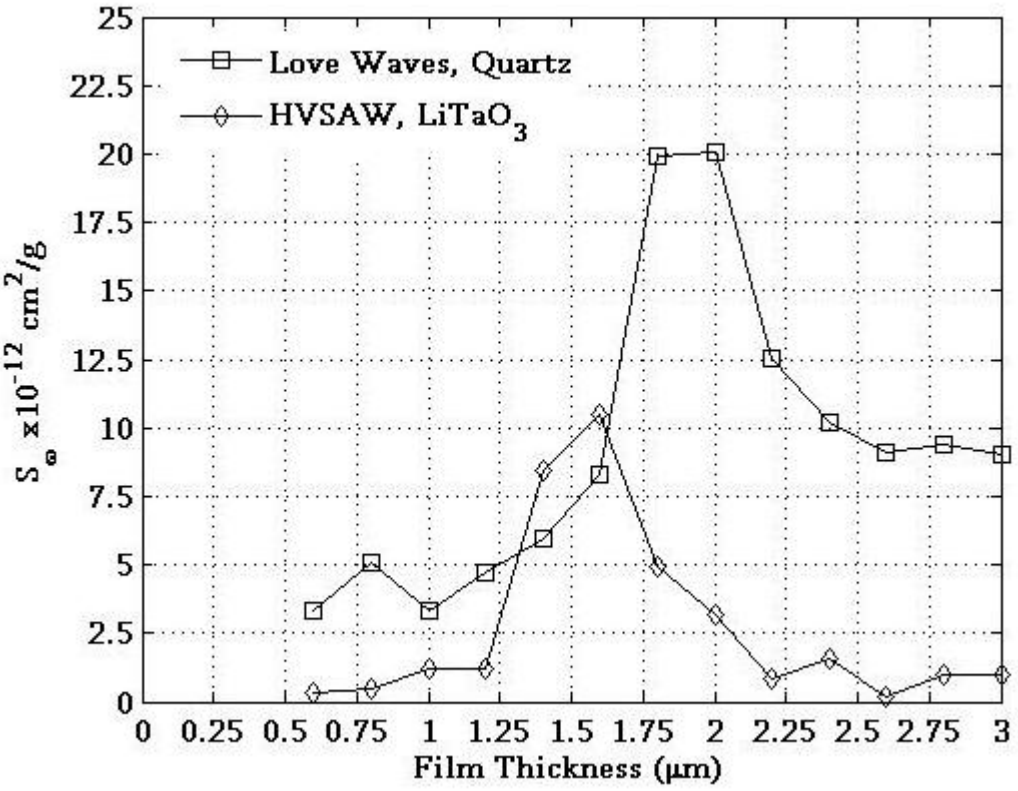

Figure 3.15. Mass Sensitivity factor for Love Wave and HVSAW devices as a function of PMMA layer thickness.

3.4 Conclusions

This chapter has introduced some novel features of the Finite Element method to investigate SAW and Layered SAW devices. Geometric transformation of the model with respect to the global coordinate system allows for analysis of different crystal orientations of piezoelectric substrates. This concept has been utilized to model SV-SAW (GSAW) and HVSAW wave propagation in ST Quartz and 77^0 Y Rotated $LiTaO_3$ along with SSBW and Love Waves in 90^0 rotated ST Quartz.

The models were investigated to determine the minimum mesh density to ensure convergence of results, occurring at 16 elements per wavelength. Transformations of global displacements into the local coordinate system allowed for investigation of wave structure for Love and HVSAW devices. These results indicate the isolation of acoustic energy in the layer associated with Love Wave propagation. Although some energy trapping in the layer occurs with the SV-SAW wave devices, a significant amount of energy remains in the substrate. The guided wave behavior of Love Wave devices was also investigated. Although the conversion from the first to the second mode is evident, the reduction of the wavelength violates the mesh density convergence resulting in skewed dispersive behavior of the second mode.

Finally, a standard relationship for mass sensitivity was used to show the sensitivity of each device as a function of overlayer thickness. As expected from the earlier analysis, the Love Wave device reached a mass sensitivity of almost twice that of the SV-SAW wave counterpart. Comparisons also show that higher sensitivities are achieved for wave excitations on the dispersive portion of the curve. The FEM model developed proved useful in predicting the behavior of Layered SAW devices. The benefits of FEM analysis were exploited to investigate features of the wave propagation that explain the increased sensitivity of certain frequency thickness combinations.

Chapter 4 Film Characterization via Layered Surface Acoustic Wave Devices

4.1 Introduction

The detection of chemical and biological analytes via Surface Acoustic Wave devices is limited by their sensitivity to surface mass perturbations [Thompson, 1997]. Such applications represent a majority for SAW sensors resulting in a vast amount of research into mass sensitivities of such devices compared to sensors based on Flexural Plate Modes (FPM), Quartz Crystal Microbalances (QCM), and Shear Horizontal-Acoustic Plate Modes (SH-APMs). Due to the confinement of acoustic energy near the surface and their typically high operating frequencies, research has shown that SAW devices can provide enhanced sensitivity over the aforementioned counterparts [Zimmerman, 2002]. The goal of this work is to compare the sensitivity of two common layered SAW devices not only to mass changes but to changes in elastic properties in general as a vehicle for characterization of the properties of thin films.

Two common wave propagation modes in layered SAW devices are the SV-SAW mode consisting of elliptical displacements in the sagittal plane and Love waves consisting of Shear-Horizontally polarized displacements. The main distinction between the two is their applicability in liquid environments. SV-SAW waves are limited due to energy leakage as a result of displacement components normal to the surface of the device. The inability to shear load a fluid allows for operation of Love Wave type devices in liquid environments.

There are two fundamental differences in these wave propagation modes that may also contribute to their sensing capabilities in layered devices. The Love waves require the overlayer to propagate and most of the energy is confined in that layer. SV-SAW wave propagate in spite of the overlayer. They require a free boundary to propagate and the addition of the overlayer simply modifies that free boundary condition. Most of the energy in SV-SAW wave devices is concentrated at the interface.

Love Wave devices have vast potential as polymer film characterization tools. The strict dependence of wave propagation on several properties of the polymer film can be exploited to monitor or characterize polymer film properties as a function of external influences. Such applications are presented in this chapter and compared with the performance of SV-SAW Wave devices.

4.2 Film Preparation and Device Characterization

Several devices were fabricated on ST Quartz with standard lithography processes (more details provided in Appendix A). For the actual experimentation, devices on 90^0 rotated ST Quartz and 77^0 Y rotated $LiTaO_3$ were obtained from researchers at Nottingham Trent University (see acknowledgements). Several films were used throughout the experimental phases of this work with the common thread of their application as photoresists in microlithography.

The two main films studied were SU-8, a cross-linking epoxy and PMMA, both made by

Microchem. These films were chosen for differing reasons. SU-8 cross-links under UV light and thus was chosen as a prime candidate for proof-of-principle for radiation detection discussed later in Chapter 5. The reported glass transition (T_g) in SU-8 is around 200^0C [Feng, 2003]. PMMA has been a common material chosen for studies of Love Wave devices and was chosen for its availability along with its use in previous Love Wave studies. PMMA has a T_g around 120^0C [Wondracsek, 2004].

A common technique of spin-casting was used for the deposition of films onto the piezoelectric substrates. A certain weight percent of the film is dissolved in solution so that the viscous liquid can be coated on the surface of the piezoelectric substrate via pipet. The "spinner" is then accelerated to a desired RPM whereby the dissolved film spreads evenly over the surface. Films such as SU-8 and PMMA have associated spin-curves provided by the manufacture. These provide relationships between the appropriate spin speeds necessary to achieve a certain film thickness depending on the weight percent of the solid in solution.

For lithography purposes, PMMA films are typically found in weight percents less than 5% which limit the potential thicknesses obtain to approximately 700nm. In order to spin thicker films, 9% PMMA dissolved in Anisole was obtained from the manufacturer in order to realize films of approximately 1.5 μm. Once applied, a small edge of the film was removed with a selective etchant (acetone in the case of PMMA) in order to verify the film thickness with a profilometer. Figures 4.1 a and b show the results from such thickness measurements.

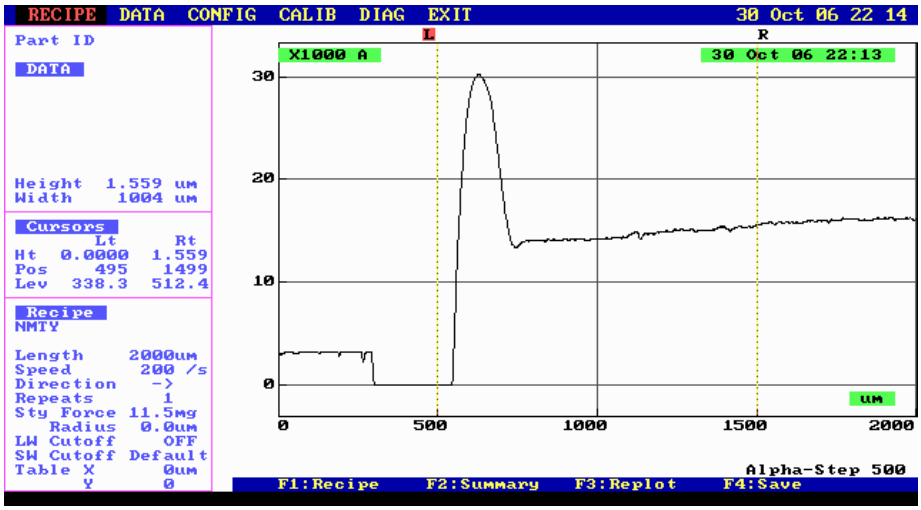

(a)

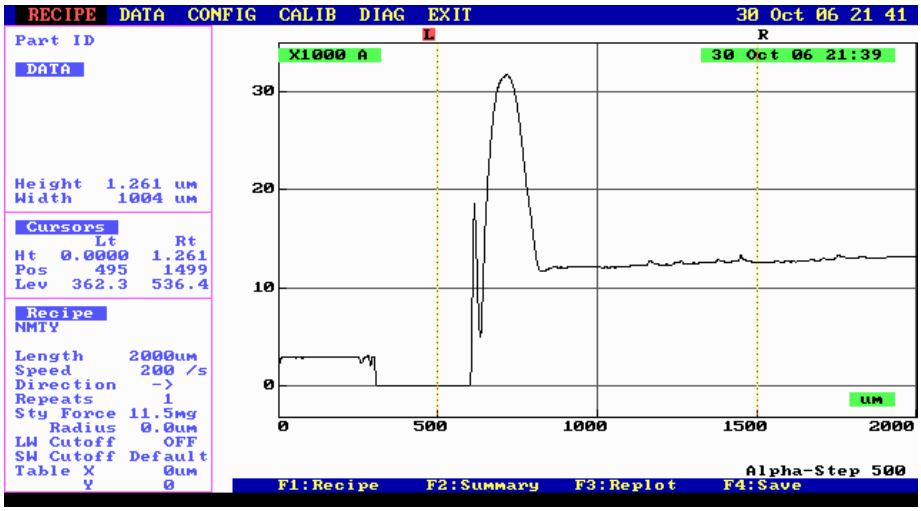

(b)

Figure 4.1. Profilometer data for (a) a 1.56 μm PMMA film and (b) a 1.26 μm SU-8 film.

The profilometer consists of an extremely small probe which scans the surface recording the deflection. Notice in the scans that on the far left there is a small step down. This is the result of the profilometer tip scanning over an IDT and then down onto the bare film. Next, one sees a large hump that occurs as a result of pile up from the etching process. Finally, a scan across the clean section of the film can be used to give an indication of the film height.

The profilometer was also used to verify the IDT thickness and spacing in order to compare with FEM results. Figure 4.2 a and b shows those results for the 90^0 rotated ST Quartz and the 77^0 Y rotated $LiTaO_3$, respectively. The associated IDT thickness for the Quartz was approximately 13 μm whereas the IDT thickness for the Lithium Tantalate was 17 μm.

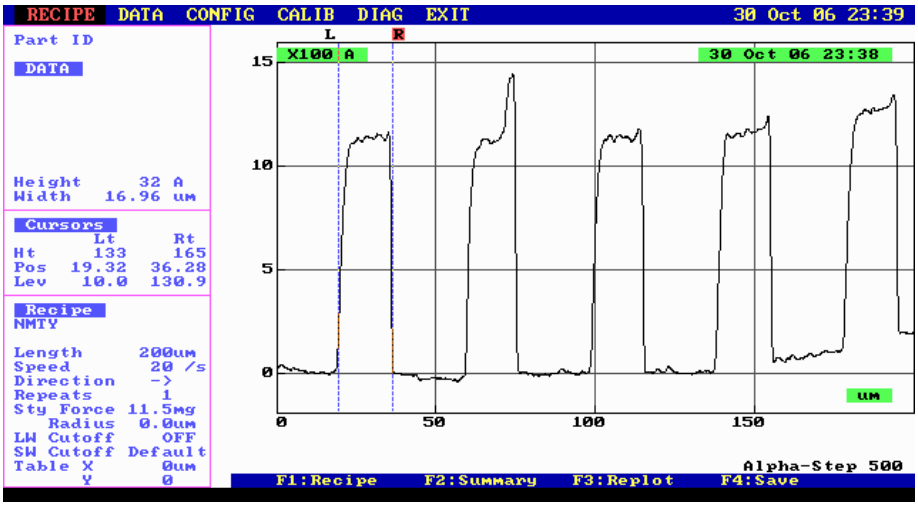

(a)

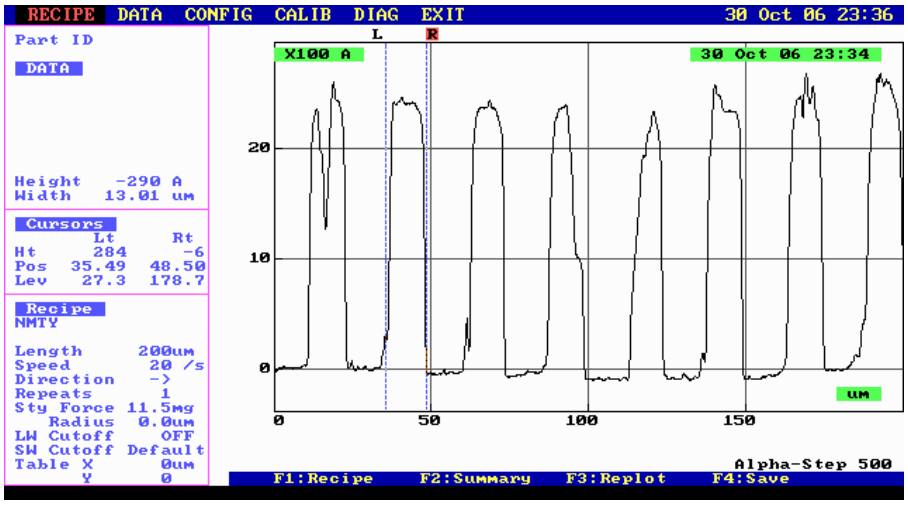

(b)

Figure 4.2. Profilometer scan over the IDTs of the (a) $LiTaO_3$ sample and (b) the ST Quartz sample showing IDT finger widths of 16.96 μm and 13.01 μm, respectively.

4.3 Polymer Curing

4.3.1 Experimental Setup

Once the films are spun onto the substrate, they are typically "soft-baked" at a prescribed temperature for a given amount of time to insure that the solvent is completely evaporated leaving only the solid film. This process is a direct correlation of polymer curing in industrial applications. As a result, devices were tested at different bake time intervals to track the removal of the solvent. The expectation is that as the solvent evaporates out of the film, the properties of the system change such that the operating frequency also changes.

This test was achieved with a simple hot plate. The difficulty was that the piezoelectric substrate plus film was heated separate from the electrical connections and the breadboard. As a result, the device had to be continually connected and disconnected from the test setup. This did not introduce any variance in frequency however some effect in insertion loss was experienced. This is to be expected as a result in the variation of the contact pressure between the wires and the electrode pads.

The temperature tests presented here were conducted on both the 90^0 rotated ST Quartz and 77^0 Y rotated $LiTaO_3$ for a PMMA film of approximately 1.4 μm. The soft bake temperature, as prescribed by Microchem, was set at 180^0C. The devices were placed on a hot plate at this temperature for intervals of approximately 20 seconds. The results are shown and

discussed below.

4.3.2 Results and Discussion

Figure 4.3 shows results for normalized frequency change as a function of time at temperature for the PMMA films on both Love Wave and HVSAW devices. This data includes two data sets for each device. Immediately apparent is the order of magnitude higher sensitivity of the Love Wave device over the HVSAW. There is also a clear convergence of frequency at approximately 40 seconds, suggesting that in this time, a majority of the solvent has been evaporated from the system.

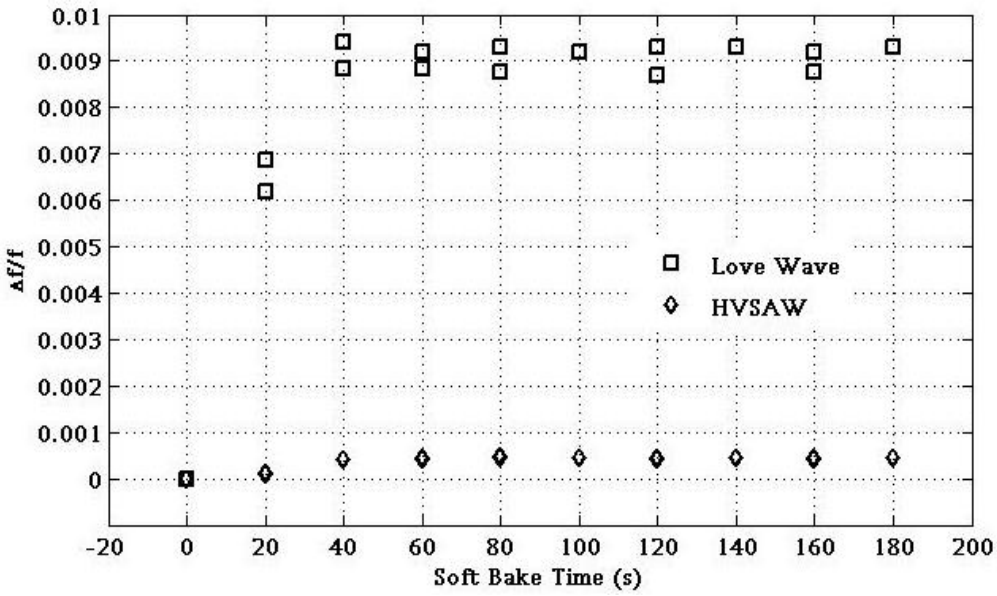

Figure 4.3. Normalized change in frequency as a function of soft bake time for a ST/90 Quartz substrated covered with a PMMA film (Love Waves) of approximately 1.4 μm.

Characteristics of the S_{21} parameter as a function of frequency also show some interesting

results. Prior to soft baking, the film is in a viscous state and the adhesion of the film to the substrate is somewhat lacking. The soft-baking process changes the behavior of the overlayer. The dominant effect is an increase in stiffness and hardness due to the evaporation of the solvent. This also promotes the adhesion of the film to the substrate. This is evident by comparing the S_{21} responses for pre-soft bake and post-soft bake in figure 4.5. Notice two significant peaks in the response from the pre-bake condition. The dominant peak is approximately 94.5 MHz with an insertion loss of approximately 34 dB. A second peak is present at 96.6 MHz which can be construed as the response from the bare device as a result of delamination between the film and the substrate. The frequency is slightly lower than the bare device (97.3 MHz), but this can be attributed to damping from mass loading associated with the film. After the soft bake, the second peak vanishes, the primary peak has shifted upward in frequency (a result of increasing the stiffness of the film) and the insertion loss has decreased to 25 dB, a result of lower attenuation due to lower viscosity.

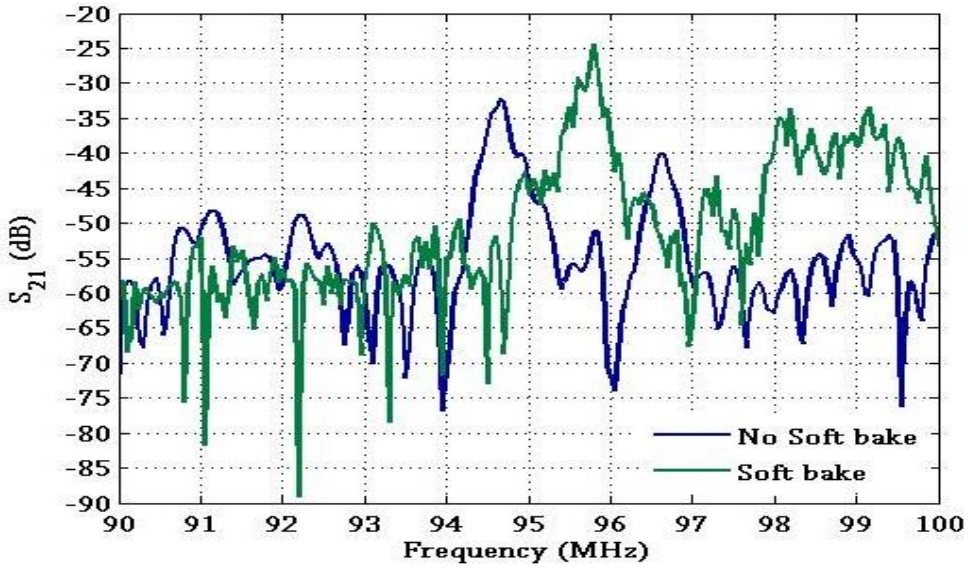

Figure 4.4 Transmission frequency response (S_{21}) from a Love Wave device consisting of a 1.4 μm PMMA film on a 90^0 rotated ST Quartz substrate both prior to and after soft bake at 180^0C for approximately 3 minutes.

Figure 4.4 illustrates the usefulness of analyzing both the centerline frequency of the S_{21} parameter but also the characteristic of the frequency response itself. As a film characterization tool, understanding the nature of the wave propagation phenomena gives significant information about the behavior and state of the film. These series of tests have shown the capability to characterize the curing properties of a polymer film as well as the potential for estimating the level of adhesion and progression of mechanical properties as the film goes through a curing process.

4.4 Glass Transition and Mechanical Changes in Polymer Films

4.4.1 Rayleigh Damping in Finite Elements for Modeling Glass Transition

Rayleigh damping is introduced in Finite Element simulations to represent complex elastic constants that arise due to the viscoelastic nature of a material. This helps in modeling the physical effects of internal attenuation. Rayleigh damping is defined by a linear combination of mass and stiffness matrices as [Kaltenbacher, 2004]:

$$[C] = \alpha[M] + \beta[K], \tag{4.1}$$

where [M] is the mass matrix and [K] the stiffness matrix as defined in Chapter 2. α and β are

damping parameters typically defined by the user in a finite element software. It is conceptually useful to express the damping parameters as fractions of a critical damping parameter for a particular mode. As long as damping is defined according to equation (4.1), it has been shown through orthogonal transformation that a critical damping relation can be expressed by [Chowdurry, 2003]:

$$2\xi\omega = \alpha + \beta\omega^2 , \tag{4.2}$$

where ξ is the critical damping ratio and ω is the angular frequency. Equation (4.2) can be rewritten as:

$$\xi = \frac{\alpha}{2\omega} + \frac{\beta\omega}{2} . \tag{4.3}$$

Equation (4.3) can be used to demonstrate a very important physical feature of Rayleigh damping. The α term is the mass proportional damping factor and is much more critical in structural vibration problems which are dominated by lower frequencies. Conversely, the stiffness proportional damping factor, β, is more crucial in wave propagation problems at higher frequencies. This phenomenon can easily be demonstrated graphically as in figure 4.5.

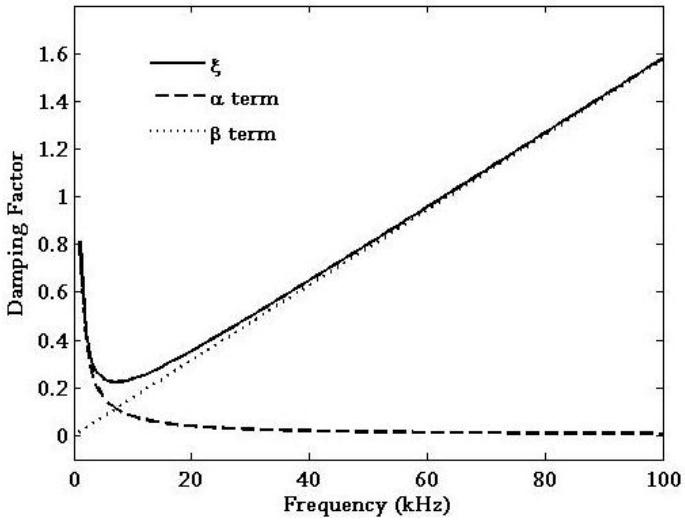

Figure 4.5. Plot of characteristic critical damping terms of Equation (4.3) as a function of frequency.

From figure 4.5, one can see that the alpha damping term dominates behavior at frequencies below 7-10 kHz. At frequencies above 20 kHz, the beta damping term dominates with a mixed alpha and beta behavior at frequencies between these values. Therefore, the following damping parameter assumption is valid for wave propagation problems above 20 to 40 kHz:

$$\xi \approx \frac{\beta\omega}{2}. \tag{4.3}$$

When dealing with polymer films, mechanical properties are often defined in the complex plane. Such is the case for the elastic modulus, E, which is typically defined by:

$$E = E' + iE'' \tag{4.4}$$

where E’ represents the storage modulus and E’’ represents the loss modulus associated with the viscoelastic nature of the polymer. Similar definitions exist for the Shear Modulus, μ, and the bulk modulus, G. In the glassy state, polymer chains typically have little mobility (i.e. higher values of E’ with respect to E’’). The rubbery state of a polymer represents a marked increase in chain mobility (i.e., lower values of E’ with respect to E’’). Toward this end, the definition of a loss tangent is useful in describing the glassy or rubbery nature of a polymer. This loss tangent, η, can be defined as [Sterling, 1992]:

$$\eta = \tan\delta = \frac{E''}{E'} \tag{4.5}$$

In this case, η can then be related to the critical damping ratio, ξ, through the following relation [Luo, 2005]:

$$\eta = 2\xi\,. \tag{4.6}$$

At this point, the effect of the loss tangent can be modeled via finite elements by adjusting the damping inputs as defined in equations (4.3), (4.5), and (4.6) such that:

$$\eta = \tan\delta = 2\xi = \beta\omega\,, \tag{4.7}$$

provided that experimental or theoretical values for the loss tangent can be determined.

As a case study, experimental data adapted from [Katime, 1994] for loss tangent as a function of temperature in isotactic PMMA was used to determine the effectiveness of the Rayleigh damping relations of the previous section along with the capability of a SAW device to monitor glass transition. Figure 4.6 shows β associated with the loss tangent taken from literature as a function of temperature. Note this does not represent the actual glass transition in the polymer film. Given the aforementioned T_g around 120^0C, a T_g measured at frequencies around 100 MHz is expected near 190^0C as a result of time-temperature superposition. The effects present here are more representative of a localized change in mechanical behavior. Notice three curves for different operating frequencies around the range of the modeled SAW device. Figure 4.7 shows the storage modulus adapted from the same report [Katime, 1994] as a function of temperature. The behavior of a Love Wave device based on these parameters was then modeled.

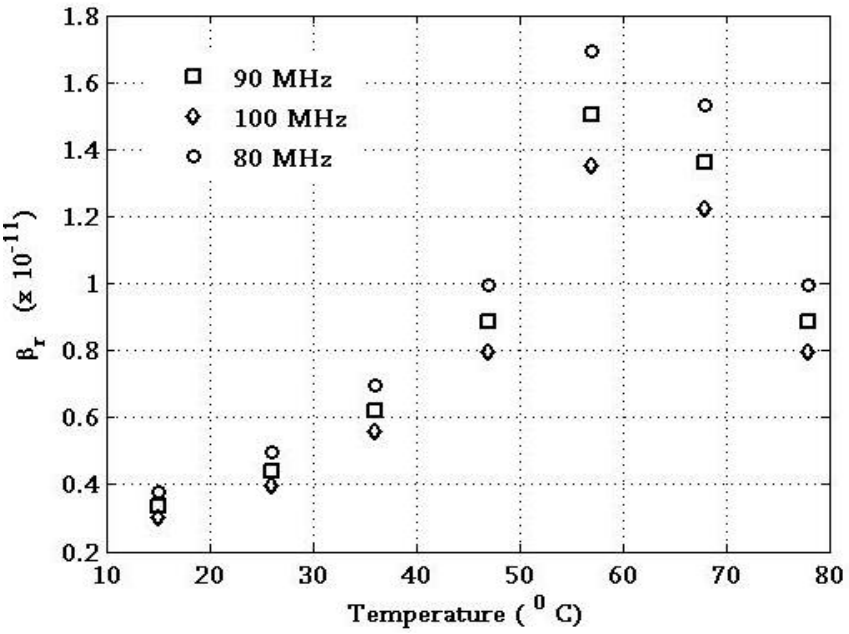

Figure 4.6. Values for the damping parameter, β, as a function of temperature for several different frequencies in the range of the modeled SAW device.

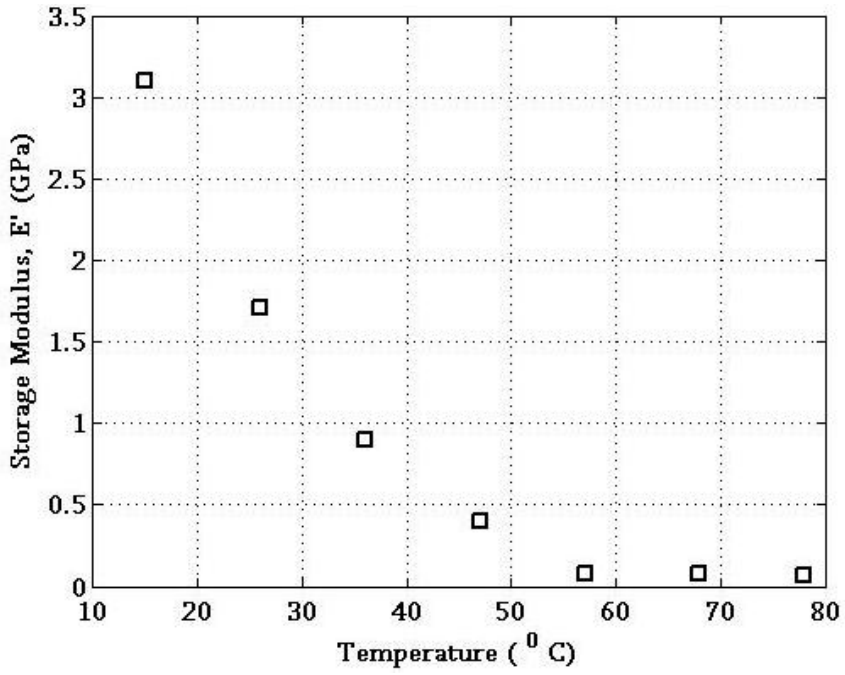

Figure 4.7. Values for the Storage Modulus, E', used for the simulation of Love Wave device behavior as a function of temperature adapted from Katime [Katime, 1994].

One must also consider film swelling. Studies have shown that PMMA films in the thickness range of 100 nm to 10 μm have a coefficient of thermal expansion of approximately 7 +/- 2 x 10^{-4} K^{-1} which reduces to about 2 x 10^{-4} K^{-1} at the glass transition temperature. Also Poisson's ratio goes from 0.35 to .48 at the glass transition temperature [Kahle, 1998]. These factors were taken into account in the iterations of the model as a function of temperature. The results of normalized frequency change as a function of temperature are shown in figure 4.8.

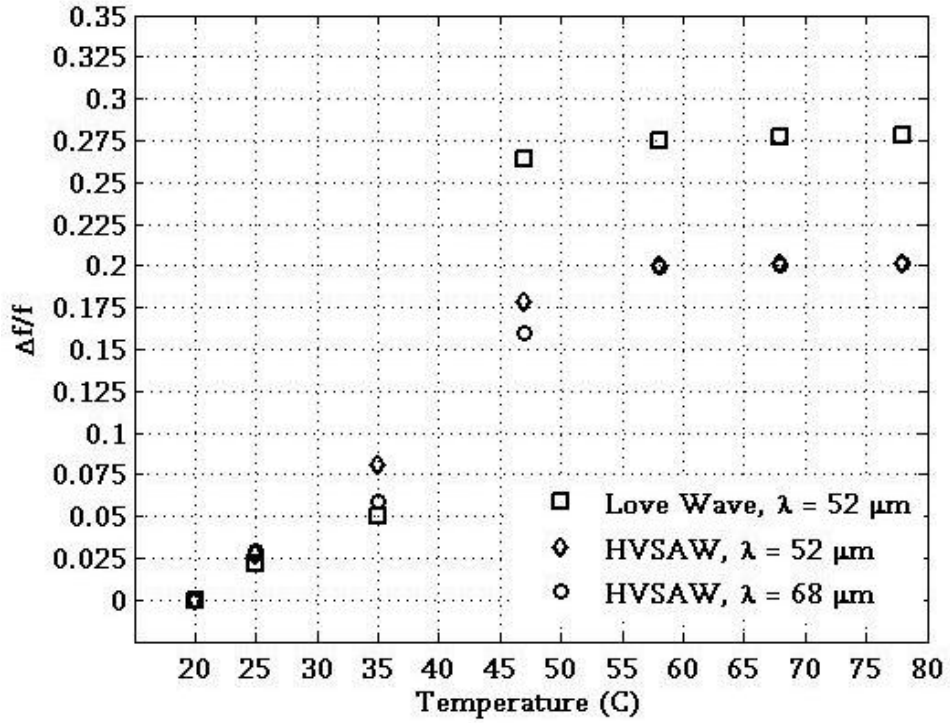

Figure 4.8. FEM results for Normalized frequency change as a function of temperature for Love Wave device (squares) on 90^0 rotated ST Quartz, HVSAW device (diamond) on ST Quartz, and HVSAW device (circles) on 77^0 Y rotated $LiTaO_3$.

One question from the data shown in figures 4.7 and 4.8 was how those two would affect the frequency of a potential Layered SAW device. Based on figure 4.7, one would expect to see a distinct change in the curve at 58^0C. On the other hand, figure 4.8 suggests a significant change around 50^0C. From the FEM results, it is plane to see that the change in Storage Modulus, E', has more of an effect on the wave propagation than the loss factor, tan δ. This is consistent with wave propagation as the characteristic of the wave behavior has a strict mathematical dependence on the Elastic modulus and is simply modified by the loss factor. Again, this temperature range is too low to be considered a glass transition but more likely represents localized changes in mechanical behavior due to the temperature variance.

4.4.2 Experimentatal Setup

The experimental setup is shown in figure 4.9a. The device was placed in thermocouple-controlled oven which has been modified with an access port for electrical connections. This port was also used to introduce a second thermocouple in order to increase the temperature measuring capability of the system. Figure 4.9b shows a close-up of the device under test. Signals were monitored with a Hewlett Packard Network Analyzer set with markers to track the minimum insertion loss and centerline frequency during the test.

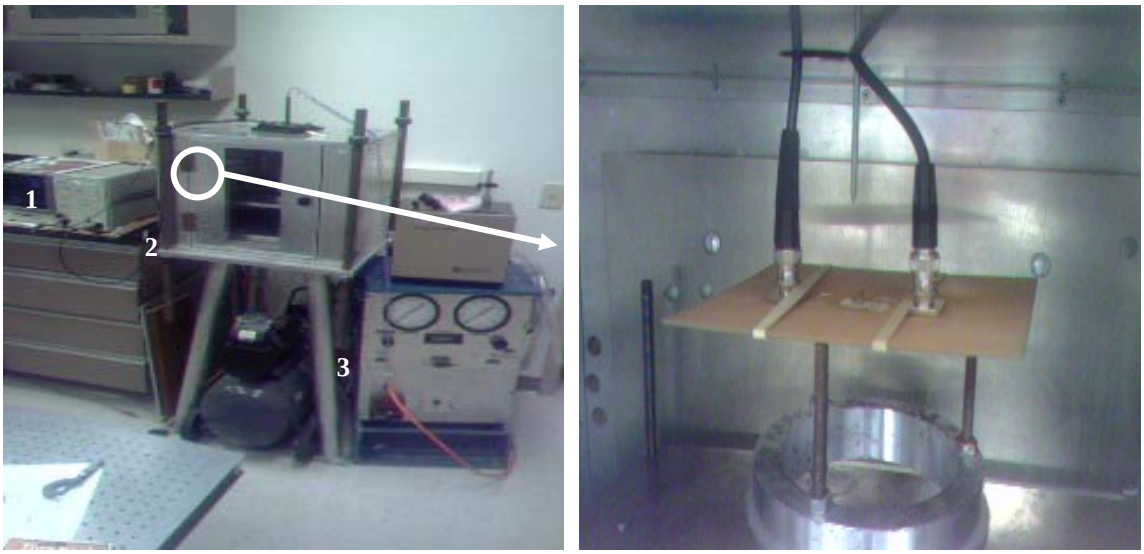

Figure 4.9. (a) Experimental setup for monitoring the localized changes in mechanical behavior of a polymer film including 1. Network Analyzer, 2. Oven, and 3. Thermocouple controller along with (b) a close up image of the device under test showing the BNC connections and the thermocouple used for temperature monitoring.

One concern was the effect of thermal hysterisis and thermal gradients on the accuracy of the data obtained. If the oven is heated to quickly, the device is not under equilibrium conditions

and the temperature is most likely not uniform throughout the film. Also, the temperature read by the thermocouple would not necessarily indicate the temperature of the device under test. To overcome this, two techniques were considered. The first was to set the oven at the maximum test temperature and then allow it to slowly cool taking data as it cooled past the appropriate temperatures. The other method was to set the oven at a particular temperature allowing it to stabilize for several minutes before taking each data point.

It was believed that the equilibrium method of setting the temperature at each point would yield the best results. In fact, this technique resulted in large temperature fluxuations due to the nature of the oven. The heating element is cycled on and off through a solid state relay when the thermocouple controller indicates that the temperature has decreased a certain value below the set temperature. This causes the oven to constantly cycle through temperatures between $+5\ ^{0}C$ and $-1\ ^{0}C$ around the set value. As a result, the cooling method was deemed the most appropriate. The repeatability of results was verified by comparing multiple runs and the results are shown below.

4.4.3 Results and Discussion

Several sets of data were taken for each of the Love Wave and SV-SAW Wave devices. Data was taken using Love Wave, Generalized SV-SAW Wave (GSAW), and High Velocity SV-SAW Wave (HVSAW) devices. The results for normalized change in frequency as a function of temperature are shown in figure 4.11. Figure 4.12 shows the associated results of insertion loss as a function of temperature.

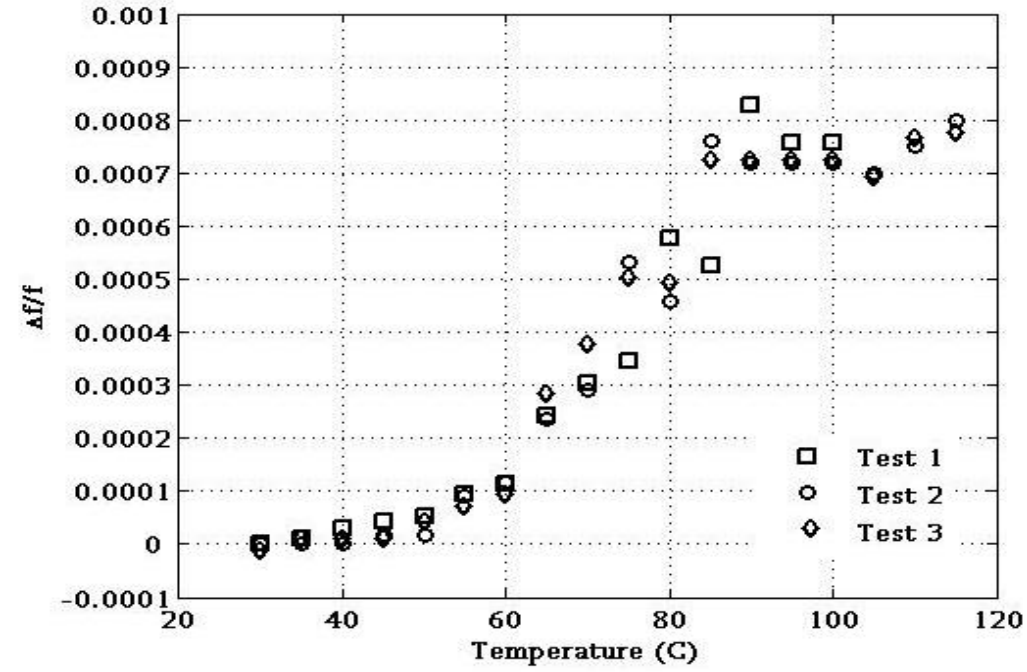
0.001
0.0009
0.0008
0.0007
0.0006
0.0005
0.0004
0.0003
0.0002
0.0001
0
-0.0001
Δf/f
20
40
60
80
100
120
Temperature (C)
Test 1
Test 2
Test 3

(a)

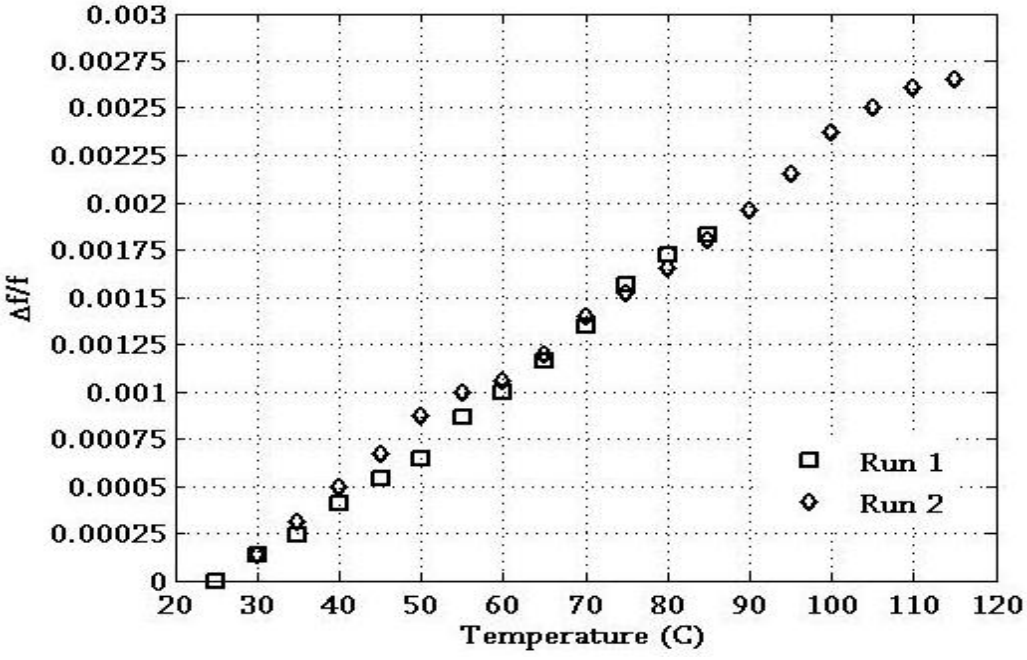
0.003
0.00275
0.0025
0.00225
0.002
0.00175
0.0015
0.00125
0.001
0.00075
0.0005
0.00025
0
Δf/f
20
30
40
50
60
70
80
90
100
110
120
Temperature (C)
Run 1
Run 2

(b)

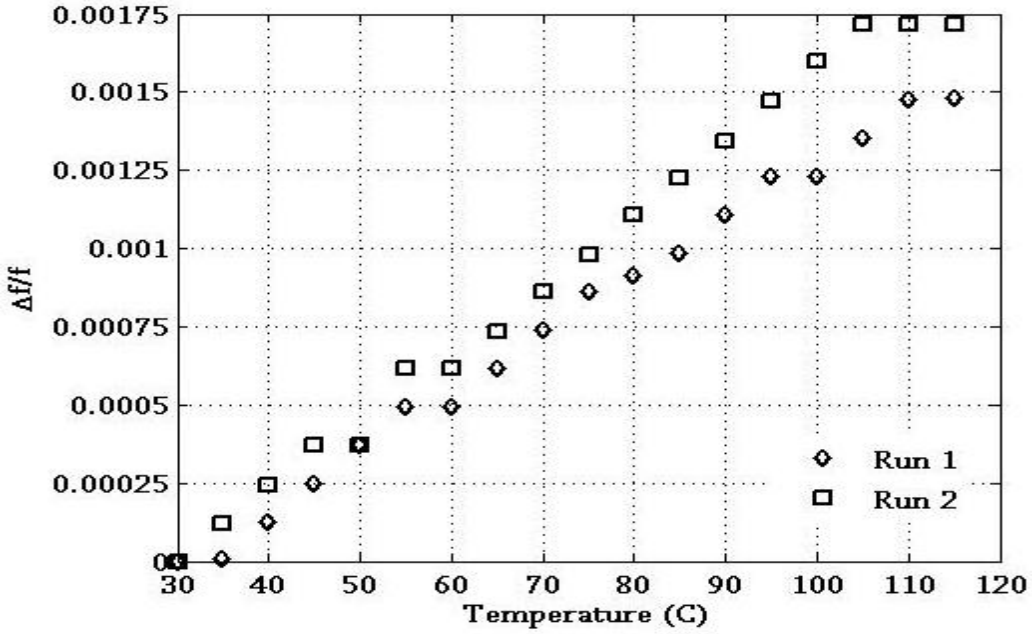

(c)

Figure 4.11. Normalized change in frequency as a function of temperature for (a) Love Wave (b) HVSAW and (c) GSAW devices.

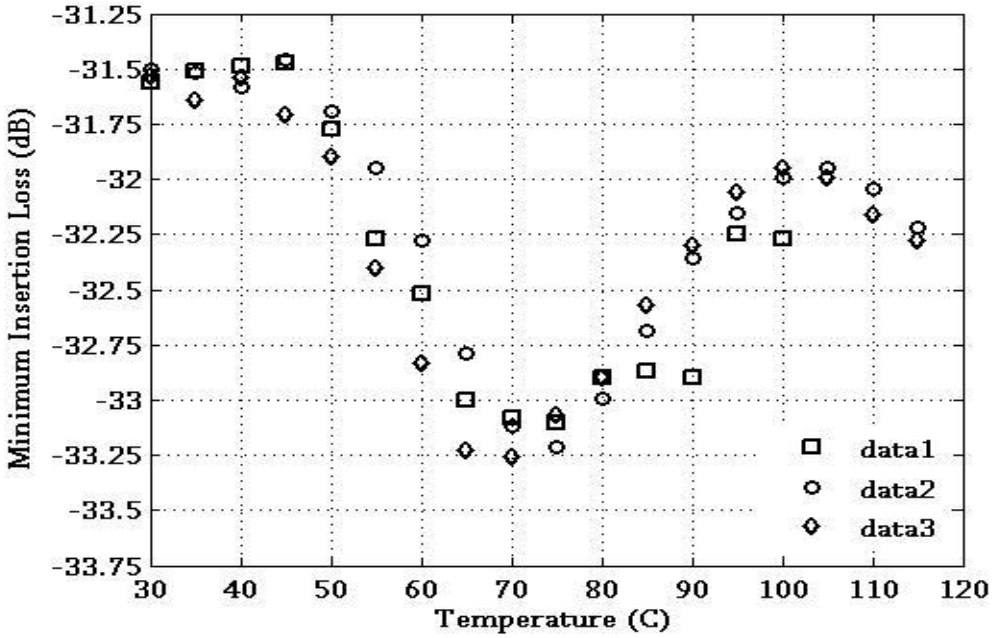

(a)

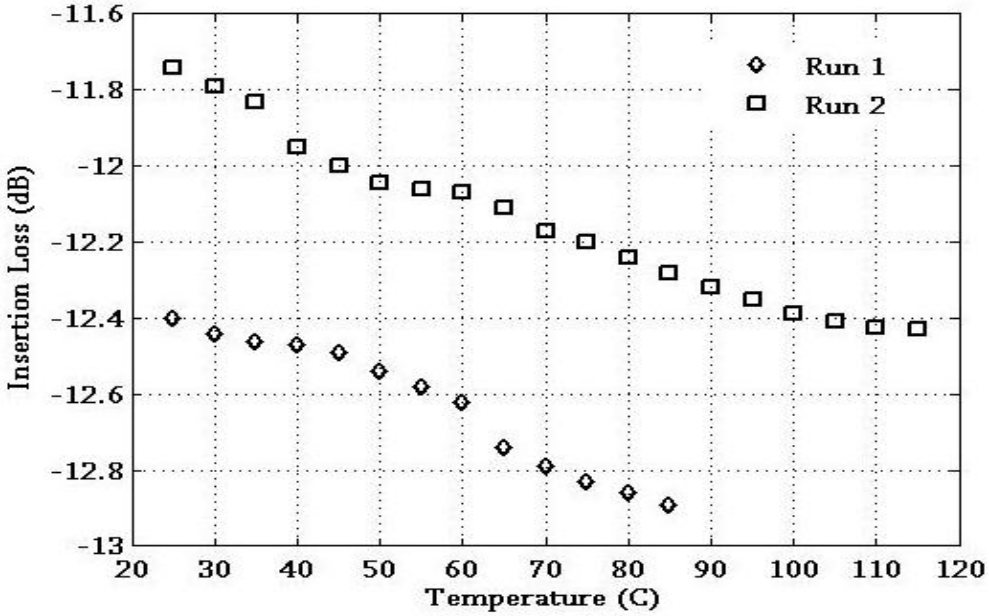

(b)

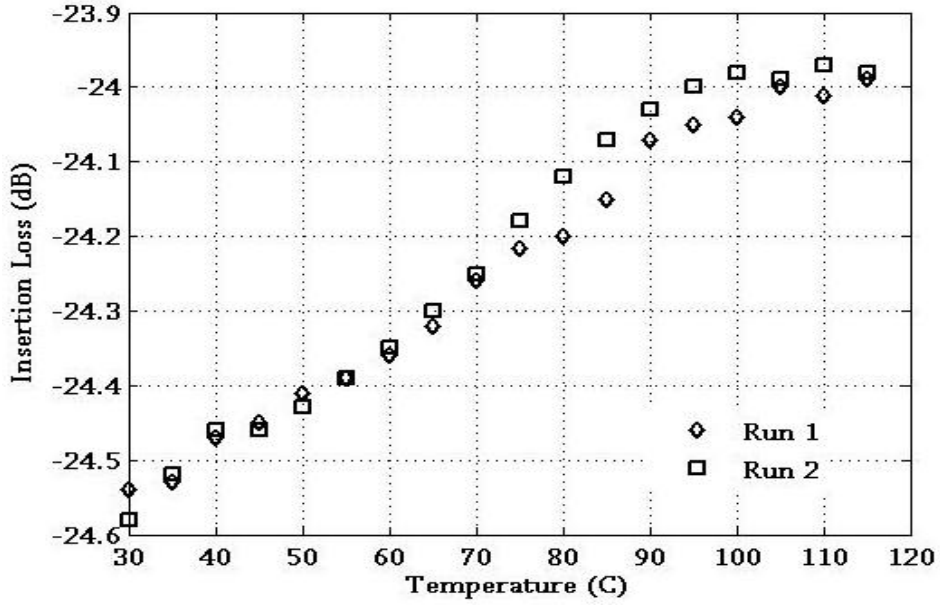

(c)

Figure 4.12. Insertion loss as a function of temperature for (a) Love Wave, (b) HVSAW, and (c) GSAW devices.

Note the somewhat clear transition in frequency for the Love Wave device compared to the SV-SAW wave counterparts. This is attributed to the Love Wave propagating most of its energy through the film compared to the SV-SAW Wave have a majority of its energy confined to the interface. The Love Wave device shows a clear minima at 70 ^{0}C providing another strong

indicator of a localized change in mechanical behavior. This behavior is much less distinguishable in the GSAW and HVSAW. The difference in initial values for the HVSAW is likely due to a change in the electrical connection and less likely due to the lack of repeatability in the measurement.

The GSAW show a slightly better indication of the film's localized mechanical change compared to the HVSAW. This is due to the GSAW confining its energy at the interface whereas, the HVSAW is a leaky wave and so energy is dissipating away from the surface. It is somewhat unclear why the insertion loss decreases as a function of temperature for the GSAW but increases for the HVSAW. The decrease in the GSAW insertion loss could be a result of the boundary becoming more like a free surface as the elastic modulus decreases. It is also unclear why there is such a marked decrease in insertion loss for the Love Wave device as the temperature increases past the point of the localized change.

Although some questions remain unanswered, this works demonstrates the capability of a Love Wave device to monitor localized changes and quite possibly glass transition in a polymer film. High temperature electronics were not designed in this work so the temperature was kept well below what would be expected for a glass transition. A distinct advantage in sensitivity is demonstrated for the Love Wave device over the SV-SAW wave counterparts with respect to both frequency and insertion loss change. Given the relationship between wavelength and film thickness, an appropriate frequency can be chosen to investigate a broad range of film thicknesses while maintaining a certain degree of sensitivity. The potential for investigating smaller films (<800 nm) is discussed in Chapter 7 under future work.

Chapter 5 Sensor Applications

5.1 Introduction

Love and SV-SAW Wave sensors are a specialized version under the broad category of Layered SAW sensors. The enhanced sensitivity over traditional SAW devices [Zimmermann, 2002; Strashilov, 2005] along with the lack of coupling to fluid loading [Petrillo, 1996; Josse, 1988; Josse, 1989; Caliendo, 1990; Hermann, 1999; Jakoby, 1997; McHale, 2001; Pan, 2001] has made Love Wave devices very attractive for practical applications. The mass loading sensitivity and large dependence on the physical and chemical state of the overlayer lends the Love and SV-SAW Wave devices to a broad range of sensing applications. The benefits of Love Wave devices over SV-SAW wave counterparts are demonstrated.

The goal of this chapter is to explore two applications for both SV-SAW and Love Wave devices: ice detection and radiation sensing. Although not a new application, the benefits of Layered SAW sensors for ice detection over more traditional techniques are discussed. Comparisons are made between sensors to further demonstrate the enhanced sensitivity of Love Wave devices. The insights gained pertaining to wave propagation earlier are explored to further enhance the sensitivity of a Love Wave device by selecting appropriate film thicknesses. Conceptual plans for wireless implementation are also explored.

The concepts of ion modification of polymer films are introduced. A model is introduced based on published data demonstrating the feasibility of Layered SAW devices for radiation

detection. Data from an accelerated modification study further demonstrate the capabilities of this technique. Sensitivity enhancement and potential applications are reviewed.

5.2 Ice Detection

Given the numerous aerospace applications for ice detection systems, a light-weight, low profile system such as those based on SAW technology could prove beneficial. The concept of Ultrasonic ice detection based on Guided wave principles has been demonstrated [Hongerholt, 2002; Rose, 1999] including a US patent for a contaminant detection system [Rose, 1999]. The concept has also been demonstrated with Love Wave devices [Vellekop, 1999]. The goal of this work is to demonstrate the capability of Love Wave devices with polymer overlayers to distinguish between air, water, and ice loading. Several SV-SAW type and Love type Layered SAW devices were investigated, particularly their frequency response to air, water, and ice loading. The capability for wireless interrogation may also prove beneficial particularly for applications were ice sensors may be implemented in a distributed network. Applications for this may include aircraft or spacecraft wings or exteriors.

Conceptually, the Love Wave device would seem far superior to the SV-SAW wave counterpart as a result of the shear horizontal displacements present in the Love Wave structure. The significant shear vertical component of the SV-SAW wave would likely cause severe attenuation under water loading and ice loading making it difficult to resolve the two. From this standpoint, the work presented here seems trivial. However, recall that waves generated in typical SAW configurations are not pure ones. The FEM studies of wave structure have shown

that non-negligible shear vertical and longitudinal wave components exist in Love Waves generated with 90^0 rotated ST Quartz. Also, the propagation path of typical delay lines is fairly small (1-10 mm). At such a small path, SV-SAW waves although attenuated may propagate from transmit to receive IDTs. The purpose of this investigation is to confirm that water and ice loading can indeed be resolved with Love Wave propagation whereas SV-SAW waves are unable to distinguish between the two loading conditions.

For this test, approximately 0.5 mL of water was applied between the transmitting and receiving IDTs on each device. Care was taken not to water load both electrode connector pads to avoid confusion from electrical shorting. In application, an insulating layer over the electrical contact pads could alleviate this concern. The frequency response (S_{21} parameter) was captured initially with no water loading, with water loading, and after the device had been in a freezer for several minutes.

Initially, ice loading was tested by placing the Layered SAW device in the freezer until the water was frozen then removing the device, connecting the electronics and testing the setup. This setup caused spurious results since the small quantity of ice would begin to melt in the time it took to establish the electrical connections. The configuration of figure 5.1 proved more effective and also more closely represents a practical situation where the electronics at the device surface will also be exposed to the extreme temperatures which are causing the ice to form.

Figure 5.1 shows the results for the three loading conditions of air, water, and ice for a SV-SAW wave device consisting of a 1.6 μm PMMA film on 36^0 Y-Rotated LiTaO3. As

expected, the water loading completely damps the SV-SAW wave response and no distinction can be made between water and ice loading. Figure 5.2 shows the same loading conditions for a Love Wave device consisting of a 1.6 μm PMMA film on 90^0 rotated ST Quartz. The water loading causes an increase in insertion loss of 11 dB from 33 to 44 dB. A frequency shift of 30 kHz from 95.3 to 95.27 kHz is also present. The decrease in frequency is attributed to the mass loading introduced by the water layer. As the water undergoes a phase change to ice, the shear horizontal displacement now leaks into the ice and is completely attenuated due to the rounded geometry of the water droplet and the internal structure of the ice.

The results of this test show that ice detection systems based on Love Wave propagation are extremely effective due to the nature of the wave structure compared to SV-SAW wave devices which are unable to distinguish between ice and water loading. Ice detection systems based on Love Wave devices have the added benefits of being light-weight, relatively low cost, low-profile, and wireless capable. These aspects make this technology ideal for aerospace applications where ice detection is vital for prevention of catastrophic failure.

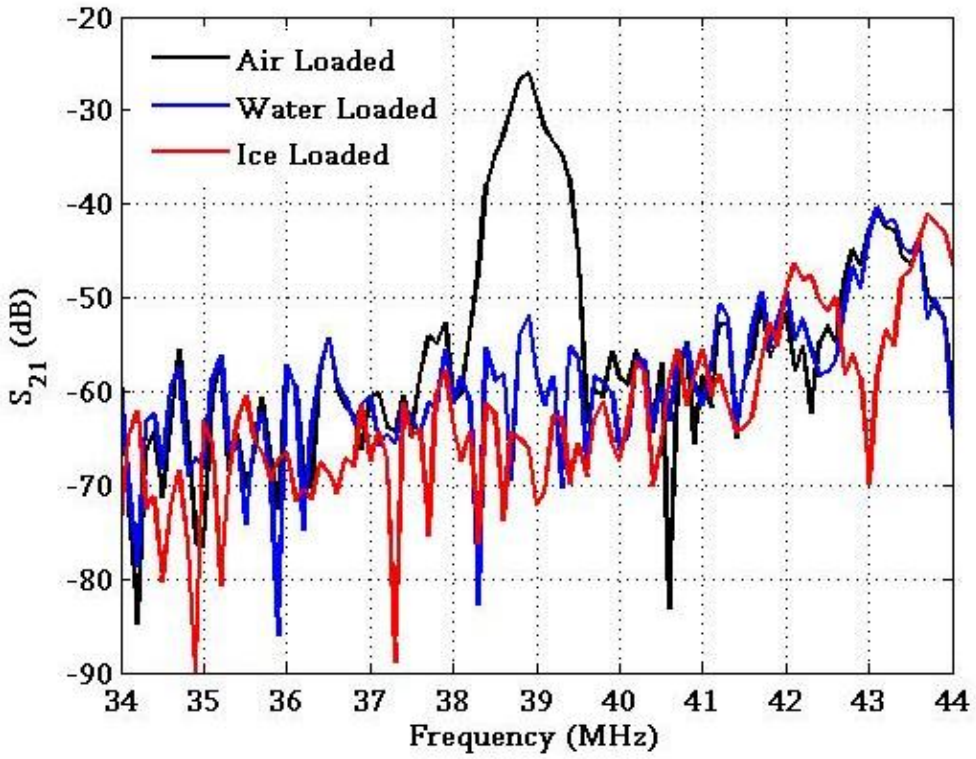

Figure 5.1. Experimental Results for S_{21} parameter of a SV-SAW wave device under air, water and ice loading conditions.

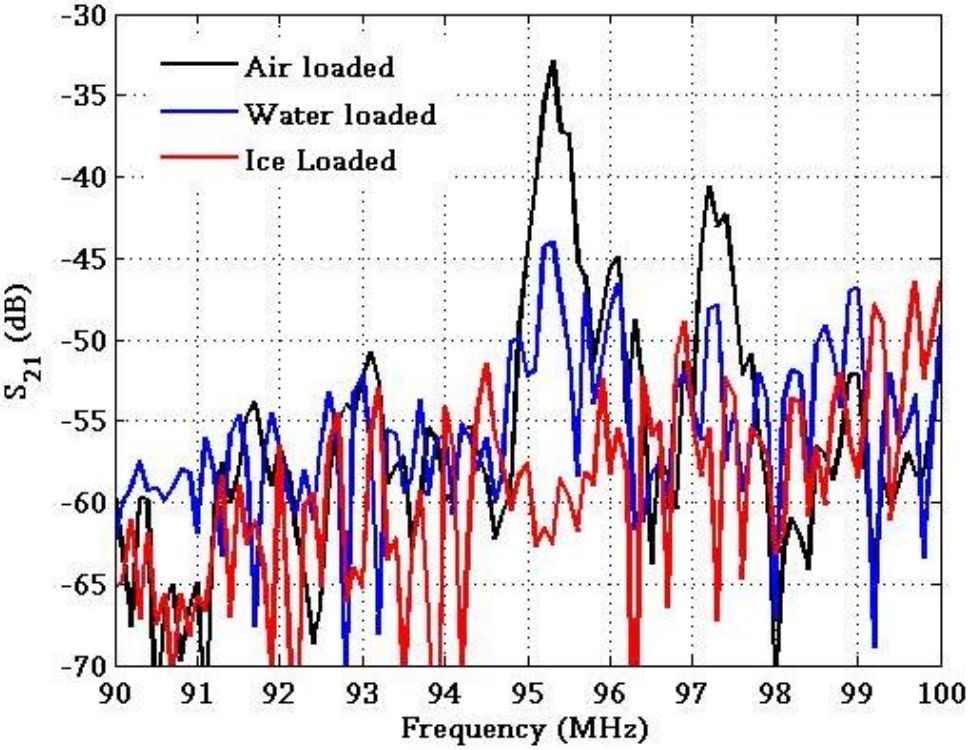

Figure 5.2. Experimental Results for S_{21} parameter of a SV-SAW wave device under air, water and ice loading conditions.

5.3 Radiation Sensing

The goal of this work was to determine feasibility and "proof-of-concept" for Ultrasonic-based neutron detectors. There could be a distinct advantage of Ultrasonic-based detectors over more standard semiconductor counterparts in that the piezoelectric effect is believed to be more impervious to radiation damage compared to semiconductors. The challenge of this work lies in determining applicable Ultrasonic sensing mechanisms for the detection of neutrons as standard Ultrasonic-based techniques are used to monitor more bulk effects.

In solid state detectors, neutrons are rarely detected directly. Often, a coincidence detection of alpha particles from converter layers is used relying on one of the following reactions:

$$
\begin{aligned}
{}^{6}_{3}Li + {}^{1}_{0}n &\rightarrow {}^{3}_{1}H + {}^{4}_{2}\alpha \\
{}^{10}_{5}B + {}^{1}_{0}n &\rightarrow \begin{cases} {}^{7}_{3}Li + {}^{4}_{2}\alpha \\ {}^{7}_{3}Li^{*} + {}^{4}_{2}\alpha \end{cases}
\end{aligned}
\tag{5.1}
$$

where the alpha energies are 2.05 and 1.47 MeV, respectively [Knoll,1989]. For the scope of this work, the actual conversion mechanism was ignored as it is a well established phenomenon. The emphasis was then put on the detection of energetic ions. The main concentration was put on the detection of alpha particles (Helium ions) but, given the right hand side of equation 5.1, consideration was also given to the detection of Hydrogen or Lithium ions.

5.3.1 Ion Modification of Polymers

The study of ion irradiation effects in materials spawned in the mid 1940's [Wigner, 1946]. The prime concern was the effect of energetic ions on mechanical behavior of metals and alloys. The generation of lattice vacancies, interstitially displaced atoms, and the diffusion/transmutation of such atoms was the source of mechanical changes [Caskery, 1987]. The obvious motivation behind these studies was the need for materials that were considerably impervious to degradation in nuclear reactor applications. The 1950's and 1960's saw a huge growth in industrial development of synthetic polymers [Sterling, 1992]. Not long after, scientists realized that radiation degradation in polymers was much more prevalent than metal counterparts. The early concern was from the standpoint of processing and sustainability of polymers in everyday applications, particularly from an environmental perspective [Shalaby, 1979].

In order to understand the overall effects of polymer modification via energetic ions, some basic concepts of radiochemistry must be highlighted. The interaction of light ions with matter occurs typically in the electronic regime [Robertson, 2002]. Although elastic collisions with nuclei are also present, the dominant effect is the Coulomb interaction between the ion and the electrons in the material lattice [Robertson, 2002; Fink, 2004]. The radiochemistry associated with these interactions is the driving force for polymer modification and will be the topic of the remainder of this section.

There are several important phenomena that relate back to the macroscale properties of an irradiated polymer. The first to be considered here is chain scissioning (CS). Chain scission is the breakage of bonds that link the polymer together. The most common implication of CS is a reduction in molecular weight, a result of the diffusion of volatiles and ultimate degassing away from the irradiated zones [Rouif, 2005]. Other scissioned units of either the side or main chain form free radicals which can be highly reactive. The reactivity of these radicals often leads to interaction with other portions of the polymer unit. This can leads cross-linking (CL) in the polymer. CL is process whereby a free end of a linear polymer chain bond to other free ends forming a polymer network and often leading to a higher molecular weight [Rouif, 2005].

Although CL can eventually take place as a result of CS, polymers are typically characterized by their preference to one over the other. It is not quite clear why certain polymers experience chain scission and others cross-link [Fink, 2004]. Polymers with linear backbones are typically candidates for CS [Rouif, 2005]. Some of these are PET, PTFE, and PI [Fink, 2004; Clegg, 1991]. Cross-linking polymers include PDMS, PE, and PS[3] [Clegg, 1991]. PMMA is interesting in that it experiences CS at low ion energy doses and transitions to CL at higher doses [Fink, 2004]. These few concepts are at the root of changes in the mechanical behavior of polymers in response to ion irradiation. An extensive investigation into the chemical modification of several polymers can be found in [Shalaby, 1979].

A major motivation for studying the irradiation of polymers is to enhance their functionality for a given application. The previous section discussed briefly the concepts of

[3] Polymer Names: PET-Poly(Ethylene Terephthalate), PTFE-Polytetrafluoroethylene, PI-Polyimide, PDMS-Poly(dimethylsiloxane), PE-Polyethylene, PS-Polystyrene.

chain scissioning and cross-linking. These processes have major implications in the macroscopic properties of the polymer. Chain scissioning is generally referred to as a process which degrades the polymer. It has been reported that chain scissioning leads to a decrease in the hardness and Young's Modulus of the polymer whereas the inverse is found in cross-linked polymers [Fink, 2004; Clegg, 1991; Kudoh, 1997; Foerster, 2004]. A similar relationship applies to the overall density of a polymer as a result of CL and CS. Chain scissioned polymers tend to show a decreased density as a result of changes in free volume due to the separation of chains [Foerster, 2004]. Cross-linked polymers tend to show an increase in density as a result of degassing and the formation of tighter chain networks [Guenther, 2004].

Some of the results of previous studies are shown here as they pertain to the propagation of a Love Wave in such a polymer. Changes in the Elastic Modulus from 1.9 GPa to 26.7 GPa of Polypropylene have been observed for helium ion fluences up to 10^{16} ions/cm^2 [Brun, 2003]. Similar studies on Polycarbonate show changes in the Elastic Modulus from 5 to 15 GPa for 160 keV Nitrogen ions for fluences upwards of $4(10)^{19}$ ions/cm^2 [Chien, 2000]. Smaller effects have been observed in Silica reinforced silicone composites exposed to Helium ion doses up to $2(10)^{12}$ ions/cm^2 [Guzman, 1998]. The modification of Elastic modulus for this dose was on the order of 200%. Boron irradiation of Polyimide at fluences of 10^{16} ions/cm^2 has yielded Elastic modifications from 5-40 GPa [Guenther, 2004]. These are examples of polymers which cross-link as a result of ion irradiation. The modification of the elastic modulus varies as a result of several factors. These include the chemical structure of the polymer, the Linear Energy Transfer (LET) of the ion irradiation, the energy and weight of the ions, and the fluence or deposited energy into the polymer. Although the specific results of modulus modification vary according

to these parameters, the general trends and mechanisms remain extremely constant.

Changes in the overall density of an irradiated polymer have been discussed conceptually as it relates to the molecular weight and free volume [Fink, 2004; Clegg, 1991]. Although a known phenomena, quantitative data in the literature is somewhat limited. Often, researchers associate the density increase due to cross-linking as an enhancement in overall stability of the polymer [Garcia, 1999; Sias, 1998]. In general, high dose irradiation of heavy ions causes an increase in polymer density [Calcagno, 1986]. This refers back to most polymers having propensity to cross-link at high irradiation doses. Results on polyimides have shown increases from 1.45 g/cm^3 to 1.85 g/cm^3 for boron fluences of 10^{16} ion/cm^2 [Guenther, 2004]. These results coincide with other reports of high ion fluences introducing density increases on the order of tens of percent [Nishimiya, 1991; Davenas, 1993]. Results of several tests in PMMA after high fluence irradiation with heavy and light ions showed density increases on the order of 20% [Fink, 2004].

5.3.2 FEM Study of Layered SAW Radiation Sensors

The feasibility of a Layered SAW Radiation sensor based on the ion modification of a polymer film is most easily explored with the FEM models discussed previously. Using data for the change in elastic modulus and density of a polyimide as a result of Boron irradiation [Guenther, 2004], the effectiveness of a SAW device in terms of frequency and insertion loss change was explored. The effect of film shrinking/swelling was ignored to simplify the

iterations of the initial model. Two models were tested representing ST cut and ST cut-90^0 rotated Quartz with PMMA overlayers of 1.2 μm thickness. This allowed for the comparison of SV-SAW and Love Wave devices.

Figure 5.3 shows the FEM results for HVSAW waves on both Quartz and $LiTaO_3$ covered with a 1.6 μm polyimide film as a result of Boron ion exposure. This data represents a change of elastic modulus from approximately 4 GPa to approximately 50 GPa. The associated density increase is approximately 20 % from 1.4 to 1.68 g/cm^3. The different values for λ are shown in the figure legend. These values were chosen for comparison reasons. The experimental Love Wave device tested has a wavelength of 52 μm and the SV-SAW wave device on Lithium Tantalate has a wavelength of 68 μm. This allowed for the comparison of Love Wave vs. SV-SAW Wave devices on Quartz along with the comparison with experimental results given the samples available for test.

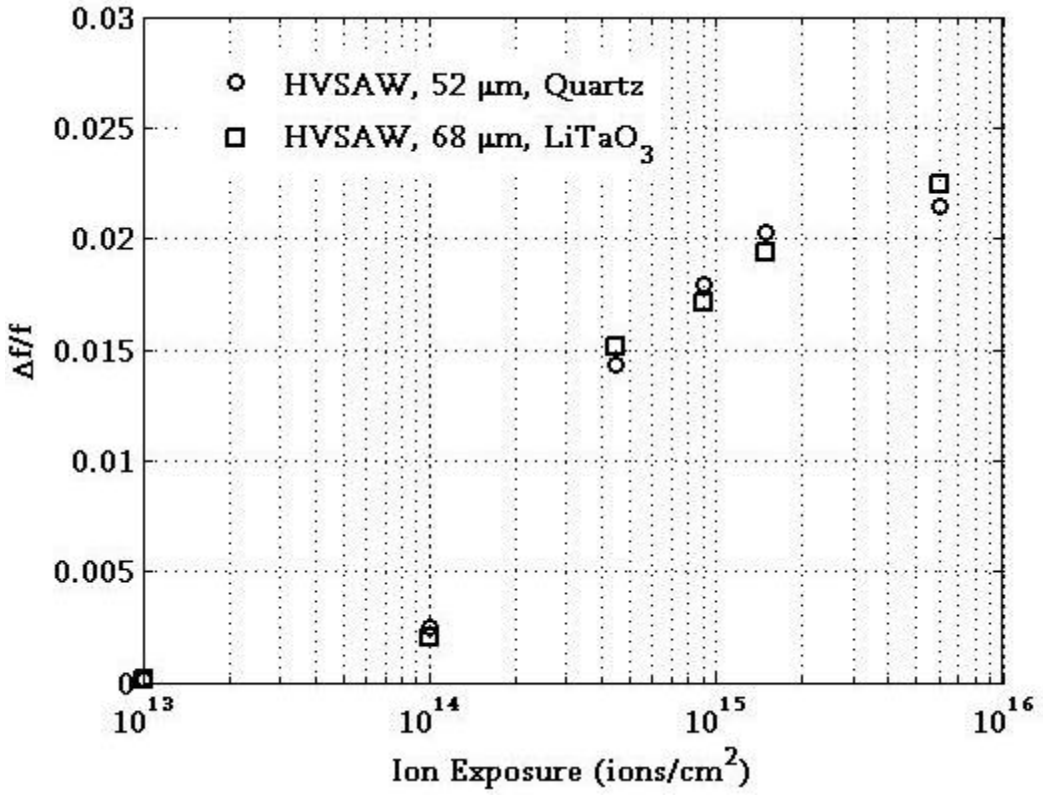

Figure 5.3. FEM Results for normalized frequency shift versus ion exposure for HVSAW devices on Quartz (circles) and Lithium Tantalate (squares) based on experimental data for Elastic modulus and density of a Polyimide film [Geunther, 2004].

The results of figure 5.3 show that a HVSAW sensor could provide a fair level of sensitivity if used as a Radiation sensor. The model predicts frequency changes of approximately 2.25% for these devices. Interesting to note is the little sensitivity difference seen between the two devices. One might expect a slightly higher sensitivity from the Quartz device compare to the Lithium Tantalate device as a result of the smaller wavelength. However, the HVSAW velocity of Lithium Tantalate (4112 m/s) is slightly higher than that of Quartz (3948 m/s) [Kalantar-Zadeh, 2003].

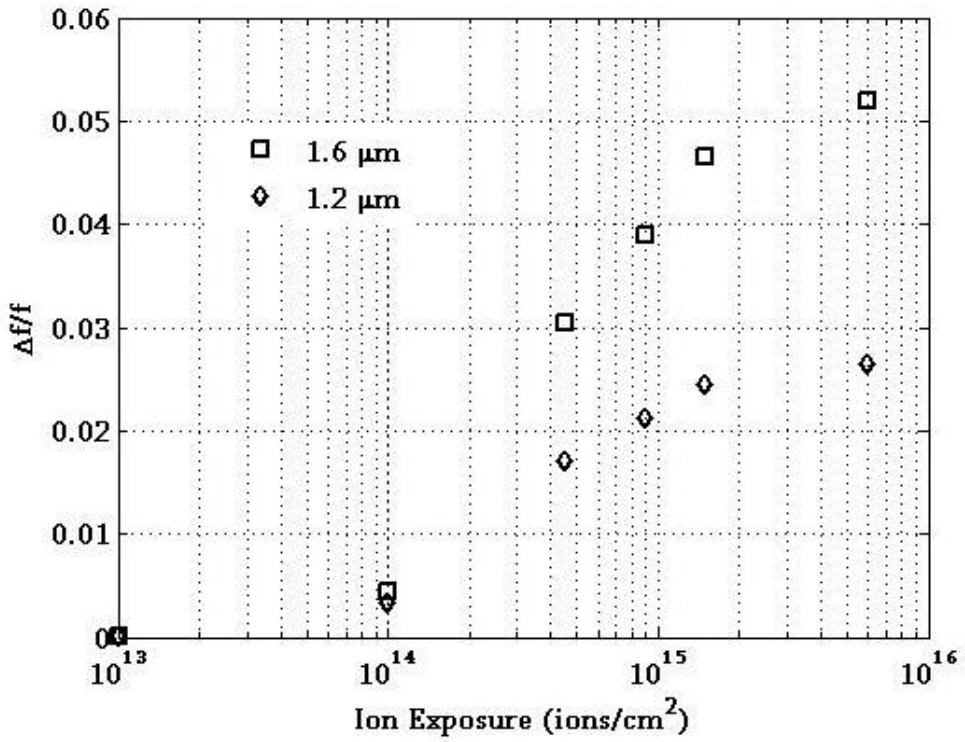

Figure 5.4. FEM Results for normalized frequency shift versus ion exposure for Love Wave devices on Quartz based on experimental data for Elastic modulus and density of a Polyimide film [Guenther, 2004]. Film thicknesses of 1.6 μm (squares) and 1.2 μm (diamonds) were simulated.

Figure 5.4 shows similar results for a Love Wave device on 90^0 rotated ST Quartz with Polyimide layers of two different thicknesses. The purpose is to show the importance of selecting appropriate film thicknesses with respect to the acoustic wavelength given the dispersive nature of Love Waves. The FEM analysis on sensitivity in chapter 3 showed the importance of exciting modes in the portion of the dispersion curve where the wave modes are somewhat dispersive. From the FEM analysis one learns that a 1.6 μm film results in a propagating frequency of 92.5 MHz. This represents an fd product of 0.148 MHz*mm. Conversely, a 1.2 μm film results in a propagating frequency of 94.5 MHz representing an fd product of 0.113 MHz*mm. Comparing the inspection points of figure 3.14 with the resulting sensitivity to radiation shown in figure 5.4, one sees the value of interrogating a dispersive

region of the Dispersion curve.

For comparison, FEM results for the Love Wave device are plotted along with the HVSAW device on $LiTaO_3$ in figure 5.5. These devices were chosen to compare sensitivities with experimental results. The Love Wave device shows a higher sensitivity compared to the HVSAW device by a factor of two. The ability to enhance the sensitivity of the Love Wave device by choosing the appropriate thickness makes it more desirable than the HVSAW counterpart.

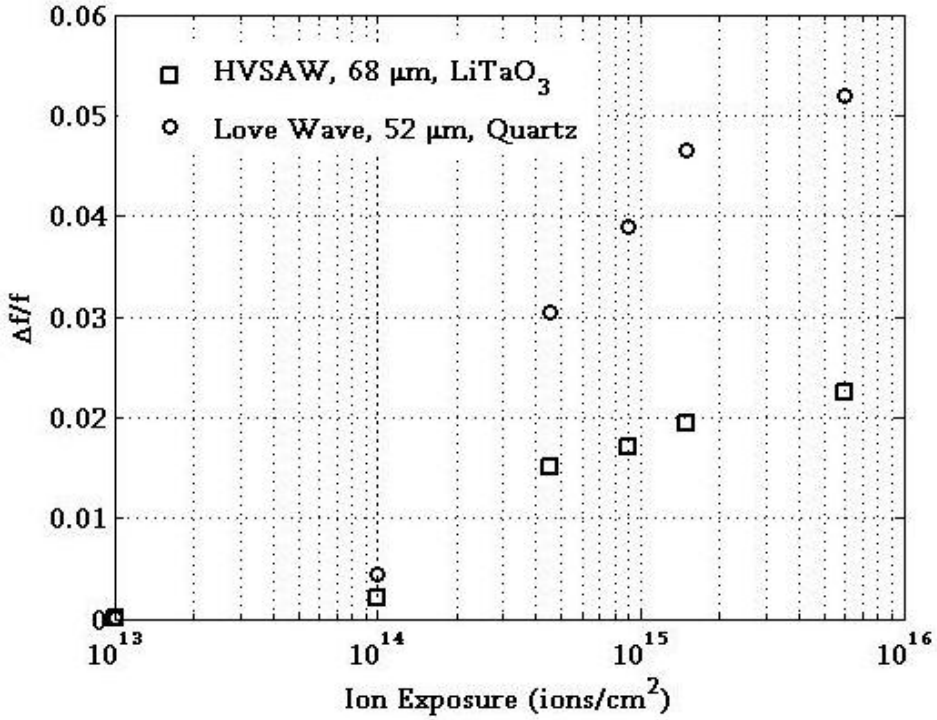

Figure 5.5. FEM Results for normalized frequency shift versus ion exposure for Love Wave devices on Quartz based on experimental data for Elastic modulus and density of a Polyimide film [Guenther, 2004]. Film thicknesses of 1.6 μm (squares) and 1.2 μm (diamonds) were simulated.

5.3.3 Experimental Verification of Layered SAW Radiation Sensing

Due to the complexities of working with a radioactive source, an alternative proof-of-concept was developed using SU-8 films. SU-8 is a cross-linking epoxy often used in microlithography as a photoresist material. Cross-linking in SU-8 is induced by exposure to Ultraviolet light. Initial tests were conducted to verify the change in mechanical properties associated with UV cross-linking. Figure 5.6 shows a photograph of several 3" diameter Silicon wafers. SU-8 films were spin-coated onto these substrates at a thickness of approximately 2 μm. Using a Karl Suss MA6 Ultraviolet exposure tool, several samples were exposed to about ten seconds of UV radiation. The elastic modulus of those films along with ones which were not exposed was tested using a Hysitron Nanoindentation system. The result of the nanoindentation test on the unexposed film is shown in figure 5.7 while figure 5.8 shows the nanoindentation curve for the exposed film.

Figure 5.6. Photograph of the 3" diameter silicon wafers coated with SU-8 films for the Nanoindentation tests comparing exposed and unexposed films.

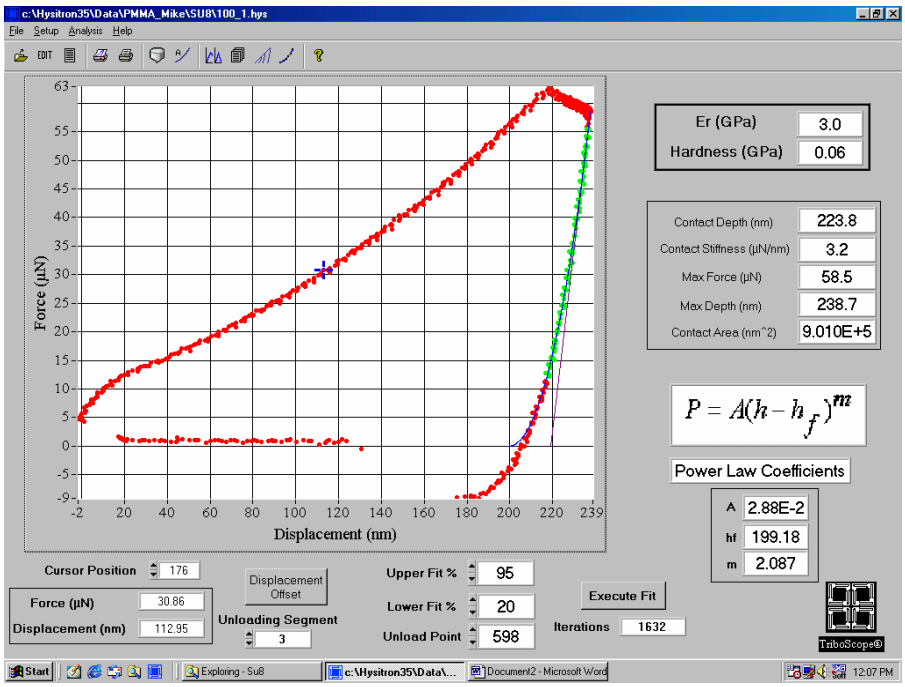

Figure 5.7. Nanoindentation data for a 2 µm SU-8 film on a Silicon substrate with no cross-linking showing an effective Elastic Modulus of 3.0 GPa. This test was conducted with a 100 µN load.

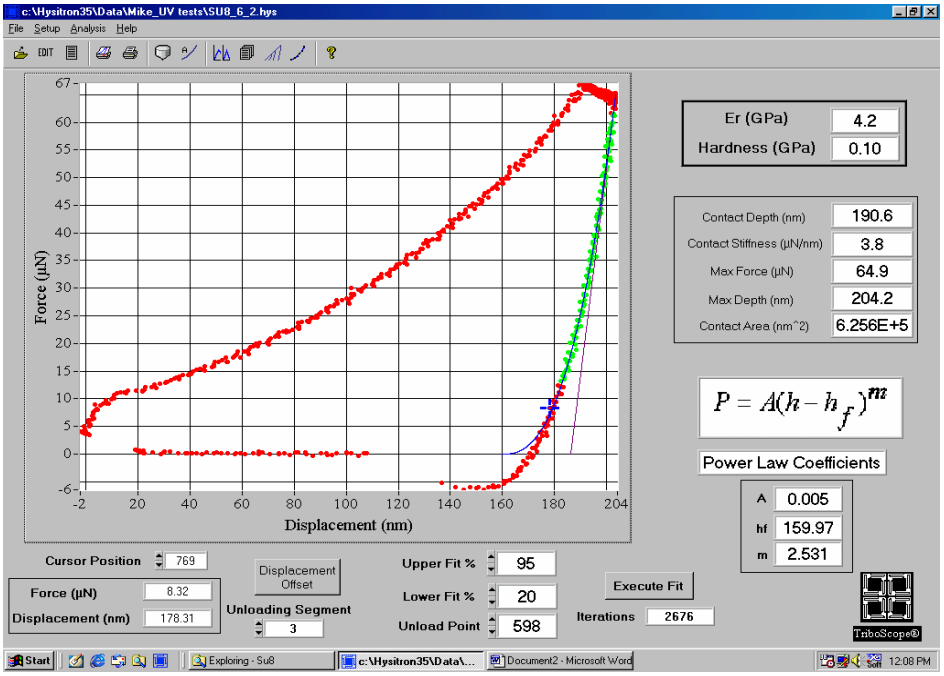

Figure 5.8. Nanoindentation data for a 2 µm SU-8 film on a Silicon substrate cross-linked via 10 seconds of UV exposure. Curve fit shows an effective Elastic Modulus of 4.2 GPa. This test was conducted with a 100 µN load.

Results from the nanoindentation tests show an increase in elastic modulus of approximately 40 % from 3.0 GPa to 4.2 GPa. Note these tests were conducted with a 100 μN load. This resulted in a nanoindentation depth of 229.8 nm for the unexposed film and 190.5 nm for the exposed film. The smaller depth associated with the exposed film is due to the increased modulus. Nanoindentation loads may vary from 10 to 1000 μN depending on the applicaton. One must take care not to penetrate too deeply into the film in order to avoid substrate influence [Fischer-Cripps, 2006]. As a rule of thumb, researchers try to keep the nanoindentation depth around 10 % of the overall thickness of the film. The approximate depth percentages for these tests were 11.5 and 9.6 % for the unexposed and exposed films, respectively.

SU-8 films were then spin-coated onto SAW devices to determine the change in wave propagation as a result of the cross-linking. Two film thicknesses were investigated for the Love Wave device. A 1.1 μm SU-8 film represents wave propagation on the non-dispersive portion of the curve. A 1.4 μm SU-8 film results in wave propagation on a slightly dispersive portion of the curve. These devices were systemically exposed to UV irradiation in 2 second intervals. Considering the short duration for complete cross-linking of SU-8 with UV irradiation (~7 to 10 seconds), the two second intervals between data points seems too sparse. This interval was chosen to allow the lamp to reach full power, giving as much of a reasonable exposure dose while keeping as much of a time resolution as possible.

Results for the exposure of two Love Wave devices are shown in figure 5.9. The device with the 1.4 μm film shows a much higher sensitivity than the device with the 1.1 μm film. This is due to larger fluctuation associated with material property changes at more dispersive regions

of the guided wave mode. At complete cross-linking, one can see the frequency reach equilibrium. This shows the potential of this type of sensor for determining exposure thresholds in microlithography.

Figure 5.10 shows a comparison of Love Wave and HVSAW devices as a function of UV exposure time. Again it is clear to see an enhanced sensitivity of the Love Wave device over the SV-SAW wave counterpart. Again, the reason for this is most likely that the Love Wave is propagating with a majority of energy in the film whereas the SV-SAW wave is propagating with a majority of energy at the interface with non-negligible contributions in the susbstrate.

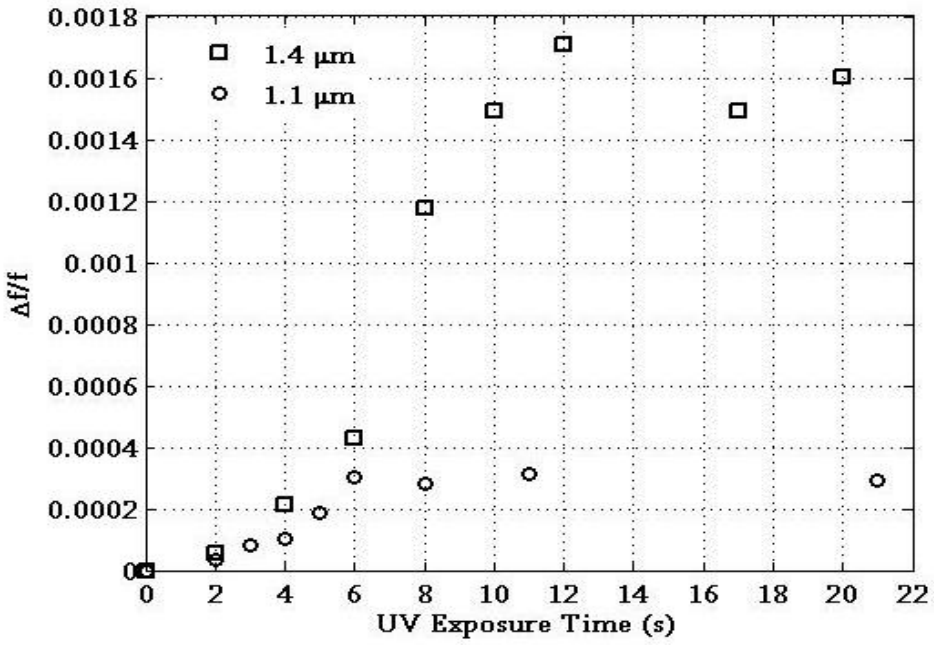

Figure 5.9. Experimental results for normalized frequency shift versus UV exposure time for Love Wave devices on Quartz Film thicknesses of 1.4 μm (squares) and 1.1 μm (diamonds) were tested.

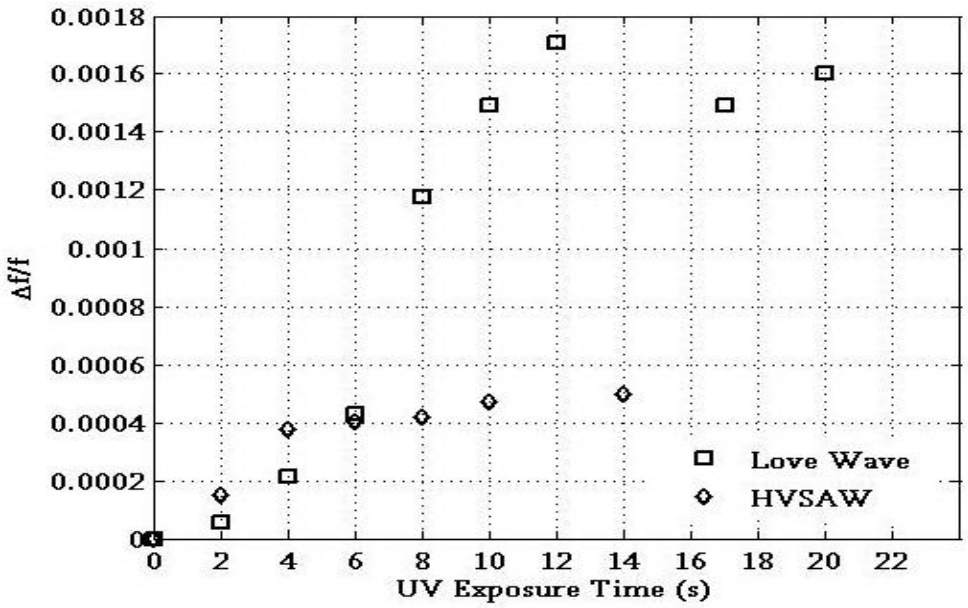

Figure 5.10. Experimental results for normalized frequency shift versus UV exposure time for Love Wave devices on Quartz and HVSAW device on $LiTaO_3$ based on experimental data for Elastic modulus and density of a Polyimide film [Guenther, 2004]. Film thicknesses of 1.6 μm (squares) and 1.2 μm (diamonds) were simulated.

5.3.4 Discussion

The results of the previous section show that normalized frequency changes of 2 parts in 1000 can be achieved due to modulus changes of approximately 40 %. Experimental results have shown the Elastic Modulus of irradiated polymer films can change on the order of 1000 % [Guenther, 2004]. This shows a great potential for radiation sensing. Those changes occur over an exposure dose of approximately 10^{16} ion/cm^2. This rivals the typical lifetimes of current semiconductor radiation based sensors. The benefit of this technique is its ability to become more cost effective with batch processing.

Chapter 6 Conclusions and Future Directions

6.1 Review of Thesis Goals and Contributions

6.1.1 Thesis Goals and Objectives

Layered SAW devices have become an integral part of the sensor community over the last several decades. The research community must continue to press the state of the art both in terms of optimizing existing sensor configurations as well as recruiting novel applications. Simply stated, this work was aimed at both of those goals. As a review, the goals of this thesis were to:

- Refine Finite Element techniques to investigate wave propagation phenomena in Layered Surface Acoustic Wave devices taking into account the crystallographic orientation of the substrate
- Demonstrate the capability to model both guided wave propagation and sensor behavior as a function of parameters key to a practical device
- Develop a Finite Element model to predict Layered SAW response to glass transition and localized change in mechanical behavior in a polymer film
- Compare the sensitivities of SV-SAW Wave and Love Wave devices and gain fundamental understanding of the benefits of one device over the other

- Apply these principles to an experimental verification of Layered SAW devices for polymer film characterization
- Evaluate/Demonstrate the potential for Love and SV-SAW wave devices for existing and novel sensing applications such as Ice detection and Radiation sensing.

6.1.2 Thesis Contributions

1. Investigation of Theoretical Aspects of Love Wave and Rayleigh Wave Propagation

This work began with an investigation into some background wave propagation theory. An extension of Auld's Love Wave derivation according to boundary conditions associated with particle velocity fields and the Transverse Resonance Method was made. This was done not only to compare with other authors but to present the equation in form more conducive to numerical solution given current computing capabilities. Theoretical aspects of Rayleigh wave propagation were investigated to show the mathematical basis for pseudo-surface acoustic wave modes associated with the complex solutions to the Rayleigh wave equation.

2. Modification of FEM Analysis to account for Crystallographic Orientation in SAW Devices

An important component of this work was the introduction of techniques for modeling SAW delay lines with Finite Elements. Special attention was given to the crystallographic orientation of the piezoelectric substrate which in practical applications, are used to generate different wave modes. Through transformation of global displacements into a local coordinate system, the wave

structure of the different modes could be verified. Results from the Finite element study showed the ability to predict the excitation of Surface Skimming Bulk Waves in 90^0 rotated ST Quartz along with SV-SAW wave and High Velocity Surface Acoustic Waves in ST Quartz and 77^0 Y Rotated Lithium Tantalate.

3. Enhanced Description of Wave Propagation Phenomena in Layered SAW Devices

The energy trapping associated with Love Wave modes operating at dispersive regions of the dispersion curve was highlighted. This became an underlying theme in the rest of the work. This phenomenon was used to demonstrate the enhanced mass sensitivity of a Love Wave device based on a 1.6 μm PMMA film compared to a HVSAW counterpart in Lithium Tantalate. Sensitivities of 20 $x10^{-12}$ cm^2/g were shown for Love waves compared to 10 $x10^{-12}$ cm^2/g for HVSAW. This represents a sensitivity increase by a factor of two. The FEM model was used to show that this occurs as a result of choosing a mode on the dispersive portion of the guided wave curve for Love Waves.

4. FEM Analysis of Polymer Film Glass Transition via Rayleigh Wave Damping Parameters

The concept of Rayleigh damping was used as a basis to derive a relationship between the damping parameter β of traditional FEM software and the loss tangent of polymer films. This paved the way for the development of an FEM model to predict the capability of a SAW delay line to predict the glass transition and localized change in mechanical behavior in a PMMA film. This model showed that the drastic decrease in Storage Modulus is the dominating effect in

SAW propagation with only slight modification due to the damping associated with the Loss Tangent. The model also showed that Love Waves have a 30% higher sensitivity compared to HVSAW in predicting the Localized change in mechanical behavior of a 1.6 μm PMMA film.

5. Demonstration of Layered SAW Characterization of Polymer Curing and Detection of Ice

The concept of acoustic energy trapping in the layer along with the Shear Horizontal displacement associated with the Love Wave structure was exploited to demonstrate the capability of Love Wave devices for monitoring Polymer curing as well as the detection of ice. An order of magnitude increase in sensitivity to polymer soft bake time was found in Love Wave devices compared to HVSAW devices. Results showed that Love Wave devices, though attenuated by approximately 12 dB, could still operate in liquid environments, unlike the HVSAW or SV-SAW wave counterparts. The complete loss of energy associated with the formation of ice was also demonstrated as the main sensing mechanism for ice detection.

5. Proof of Concept for Novel Application of Radiation Sensing for Layered SAW devices

Finally, a novel sensing application was introduced for both SV-SAW wave and Love Wave devices. Based on the ion modification of polymer films, a conceptual description of a Layered SAW radiation sensor was introduced. Based on experimental data for Boron irradiation of a Polyimide film, a Finite Element model was developed to demonstrate the feasibility of such a device. The model predicted normalized changes in frequency of approximately 5 % for Love Wave devices compared to 2.5 % for SV-SAW and HVSAW

devices. A proof-of-concept experiment was developed based on the UV cross-linking of the photoresist SU-8. Although on a different scale, experimental data showed similar trends of sensitivity and response to polymer modification. The Love wave device had a sensitivity of approximately 2.5 times that of the HVSAW counterpart.

Overview of Thesis Accomplishments

In summary, the milestones set forth for this work were met.

1. The ability to account for crystallographic orientation in a Finite Element model of a SAW device was shown.
2. Fundamental understanding of the wave propagation phenomena allowed for the demonstration and explanation of enhanced sensitivity present in Love Wave devices vs. SV-SAW wave or HVSAW devices.
3. Finite element models were extended to predict the behavior of Layered SAW devices for glass transition monitoring as well as radiation sensing.
4. Experimental validation of film characterization and highlighted sensor applications was also completed.
5. In the end, a greater understanding of wave propagation and enhanced modeling techniques allowed for further optimization of existing Layered SAW applications as well as the development of a novel applications, i.e., Radiation sensing.

6.2 Future Directions of Research

Based on the research discussed in this work, many avenues are still unexplored. A multitude of applications for Surface Acoustic waves on a macroscopic scale have been demonstrated for structural health monitoring applications [Tittmann, 2003] as well as, materials characterization [Tittmann, 1995]. The purpose of this section is to highlight some research directions that may prove beneficial in the future for sensors based on smaller scale SAW devices.

6.2.1 Improved Finite Element Models

The FEM model presented here involves some assumptions that may affect the results of the model. In this model, electrodes are created by applying electrical boundary conditions/loads to the surface of the substrate. The underlying assumption of this boundary condition is that the electrodes are mass-less and two dimensional. Over the past several years, researchers have begun to account for both the mass and dimension of the electrodes showing that they do play a role on the resulting frequency response [Laude, 2002]. Future modeling efforts should concentrate on determining the consequence of the mass-less electrode assumption. This is particularly of concern when dealing with Layered SAW devices concerning thin films. Typical electrodes are deposited at thicknesses of around 300 μm. This could play a significant role when investigating films that are less than 2 or 3 μm.

A miniaturized model was presented in this work. This is due to the memory

requirements associated with the fine mesh density required for modeling devices which operate around 100 MHz. Although only a small portion of the model is of concern from a wave propagation perspective, care must be taken to avoid edge effects. This problem could be avoided by developing effective absorbing boundary conditions. These boundary conditions exist and have been utilized for fluid media [Bezdek, 2006] in CAPA, however, the mode conversion and oblique incidence make effective absorbing boundary conditions difficult for solids. A single frequency can be effectively damped but, given the bandwidth of typical wave propagation scenarios, significant energy will still propagate. If effective absorbing boundary conditions could be developed, model sizes could be cut down to only the essential propagation paths of interest. This may also provide enough available computer memory to include a larger number of finger pairs in the transmitting and receiving IDTs.

This work also concentrated on modeling and proof-of-concept for particular sensor applications. Sensitivity analysis for proper mode selection is critical in realizing these applications. This presents an opportunity for the Semi-Analyitical Finite Element (SAFE) Method. SAFE methods help to avoid long computation times associated with the finite element method while providing vital dispersion characteristics and sensitivity prediction through proper mode selection [Hayashi, 2003; Hayashi, 2003]. A background study on sensitivity analysis for different sensor configurations can provide useful thumb rules for researchers to maximize sensitivity in a particular application while minimizing the computation time.

6.2.2 **Alternative Fabrication Strategies for Diverse Applications**

This work has presented the potential for Layered Surface Acoustic Wave devices for monitoring glass transition and localized change in mechanical behaviors in polymer films. A limitation of these devices is in their profile. An increased interest in this technology would arise if these devices were able to characterize the glass transition and localized change in mechanical behavior behavior of films smaller than 100 nm. With electrode thicknesses of 300 nm, this is not feasible. For that reason, a modified lithography process allowing for a flush device surface would prove beneficial. This would require etching of the piezoelectric substrate. If grooves could be etched into the piezoelectric substrate, the electrodes could fill the grooves leaving a flush surface. A schematic representation of the proposed process is shown in figure 6.1.

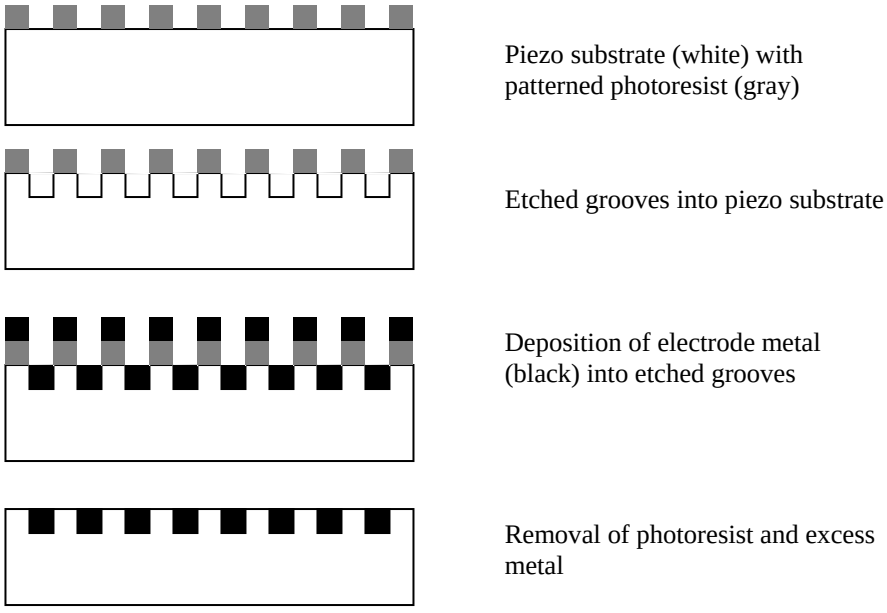

Figure 6.1. Schematic representation of the lithography process for depositing electrodes into etched grooves into the substrate.

6.2.3 Further Radiation Sensing

The work of this thesis represents the first introduction of experimental results on radiation sensing based on Layered Surface Acoustic Wave devices. Given the proof of concept level of this effort, much more research should be done to investigate these devices.

The first aspect of future work should concentrate on the materials research aspect of this project. Investigation of potential overlayers that may maximize the effect from ion modification should be conducted. Based on the FEM results of this work, an investigation of optimal film thickness should be conducted experimentally. Tests with an actual radiation source (i.e. ion source) should be conducted to further validate the technique for practical application. This would also help to assess the ion effects on the piezoelectric substrate as that may affect the performance of the device.

Once parameters such as overlayer material and thickness have been identified, a more permanent electrical connection should be established that is fairly rugged. The setup should withstand degradation due to elevated temperatures, radiation damage, and other harsh operating conditions which replicate a field environment. This setup could also be useful in many of the applications where Layered Surface Acoustic waves may be desirable.

Appendix A: Review of SAW Fabrication

One of the more common lithography techniques used for IDT patterning is the "Lift-Off" process. This technique involves the use of a positive photoresist such that the image resulting on the substrate exactly mimics the image on the photoresist. This appendix aims to introduce this procedure to those unfamiliar with the process as well as highlight some special considerations for this specific work to those more intimately involved with microlithography. More detailed descriptions of lithography processes for sensor technologies can be found in literature [Varadan, 2001].

A schematic of the key components of the Lift-Off process is shown in figure A.1. The first step is the creation of the pattern which was done with the commercial software L-Edit software. Next this pattern must be transferred to the mask shown in the first step of figure A.1. The mask used was a soda-lime glass covered with a chrome layer as well as a negative photoresist. The mask was "written" with a Heidleburg DWL 66 Laser Writer. The photoresist was then removed in the exposed portion with a chemical developer followed by the removal of the subsequently exposed chrome areas with an appropriate chrome etchant.

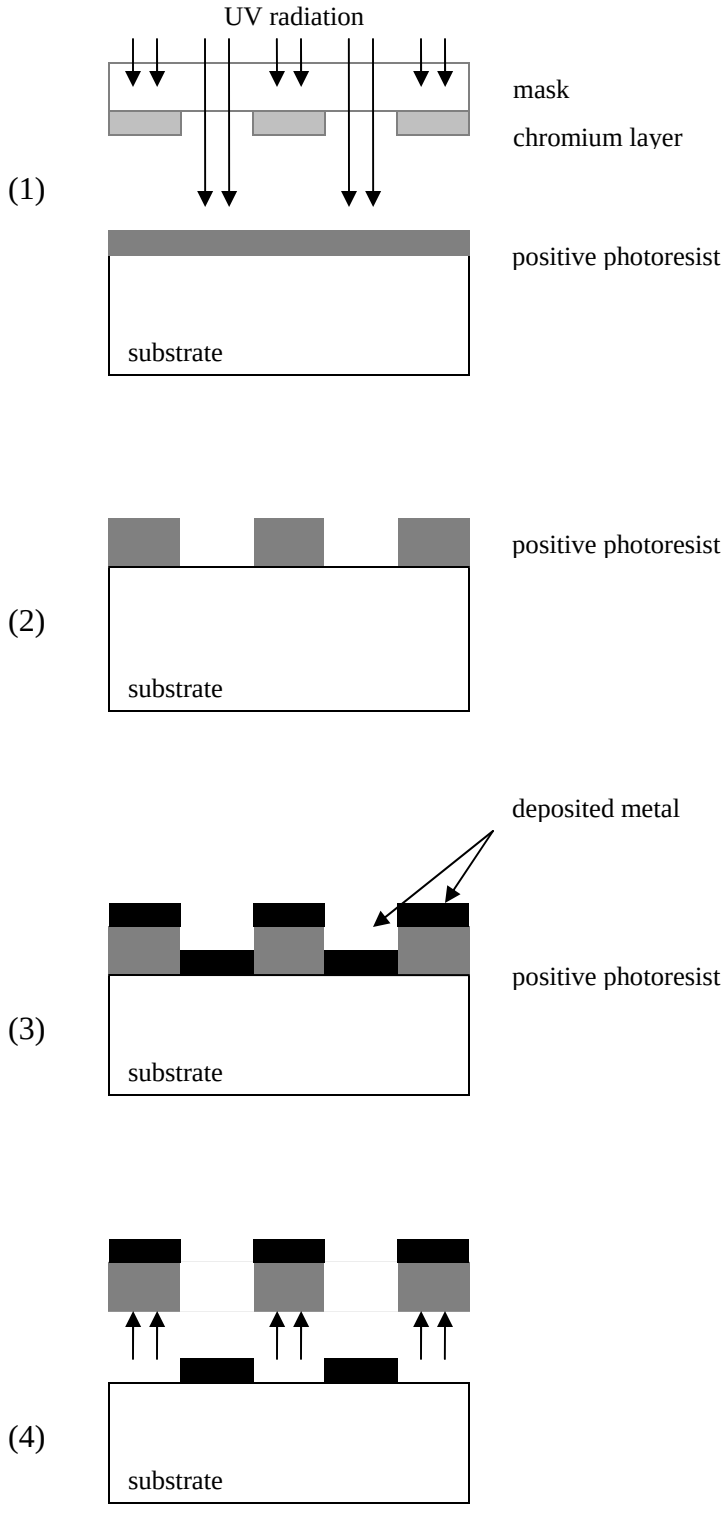

Figure A.1. Schematic representation of the steps associated with the "Lift Off" Process involving (1) pattern exposure, (2) photoresist development, (3) metal deposition, and (4) lift-off.

Several film layers were added to the sample for various reasons. Many piezoelectric substrates (Quartz included) are somewhat translucent. Under UV exposure, this can introduce image blurring as the light actually travels through the substrate reflecting off of the back surface and dispersing back into other portions of the photoresist. A schematic of this phenomenon is shown in figure A.2 with a translucent substrate A.2a compared to a traditional opaque substrate A.2b. For this reason, a thin (50-100 nm) anti-reflective coating was applied to the front surface of the Quartz. Secondly, a "lift-off" resist is deposited on the surface. This layer is provided to ensure enough height separation between areas where metal deposition is desired and areas where no metal deposition is required. The lack of this layer could result in "bridging" during the deposition process where the metals of two areas separated by a gap connect impeding the removal of the sacrificial layer. Finally, a positive photoresist is applied to the layer to help transfer the mask pattern onto the substate.

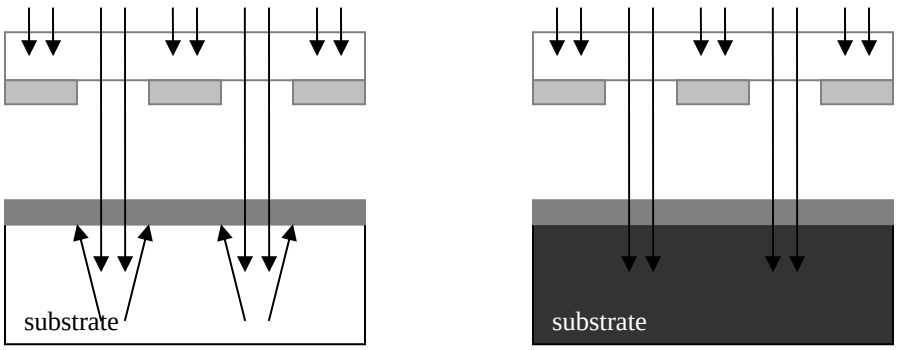

(a) (b)

Figure A.2. Schematic representation of pattern transfer consisting of (a) a translucent substrate where back-scatter light can expose unwanted areas of the film and (b) an opaque substrate where light that penetrated the photoresist is absorbed by the material.

Once the substrate is prepared, the mask is used to expose the areas of the substrate which will ultimately be exposed for metal deposition. This was done with a Karl Suss MA6 UV exposure tool. The photoresist is then developed exposing the desired areas of the substrate for metal deposition. At this point, the metal was deposited via the evaporation process. Gold is a preferred metal for electrodes due to its electrical properties however, the adhesion of gold to the substrate is often difficult. In order to promote adhesion, a layer of chromium is often deposited prior to the gold layer. Chromium was deposited at a thickness of 100 angstroms followed by a gold layer of 300 nm using a Semicore Evaporator tool. This works by hanging the substrate upside down in a vacuum chamber while heating the metal "slugs" such that they evaporate and transfer onto the surface of the sample. The deposition of metal typically occurs at a rate 0.5-5 angstroms/sec so this process can become quite time consuming for deposition targets of 1 μm or higher. The final step of the process is the removal of the access metal and sacrificial layers with the appropriate chemical. Figure A.3a shows an image of the patterned mask and figure A.3b shows the Quartz substrate just prior to metal deposition. The IDT pattern is clearly visible. Figure A.4 shows an optical microscope image of a closeup on on IDT showing the widths and spacings.

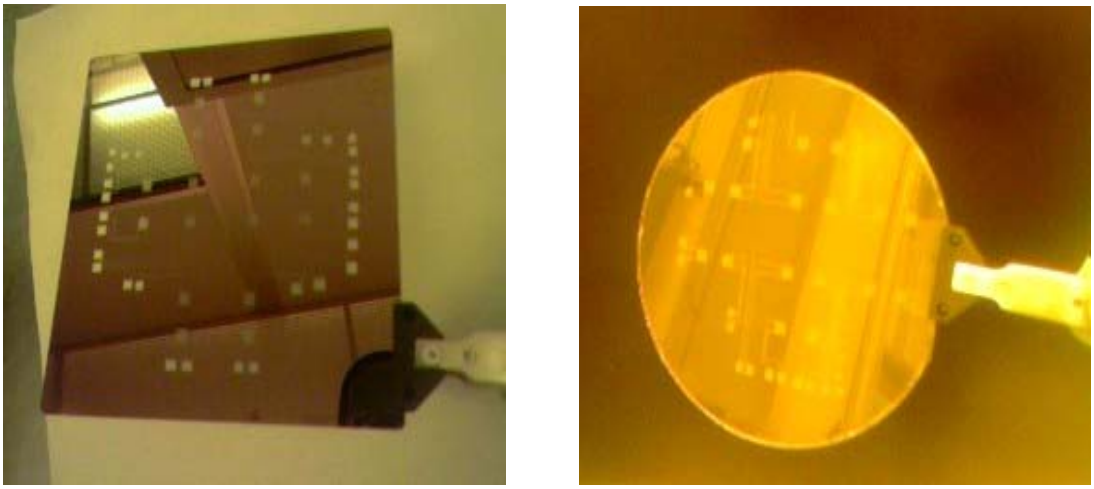

(a) (b)

Figure A.3. (a) Image of the Soda Lime glass mask showing the IDT patterns. The IDTs are in the center of the cross structure and the electrode pads are around the outside. (b) The Quartz substrate with the transferred pattern from the Mask just prior to metal deposition.

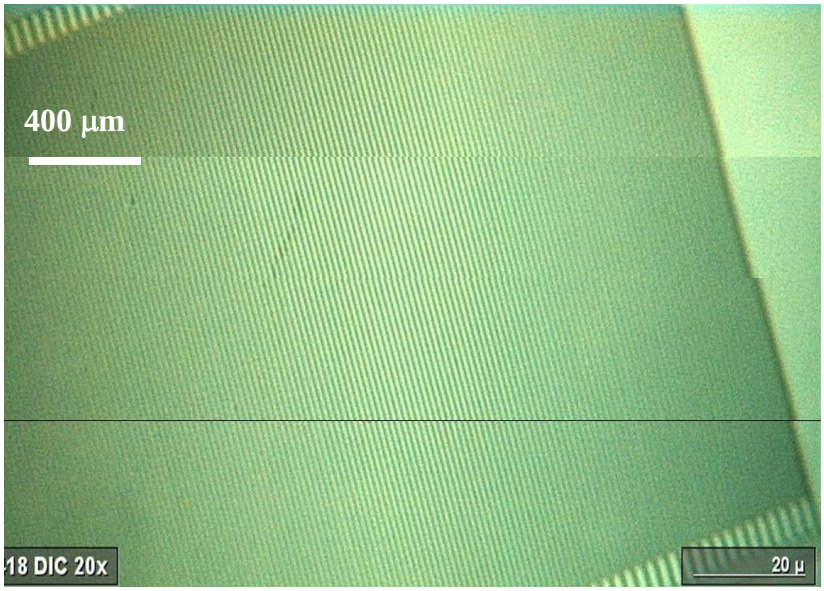

Figure A.4. Optical Microscope close-up of one of the IDTs. The finger spacings and thicknesses are 10µm.

In patterning IDTs onto piezoelectric substrates, one must take caution in the alignment. Alignment can be aided by the addition of markers and reference crosses in the mask design.

This will allow alignment with the exposure tool ensuring that the IDTs are completely in line with the desired crystallographic orientation. This can help to optimize the performance of the resulting device. Also, the anti-reflective coating can introduce another concern for applications discussed in this thesis. A more ideal situation is the deposition of the anti-reflective coating on the back surface of the substrate. In this fashion, it does not interfere with the finalized sensor. Although the anti-reflective coating outside the areas of deposited metal can be removed, the areas between the substrate and metal cannot. This may have a slight effect on the electric conductivity between the gold and the substrate ultimately increasing the insertion loss of the device.

Appendix B: ANSYS/CAPA Interface

ANSYS is a very common commercial software whereas, Coupled-Piezoelectric Acoustic Analysis (CAPA) is a smaller software found only in circles involved in sensors and actuators. The purpose of this Appendix is to provide some background information on the methodologies of CAPA and how it interfaces with the more standard ANSYS package. Although ANSYS is capable of handling the problems presented in this thesis, CAPA proved more beneficial for several reasons which are also discussed.

CAPA is a software offered by WisSoft and developed at the Department of Sensor Technology, University of Erlangen-Nuremberg[4] that can be used as a stand alone software or interfaced with ANSYS. CAPA has the ability to handle both Finite element and Boundary element problems with an emphasis on the governing equations associated with piezoelectric coupled-field modeling. Prescribed element definitions include the wave equation for fluids and Navier-Stokes equations for solids. CAPA also has the ability to simulate moving fluids which has been demonstrated in simulations of Ultrasonic Flowmeters [Bezdek, 2006]. CAPA offers a unique flexibility of user specified solvers. This is a major benefit over ANSYS. Since wave propagation is a critical aspect of CAPA, more sophisticated solvers are a benefit as these problems are inherently more complex.

Interfacing ANSYS and CAPA allows the user to exploit the strengths of both programs to solve FEM/BEM problems in the most efficient manor. Typical FEM problems involve three

[4] Information is provided at the website www.wissoft.de

main steps: Pre-processing, Solving, and Post-processing. Pre-processing typically consists of defining model geometry, boundary conditions, material properties, and solution parameters. Due to its global commercialization, ANSYS has developed a highly sophisticated User interface with extremely versatile pre-processing and post-processing capabilities. As discussed, CAPA has the benefit of element definitions and solver capabilities that are specifically designed for wave propagation problems. In this fashion, the most efficient combination is the use of the ANSYS pre- and post-processor while solving the system with CAPA. Figure B.1 shows a process flow diagram for the interface between ANSYS and CAPA along with some post-processing options depending on the nature of the problem being explored.

The input script can be written as a text file and involves an ANSYS language (ADPL) modified with CAPA specific commands. This file is then read into the ANSYS pre-processor along with file definitions for the excitation function and element mapping files to interface between CAPA and ANSYS element definitions. Conversion rules are used to convert the resulting model definitions of the pre-processor into a .DAT file readable by the CAPA solver. The .DAT file along with a material property database is fed into the CAPA solver which is run via command line prompts. Once the solution is complete, a universal results file is written at which point the user has several options for proceeding with the post-processing. A conversion command (unv2rst) can be used to write the universal results into the standard ANSYS results file, .RST. The ANSYS post-processor can then be used in a standard fashion for interpreting results. The second option is to use a “history” tool to write the results into a text file which can then be exported to analysis programs such as MatLab or Excel. The results can also be analyzed with an “inner-imp” tool which has some prescribed definitions for transducer

impedance analysis. Finally, the results can be written into a matrix file via the "unvsplit" command at which point combinations of the above post-processing options can be utilized.

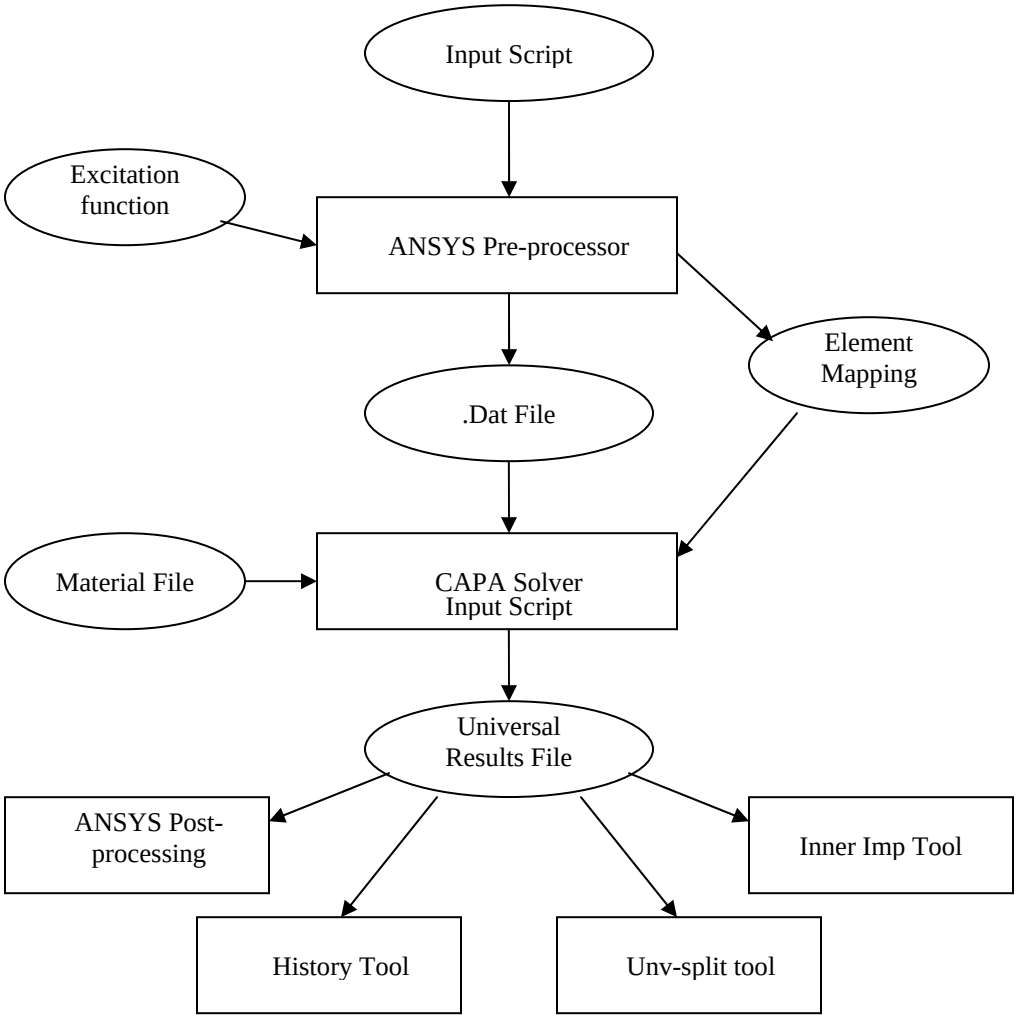

Figure B.1. Process flow diagram for the ANSYS/CAPA Interface.

Appendix C: Catalog of Written Software

C.1 Input Script for FEM Model of SAW Devices

```
!----------Love Waves on Quartz----------!
!            July 18, 2006                !
!                                         !
!  3D Coupled Field model of polymer overlayer on   !
!  quartz substrate with Transmitting and Receiving  !
!  IDTs containing two finger pairs. Meant to sim.   !
!  propagation orthogonal to X in ST Quartz, known   !
!  to generate SSBW leading to Love Waves            !
!                                  Michael Pedrick  !
!-----------------------------------------!

FINISH

/clear
/filename,quartz
/title,Love Waves on Quartz

!-CONSTANTS----------

f = 115e6                               !nominal frequency
length = 500e-6                         !dimension in the x direction
width = 200e-6                          !dimension in the y direction
height = 80e-6                          !dimension in the z direction
thick = .6e-6                           !film thickness
xinset = 80e-6                          !nearest distance to y-z plane edge
yinset = 40e-6                          !symmetric distance to x-z plane edges
IDT = 13e-6                             !IDT thickness and spacing
theta = 43                              !Rotation angle


!-MODEL----------

/PREP7

!___Geometry_____

btol,0.1e-6                             !Sets a small tolerance for nodal distance
wprota,,theta
cswpla,11,0
block,,width,,length,,height-2*IDT
block,,width,,length,height-2*IDT,height
block,,width,,length,height,height+thick
/color,volu,gree
wprota,,90,
wpoffs,,,-xinset
```

```
vsbw,all,,delete
*do,IDTstep,1,7,1
 wpoffs,,,-IDT
 vsbw,all,,delete
*enddo
wpoffs,,,(xinset+7*IDT)
wpoffs,,,-length+xinset
vsbw,all,,delete
*do,IDTstep,1,7,1
 wpoffs,,,IDT
 vsbw,all,,delete
*enddo
wprota,,,90
wpoffs,,,yinset
vsbw,all,,delete
wpoffs,,,(width-2*yinset)
vsbw,all,,delete
vglue,all
wpcsys,-1,11
asel,all

!___Components_____________

asel,s,loc,z,height,,,,
asel,r,loc,x,width/2,,,,
asel,r,loc,y,xinset+IDT/2,,,,
asel,a,loc,y,xinset+9*IDT/2,,,,                 !positive Trans. electrodes
asel,r,loc,x,width/2,,,,
asel,r,loc,z,height,,,,
cm,pos_elecT,area

asel,s,loc,z,height,,,,
asel,r,loc,x,width/2,,,,
asel,r,loc,y,xinset+5*IDT/2,,,,
asel,a,loc,y,xinset+13*IDT/2,,,,            !ground Trans. electrodes
asel,r,loc,x,width/2,,,,
asel,r,loc,z,height,,,,
cm,neg_elecT,area

asel,s,loc,z,height,,,,
asel,r,loc,x,width/2,,,,
asel,r,loc,y,Length-(xinset+13*IDT/2),,,,
asel,a,loc,y,Length-(xinset+5*IDT/2),,,,    !positive Rec. electrodes
asel,r,loc,x,width/2,,,,
asel,r,loc,z,height,,,,
cm,pos_elecR,area

asel,s,loc,z,height,,,,
asel,r,loc,x,width/2,,,,
asel,r,loc,y,Length-(xinset+9*IDT/2),,,,
asel,a,loc,y,Length-(xinset+IDT/2),,,,          !ground Rec. electrodes
asel,r,loc,x,width/2,,,,
asel,r,loc,z,height,,,,
cm,neg_elecR,area

vsel,s,loc,z,(height-2*IDT)/2,,,,           !substrate
```

```
cm,substrate,volu

vsel,s,loc,z,height+thick/2,,,,                    !film
cm,film,volu,,,,

allsel

!___Element Types_____________

setgroup,1,piezo3d,lin,,640,!save
setgroup,2,mech3d,lin,,870,!save          !Define elem type and mat props
attgroup,2,addshape

!___Meshing_____________________

mshkey,1
esize,4*IDT/elemrate
lsel,s,loc,z,height+thick/2
lsel,r,loc,x,0
lsel,r,loc,y,0
lesize,all,,,2
cmsel,s,film
vmesh,all

esize,4*IDT/elemrate
lsel,s,loc,z,height-IDT
lsel,r,loc,x,0
lsel,r,loc,y,0                                    !mesh the layer
lesize,all,,,4
vsel,s,loc,z,height-IDT
vmesh,all

esize,4*IDT/elemrate
lsel,s,loc,z,(height-2*IDT)/2
lsel,r,loc,x,0
lsel,r,loc,y,0                                    !mesh substrate
lesize,all,,,2
cmsel,s,substrate
vmesh,all

cmsel,s,film
eslv,s                                            !assign properties to film
type,2
emodif,all
/color,elem,red
/color,volu,red
/color,area,red

cmsel,s,substrate
eslv,s                                            !assign properties to substrate
type,1
emodif,all
/color,elem,dgra
/color,volu,dgra
/color,area,dgra
vsel,s,loc,z,height-IDT,,,,
```

```
eslv,s
type,1
emodif,all
/color,elem,dgra
/color,volu,dgra
/color,area,dgra


allsel
numcmp,node
numcmp,elem
eplot

!___CAPA Initialization_____________

function,import,1,pulse500,fnc                  !Synthesized pulse
savedofs,ep_
analysis,fem+trans+cons+rayl
transient,1000,1,1000,10,1e-10,0.,0.25,0.5,0.5  !Model parameters
!solver,iterstd+gmres,,0,1,1,,0.00001,40
solver,direct+explicit,1,0

!___Boundary Conditions_____________


nsel,s,loc,z,0
nsel,r,loc,x,0
nsel,r,loc,y,0
dofs,all,,,dx_
dofs,all,,,dy_
dofs,all,,,dz_
nsel,s,loc,z,0
nsel,r,loc,x,0
nsel,r,loc,y,length
dofs,all,,,dx_
dofs,all,,,dy_
dofs,all,,,dz_
nsel,s,loc,z,0
nsel,r,loc,x,width                      !Fix displacements on bottom corner nodes
nsel,r,loc,y,length
dofs,all,,,dx_
dofs,all,,,dy_
dofs,all,,,dz_
nsel,s,loc,z,0
nsel,r,loc,x,width
nsel,r,loc,y,0
dofs,all,,,dx_
dofs,all,,,dy_
dofs,all,,,dz_

cmsel,s,neg_elecT
cmsel,a,neg_elecR                           !Set potential to zero on ground electrodes
nsla,s,1
dofs,all,,,ep_

nsel,s,loc,z,0                              !Ground substrate bottom to eliminate feed-through
```

```
dofs,all,,,ep_

cmsel,s,pos_elecT
nsla,s,1
restraints,all,,,ep_,1,1                    !Apply voltage excitation to transmit IDT
cmsel,s,pos_elecR
nsla,s,1
constraints,all,,,ep_                       !Constrain receiver IDTs

vsel,all
nslv,s,1

*get,mstr,node,,num,min
nsel,s,,,mstr                               !Get master node on receiver IDT for plotting

!lsel,s,loc,x,yinset
!lsel,r,loc,y,length-xinset-7*IDT           !Select lines for Wave Structure analysis
!nsll,s,1



!___Solution_____________________

history,all
allsel
setfile,quartz,dat
stop
```

C.2 MatLab Love Wave Dispersion

```
%Numerical Solution For Love Waves based on the Longitudinal Velocities and Shear Moduli
%of the Layer and the Substrate

%       Mike Pedrick


d=1;      %input('Layer Thickness (m):  ');
c1=1000;          %input('Shear Velocity in Layer (m/s):  ');
c2=5100;          %input('Shear Velocity in Substrate (m/s):  ');
mu1=1430000000;          %input('Shear Modulus in Layer (Pa):  ');
mu2=69000000000;%input('Shear Modulus in Substrate (Pa):  ');
modes=7;          %input('Number of Modes to Solve for (5 or less):  ');

c_search=[c1+1:.005:c2];
w=[1:25:2951];
```

```
n=1;
cp1=zeros(size(w));
cp2=zeros(size(w));
cp3=zeros(size(w));
cp4=zeros(size(w));
%cp5=zeros(size(w));
root=1;
 while n<length(w)+1
    m=2;
    y=tan(sqrt(1./c1^2-1./c_search.^2).*w(n).*2.*pi)-(mu2.*sqrt(1-c_search.^2./c2^2))./(mu1*sqrt(-
1+c_search.^2./c1^2));
  while m<length(y) & root<modes+1
    z=y(m)*y(m-1);
    if z<0 & root==1 & y(m)<y(m+1)
       cp1(n)=c_search(m+1);
       m=m+1;
       root=root+1;
    elseif z<0 & root==2 & y(m)<y(m+1)
       m=m+1;
       root=root+1;
    elseif z<0 & root==3 & y(m)<y(m+1)
       cp2(n)=c_search(m+1);
       m=m+1;
       root=root+1;
    elseif z<0 & root==4 & y(m)<y(m+1)
       m=m+1;
       root=root+1;
    elseif z<0 & root==5 & y(m)<y(m+1)
       cp3(n)=c_search(m+1);
       m=m+1;
       root=root+1;
    elseif z<0 & root==6 & y(m)<y(m+1)
       m=m+1;
       root=root+1;
    elseif z<0 & root==7 & y(m)<y(m+1)
       cp4(n)=c_search(m+1);
       m=m+1;
       root=root+1;
       %elseif z<0& root==9 & y(m)<y(m+1)
       %cp5(n)=c_search(m+1);
       %m=length(y)+5;
       %root=root+1;
   end
    m=m+1;
  end
  root=1;
  n=n+1;
 end

skip=5;
threshold=1200;
clear n
n=1;
while cp1(n)==0
  n=n+1;
end
```

```
cp1=cp1(n:length(cp1));
w1=w(n:length(w));


p=n+skip;
while cp2(p)<threshold
   p=p+1;
end
cp2=cp2(p:length(cp2));
w2=w(p:length(w));


p=p+skip;
while cp3(p)<threshold
   p=p+1;
end
cp3=cp3(p:length(cp3));
w3=w(p:length(w));

p=p+skip;
while cp4(p)<threshold
   p=p+1;
end
cp4=cp4(p:length(cp4));
w4=w(p:length(w));

p=p+skip;
%while cp5(n)<threshold
%    n=n+1;
%end
%cp5=cp5(n:length(cp5));
%w5=w(n:length(w));



plot(w1./1000,cp1./1000,'k');
xlabel('fd Product (MHz mm)');
ylabel('Velocity (mm/\musec)');
hold on
plot(w2./1000,cp2./1000,'k');
plot(w3./1000,cp3./1000,'k');
plot(w4./1000,cp4./1000,'k');
%plot(w5./1000,cp5./1000,'k');

cg1=zeros(size(cp1));
clear n
for n=1:length(cp1)-1
 cg1(n)=cp1(n)^2/(cp1(n)-(w1(n)*((cp1(n+1)-cp1(n))/(w1(n+1)-w1(n)))));
 wg1=w1;
end
cg1(length(cg1))=cg1(length(cg1)-1);

cg2=zeros(size(cp2));
clear n
for n=1:length(cp2)-1
 cg2(n)=cp2(n)^2/(cp2(n)-(w2(n)*((cp2(n+1)-cp2(n))/(w2(n+1)-w2(n)))));
```

```
 wg2=w2;
end
cg2(length(cg2))=cg2(length(cg2)-1);

cg3=zeros(size(cp3));
clear n
for n=1:length(cp3)-1
 cg3(n)=cp3(n)^2/(cp3(n)-(w3(n)*((cp3(n+1)-cp3(n))/(w3(n+1)-w3(n)))));
 wg3=w3;
end
cg3(length(cg3))=cg3(length(cg3)-1);

cg4=zeros(size(cp4));
clear n
for n=1:length(cp4)-1
 cg4(n)=cp4(n)^2/(cp4(n)-(w4(n)*((cp4(n+1)-cp4(n))/(w4(n+1)-w4(n)))));
 wg4=w4;
end
cg4(length(cg4))=cg4(length(cg4)-1);

plot(wg1./1000,cg1./1000,'k --');
hold on;
plot(wg2./1000,cg2./1000,'k --');
plot(wg3./1000,cg3./1000,'k --');
plot(wg4./1000,cg4./1000,'k --');
```

C.3 MatLab Love Wave Structure

```
%Displacement Vector Plots for Love Waves
%          Mike Pedrick



ct1=1100; %Shear velocity of Layer
ct2=5050; %Shear velocity of Substrate

cp=3300; %Phase Velocity at desired fd product
f=250; %represents fd product in Hz*m assuming the layer thickness is 1.

w=2*pi*f;
k=w/cp;
d=.001;
beta1=sqrt(1-cp^2/ct1^2);
```

```
beta2=sqrt(1-cp^2/ct2^2);
t=0;
lambda=cp/f;

z=-d:.0005:5*d;
x=0:lambda/5:5*lambda;
n=1;
m=1;
u1=zeros(length(z),length(x));
u2=zeros(length(z),length(x));
while m<length(z)+1
   while n<length(x)+1
      u1(m,n)=cosh(beta1*k.*(z(m)+d))*exp(i*w*t-i*k.*x(n));
      u2(m,n)=cosh(beta1*k*d)*exp(-beta2*k.*z(m))*exp(i*w*t-i*k.*x(n));
      n=n+1;
   end
   n=1;
   m=m+1;
end
```

Appendix D: Non-Technical Abstract

Sensors operate on a cause and effect principle where the cause represents the entity one wishes to detect and the effect is the mechanism by which that entity is detected. The value of a particular sensor is largely based on its sensitivity. The goal of any sensor is to produce the largest effect from the smallest cause possible. Toward this end, Surface Acoustic Wave (SAW) sensors have proven valuable for their extremely high sensitivity to certain causes. SAW devices operate on a principle analogous to generating ripples in water by throwing a stone into a pond. The ripples traverse across the surface of the pond at a speed dictated by the properties of the water. A SAW device can be thought of as a solid "pond" (typically the size of nickel or dime) containing ripples almost a billion times smaller induced by an electrical signal acting as a stone. As a result of this miniature scale, SAW devices are extremely sensitive to very small changes in the "water."

Researchers have used this technology extensively to detect and quantify the presence of minute traces of certain biological and chemical constituents in a particular environment. Theoretical work has been aimed at using certain mathematical analogies to predict the behavior of the device under certain conditions as well as testing different configurations to determine the most sensitive device for a particular application. The aim of this work is to expand on some of these mathematical tools to provide a better description of these devices as well as, use these descriptions to develop novel sensor applications for devices of this type.

The Finite Element Method (FEM) was used to predict the behavior of certain types of

SAW devices. A device can be modeled via FEM by dividing its geometry into many smaller components and solving the associated mathematical equations that govern the materials behavior for each component making up the entire system. This technique has been applied on a limited basis for the modeling of SAW device behavior. The nature of the waves generated in a SAW device depends heavily on the orientation of the substrate (i.e. the relationship between the pond and the trajectory of the stone). This work introduces a technique to account for that orientation and uses that ability to effectively model several practical scenarios to gain understanding about the sensor's behavior under certain conditions. This represents an extremely cost effective tool as several parameters can be tested on a computer without having to build test specimens.

The principles learned via the device modeling were applied to the characterization of key properties of thin films that are deposited on SAW devices. These concepts were applied to an existing application to show enhanced sensitivity to the presence of water and ice, an application of particular interest in the aerospace community. Finally, a novel application for these devices was introduced involving the detection of tiny charged particles due to their accumulative effect on the material properties of a thin polymer film. This technology could provide a cost effective sensing alternative in such industries as: power generation, environmental protection, and homeland security.

References

Achenbach, J., Wave Propagation in Elastic Solids, North-Holland, New York, 1984.

Allik,H. and Hughes, J.R. "Finite Element Method for Piezoelectric Vibration", *International Journal for Numerical Methods of Engineering*, vol. 2(2), pp. 151-157, 1970.

Anastasiou, T., Tsertos, H., Christofides, S., and Christoduolides, G., "Indoor Radon Concentration Measurements in Cyprus Using High-Sensitivity Portable Detectors", *J of Environ. Radioactivity*,,vol 68, no 2, pp. 159-169, 2003.

Atashbar, M., Bazuin, B., Simpeh, M., and Krishnamurthy, S., 3-D Finite Element Simulation Model of SAW Palladium Thin Film Hydrogen Sensor, *IEEE Proc. Ultras, Ferro, and Freq Control*, pp. 549-553, 2004.

Auld, B., "Acoustic Fields and Waves in Solids, Vol II", Krieger, New York, 1990.

Ballantine, D., White, R., Martin, S., Ricco, A., Zellers, A., Frye, G., and Wohltjen, H., Acoustic Wave Sensors: Theory, Design, and Physico-Chemical Applications, Academic Press, San Diego, CA, 1997.

Bathe, K., "Finite Element Procedures", Prentice-Hall, California, 1996.

Bezdek, M., A Boundary Integral Method for Modeling Sound Waves in Moving Media and its Application to Ultrasonic Flow Meters, *PhD Thesis*, University of Erlangen-Nuremberg, Germany, 2006.

Bleustein, J.L., "A New Surface Wave in Piezoelectric Materials", *Applied Physics Letters*, vol 13, pp. 412-413, 1968.

Branch, D.W. and Brozik, S.M., "Low-Level Detection of a Bacillus Antracis Simulant Using Love-Wave Biosensors on 36^0 YX $LiTaO_3$", *Biosensors and Bioelectronics*, vol 19, no 8, pp. 849-859, 2004.

Brekhovskikh, L., Waves in Layered Media, Academic Press, New York, 1960.

Brun, C., Fromm, M., Berger, F., Delobelle, P., Takadoum, J., Beche, E., Chambauolet, A., and Jaffiol, F., Modifications of Polypropylene Surface Properties by He^+ Ion Implantation, *J. of Polym. Sci B: Polym Phys*., Vol 41 (11), pp. 1183-1191, 2003.

Cabrerra, B., Martoff, J., and Neuhauser, B., "Acoustic Detection of Single Particles", *Nucl Inst and Meth in Phys Res B*, vol 275, no 1, pp. 97-111, 1989.

Calcagno, L. and Foti, G., "Density Enhancement in Ion Implanted Polymers", *Nucl Inst and Meth in Phys Res. B*, vol.

B19-20, no 2, pp. 895-898, 1986.

Caliendo, C., D'Amico, A., Verardi, P., and Verona, E., "K^+ Detection using Shear Horizontal Acoustic Modes", *Proc. IEEE Ultrasonics Symposium*, vol 1, pp. 383-387, 1990.

Carlotti, G., Fioretto, D., Socino, G., Palmieri, L., Petri, A ., and Verona, E., Surface Acoustic Waves in C-Axis Inclined ZnO films, *Ultrasonics Symp. Proc.*, Vol 1, pp. 449-453, 1990.

Caskery, G., Irradiation Effects in Metals, *Proc. Environmental Degredation of Engineering Materials*, Vol 3, pp. 627-630, 1987.

Chandrupatla, T. and Belegundu, A., "Introduction to Finite Elements in Engineering", Prentice-Hall, New Jersey, 2002.

Chang, R.-C., S.-Y. Chu, C.-S. Hong, Y.-T. Chuang. An Investigation of Preferred Orientation of Doped ZnO Films on 36^0 YX-$LiTaO_3$ Substrates and Fabrications of Love-Mode Devices. *Surface and Coating Technologies*, Vol 200 no 10, 3225-3240, 2006.

Cheeke, J., Tashtoush, N., and Eddy, N., Surface Acoustic Wave Humidity Sensor Based on the Changes in the Viscoelastic Properties of a Polymer Film, *Proc IEEE Ultrasonics Symposium*, Vol 1, pp. 449-452, 1996.

Chien, A., Felter, T., LeMay, J., and Balooch, M., Nanoscale Mechanical Properties of Polymer Composites: Changes in Elastic Modulus and Measurement of Ion Penetration Depth Due to α-Radiation, *J of Mater Res.*, Vol 15 (4) pp. 838-841, 2000.

Cho, Y., Rose, J., Lee, C., and Bogan, G., Elastic Guided Waves in Composite Pipes. *ASME PVP: Recent Advances in NDE Techniques for Materials Science and Industries*, Vol 484, pp. 47-52, 2004.

Chowdhury, I., and Dasgupta, S., "Computation of Rayleigh Damping Coefficients for Large Systems," *The Electronic Journal of Geotechnical Engineering*, vol 8, Bundle 8C.

Clatot, S., Laude, V., Reinhardt, R., Wilm, M., Daniau, W., Ballandras, S., Lardat, R., and Solal, M., Sensitivity of Interface Acoustic Waves to the Nature of the Interface, *Proc. IEEE Ultrasonics Symp.*, Vol 2, pp. 2126-2129, 2003.

Clegg, D.and Collyer, A. (editors), *Irradiation Effects on Polymers*, Elsevier Science Publishing Co, New York, 1991.

Cole, M., Sehra, G.S., Gardner, J.W., and Varadan, V.K., "Fabrication and Testing of Smart Tongue Devices for Liquid Sensing", *Proc. IEEE Sensors*, vol 1, no 1, pp. 237-241, 2002.

da Cunha, M., and Adler, E., "High Velocity Pseudosurface Waves (HVPSAW)", *IEEE Trans. on Ultrasonics,*

Ferroelectrics, and Frequency Control, vol 42(5), pp. 840-844, 1995.

Davenas, J., and Thevenard, P., The Multi-Aspects of Ion Beam Modification of Insulators, *Nucl Inst and Meth in Phys Res B*, Vol B80-81, pp. 1021-1027, 1993.

D'Errico, "Radiation Dosimetry and Spectrometry with Superheated Emulsions", *Nucl Inst and Meth in Phys Res B*, vol 184, no 1-2, pp. 229-254, 2001.

Ditri, J., "Determination of Nonuniform Stresses in an Isotropic Elastic Half Space from Measurements of the Dispersion of Surface Waves". *Journal of Mechanics and Physics in Solids*, vol. 45(1), pp. 51-66, 1997.

Dong, H. and Bell, T., "State of the Art Overview: Ion Beam Surface Modification of Polymer Towards Improving Tribological Properties", *Surface and Coatings Technology*, vol 111, pp. 29, 1999

Du, J., Harding, G.L., Collings, A.F., Dencher, P.R., "Experimental Study of Love Wave Acoustic Sensors Operating in Liquids", *Sensors and Actuators A: Physical*, vol 60, no 1-3, pp. 54-61, 1997.

El-Kettani, E., Luppe, F., and Guillet, A., Guided Waves in a Plate with Linearly Varying Thickness: Experimental and Numerical Results, *Ultrasonics*, Vol 42 (1-9), pp. 807-812, 2004.

Endoh, G., Hasimito, K., and Yamaguchim M., Surface Acoustic Wave Propagation Characterization by Finite-Element Method and Spectral Domain Analysis, *Jap J of App Phys*., Vol 34 (5B), pp. 2638-2641, 1995.

Ewing, W., Jardesky, W., and Press, F., Elastic Waves in Layered Media. McGraw-Hill, New York, 1957.

Feng, R. and Farris, R., Influence of Processing Conditions on the Thermal and Mechanical Properties of SU8 Negative Photoresist Coatings, *Journal of Micromech. and Microeng*., Vol 13, 80-88, 2003.

Fink, D. (editor)., Fundamentals of Ion-Irradiated Polymers, Springer, Berlin, 2004.

Fischer-Cripps, A., Critical Review of Analysis and Interpretation of Nanoindentation Test Data, *Surface and Coatings Technology*, vol 200 pp.4153-4165, 2006.

Foerster, C., Garcia, I., Zawislak, F., Serbena, F., Lepienski, C., Schreiner, W., and Abbate, M., Ion Irradiation effects on Hardness and Elastic Modulus in AZ 1350J Photoresist Film, *Thin Solid Films*, Vol 411, pp. 256-261, 2004.

Garcia, I., Zawislak, F., and Samios, D., Thermal Stability of He Irradiated Photoresist Films, *Nuc. Inst. and Meth. in Phys Res. B*, Vol 148 (1-4), pp. 1111-1115, 1999.

Gardner, J., and Bartlett, P., "Sensors and Sensory Systems for an Electronic Nose", *NATO ASI Series E: Applied Sciences*, vol 212, Kluwer Academic Publishers, Dordrecht, Netherlands, 1992.

Gizeli, E., "Design Considerations for the Acoustic Waveguide Biosensor", *Smart Mat. and Struct*., vol 6, no 6, pp. 700-706, 1997.

Gizeli, E., "Study of the Sensitivity of the Acoustic Waveguide Sensor", *Anal. Chem.*, vol 72, n24, pp. 5967-5972, 2000.

Gizeli, E., Bender, F., Rasmusson, A., Saha, K., Josse, F., and Cernosek, R., *Sensitivity of the Acoustic Waveguide Biosensor to Protein Binding as a Function of Waveguide Properties*, Biosensors and Bioelectronics, vol 18, no 11, pp. 1399-1406, 2003.

Gizeli, E. and Glad, J., "Single-Step Formation of a Biorecognition Layer for Assaying Histidine-Tagged Proteins", *Analy. Chem*., vol 76, no 14, pp. 3995-4001, 2004.

Gizeli, E., Stevenson, A., Goddard, N., and Lowe, C., "Surface Skimming Bulk Waves: A Novel Approach to Biosensors", *Transducers*, pp. 690-692, 1991.

Greve, D., Neumann, J., Nieuwenheis, J., Oppenheim, I., and Tyson, N., Use of Lamb waves to monitor plates: Experiments and simulations, *Proc. SPIE: Smart Materials and Structures*, Vol 5765 (1), pp. 281-92, 2005.

Griffith, A., Engoy, T., Diashev, A., and Krumrine, P. H., "Solid State Radiactive Waste Treatment Initiatives for Nuclear Submarine Decommisioning Wastes Under the AMEC Program", *Proc. Waste Management Conference*, 2001.

Guenther, M., Gerlach, G., Suchaneck, G., Sahre, K., Eichhorn, K., Baturin, V., and Duvanov, S., Physical Properties and Structure of Thin Ion-Beam Modified Polymer Films, *Nuc. Inst. Meth. in Phys. B*., Vol 216, pp. 43-148, 2004.

Guenther, M., Gerlach, G., Suchaneck, G., Schneider, D., Wolf, B., Deineka, A., and Jastrabik, L., "Physical Properties and Structures of Thin Conducting Ion-Beam Modified Polymer Films", *Macromolecules Symp*., vol 212, pp. 245-250, 2004.

Gulyaev, Y.V., "Electroacoustic Surface Waves in Solids", *Soviet Physics JETP Letters*, vol 9, pp. 37-38, 1969.

Guzman, L., Celva, R., Miotello, A., Voltolini, E., Ferrari, F., and Adami, M., Polymer Surface Modification by Ion Implantation and Reactive Deposition of Transparent Films, *Surface and Coatings Tech*., Vol 103-104, pp. 375-379, 1998.

Harding, G.L., "Mass Sensitivity of Love-Mode Acoustic Sensors Incorporating Silicon Dioxide and Silicon-Oxy-Fluoride Guiding Layers", *Sensors and Actuators A: Physical*, vol 88, pp. 20-28, 2001.

Harding, G.L. and Du, J., "Design and Properties of Quartz-Based Love Wave Acoustic Sensors incorporating Silicon Dioxide and PMMA Guiding Layers", *Smart Mater. Struct*., vol 6, pp. 716-720, 1997.

Hasegawa, K. and Koshiba, M., Coupled-Mode Equations for Interdigital Transducers for Leaky Surfaces Waves. *Jap J of App Phys*., Vol 42 (5B), pp. 3157-3160, 2003.

Hayashi, T., Nagamizo, H., Nakamra, S., Murase, M., and Kawashima, K., Circumferential Guided Wave Inspection for a Defect of Inner Surface of a Pipe, *ASME PVP: Recent Advances in Nondestructive Evaluation Techniques for Material Science Industries*, Vol 484, pp. 13-17, 2004.

Hayashi, T., and Rose, J., Guided Wave Simulation and Visualization by a Semi Analytical Finite Element Method, *Materials Evaluation*, Vol 60, pp 75-79, 2003.

Hayashi, T., Song, W., and Rose, J., Guided Wave Dispersion Curves for a Bar with an Arbitrary Cross-Section, A Rod and Rail Example, *Ultrasonics*, Vol 41, pp. 175-183, 2003.

Hayashi, T., Tamayama, C., Murase, M., Wave Structure Analysis of Guided Waves in a Bar with Arbitrary Cross Section, *Ultrasonics*, Vol 44 (1), pp. 17-24, 2006.

Hermann, F., Hahn, D., and Buttgenbach, S., Seperation of Density and Viscosity Influence on Liquid Loaded Acoustic Wave Devices, *Applied Physics Letters*, vol 74, no 22, pp. 3410-3412, 1999.

Herrmann, F., Weihnacht, M., and Buttgenbach, S., "Properties of Sensors based on Shear-Horizontal Surface Acoustic Waves in $LiTaO_3/SiO_2$ and Quartz/SiO_2 Structures", *IEEE Trans. Ultrason., Ferro., and Freq. Control*, vol 48, no 1, pp. 268-273, 2001.

Hickernell, F., and Adler, E., "The Experimental and Theoretical Characterization of SAW Modes in ST-X Quartz with a Zinc Oxide Film Layer", *Proc. IEEE Int'l Frequency Control Symp.*, pp. 852-857, 1997.

Hongerholt, D., Willms, G., and Rose, J., Summary of Results from an Ultrasonic In-Flight Wing Ice Detection System, *Proceeds: Quantitative Nondestructive Evlauation*, Vol 615, pp. 1023-1028, 2002.

Ippolito, S., Kalantar-zadeh, K., Powell, D., and Wlodarski, W., A 3-Dimensional Finite Element Approach For Simulating Acoustic Wave Propagation in Layered SAW Devices, *Proc. IEEE of Ultrasonics Symp*., Vol 1, pp. 303-306, 2003.

Jacesko, S., Abraham, J.K., Ji, T., Varadan, V.K., Cole, M., and Gardner, J.W., "Investigations on an Electronic Tongue with Polymer Microfluidic Cell for Liquid Sensing and Identification", *Smart Mater. Struct.*, vol 14, no 5, pp. 1010-1016, 2005.

Jakoby, B. and Vellekoop, M.J., "Analysis and Optimization of Love Wave Liquid Sensors", *IEEE Trans. Ultrason., Ferro, and Freq. Control*, vol 45, no 5, pp. 1293-1302, 1998.

Jakoby, B. and Vellekoop, M.J., "Properties of Love Waves: Applications in Sensors", *Smart Mater. Struct*., vol 6, pp. 668-679, 1997.

Jacoby, B. and Vellekoop, M.J., "Viscous Losses of Shear Waves in Layered Structures for Biosensing", *Proc. IEEE Ultrasonics Symposium*, vol 1, pp. 493-496, 1998.

Jacoby, B., Venema, A., and Vellekoop, M.J., "Viscosity Sensing Using Love Wave Devices. *Sensors and Actuators A: Physical*", vol 68, no 1-3, pp. 275-281, 1998.

Jin, X., Gao, Z., Pan, H., Zhu, H., Zhou, M., and Chen, H., "The Surface Acoustic Wave Biosensor for Detecting the Gene of Staphylococcal Enterotoxin B", *Proc Int Symp on Test and Measurement*, vol 1, pp. 261-264, 2003.

Josse, F., "Temperature Dependence of SH-Wave on Rotated Y-Cut Quartz with SiO_2 Overlay", *IEEE Trans on Sonics and Ultrason*, vol SU-31, no 3, pp. 162-168, 1984.

Josse, F. and Lee, D.L., "Analysis of the Excitation Interaction and Detection of Bulk and Surface Acoustic Waves on Piezoelectric Substrates", *IEEE Trans on Sonics and Ultrason*, vol SU-29, no 5, pp. 261-273, 1982.

Josse, F. and Shanna, S., "Analysis of Shear Horizontal Waves at a Boundary between a Piezoelectric Crystal and a Viscoelastic Fluid Medium", *J Acous. Soc. Am,*, vol 84, no 3, pp. 978-984, 1988.

Josse, F. and Shanna, S., "Effects of Liquid Relaxation Time on SH Surface Waves Liquid Sensors", *J Acous. Soc. Am*., vol 85, no 4, pp. 1556-1559, 1989.

Kahle, O., Wielsch, U., Metzner, H., Bauer, J., Uhlig, C., and Zawatski, C., "Glass Transition Temperature and Thermal Expansion Behavior of Polymer Films Investigated by Variable Temperature Spectroscopic Ellipsometry", *Thin Solid Films*, vol. 313-314(1-2), pp. 803-807, 1998.

Kalantar-Zadeh, K., Powell, D.A., Wlodarski, W., Ippolito, S., Galatsis,K., "Comparison of Layered Based SAW Sensors", *Sensors and Actuators B*, vol. 91, pp. 303-308, 2003.

Kalantar-Zadeh, K., Trinchi, A., Wlodarski, W., Holland, A., and Galatsis, K., "Mass Sensitivity of Layered Shear Horizontal Surface Acoustic Wave Devices for Sensing Applications", *Proc. SPIE*, vol 4591, pp. 113-124, 2001.

Kaltenbacher, M., "Numerical Simulation of Mechatronic Sensors and Actuators", Springer, Berlin, Germany, 2004.

Kambara, T., "Detection of Acoustic Signals by Heavy Ion Impact: Ion Beam Seismology", *Nucl Inst and Meth in Phys Res B*, vol 230, no 1-4, pp. 601-607, 2005.

Katime, I., and Calleja, R., "Dynamic Mechanical Properties of Isotactic PMMA", *Polymer International*, vol 35, pp 281-285, 1994.

Kielczynski, P. and Cheeke, J.D.N., "Propagation of Love Waves in Lossy Media", *Proc. IEEE Ultrasonics Symposium*, pp. 403-405, 1996.

Kleinknecht, K., Detectors for Particle Radiation, 2nd Ed., Cambridge University Press, 1998.

Knoll, G.F., Radiation Detection and Measurement, 2nd Ed., John Wiley and Sons, New York, 1989.

Knoll, G.F. and McGregor, D.S., "Fundamentals of Semiconductor Detectors for Ionizing Radiation", *Proc. Mat. Res. Society Symp*., vol 302, pp. 3-17, 1993.

Kovacs, G., Vellekoop, M.J., Haueis, R., Lubking, G.W., and Venema, A., "A Love Wave Sensor for (Bio)Chemical Sensing in Liquids", *Sensors and Actuators A: Physical*, vol 43, no 1-3, pp. 38-43, 1994.

Kudoh, H., Sasuga, T., and Seguchi, T., High Energy Ion Irradiation Effects on Polymer Materials-LET Dependence of G Value of Scission of Polymethylmethacrylate (PMMA), *Radiat. Phys. Chem.*, Vol 50 (3), pp. 299-302, 1997.

Laude, V, and Ballandras, S., Characteristics of Surface Acoustic Waves Propagating Obliquely in Periodic Electrode Gratings. *Proc. IEEE Freq Control Symp*, pp.652-657, 2002.

Lou, S., "Ultrasonic Guided Wave Scattering Viscoelastic Coated Hollow Cylinders", PhD Thesis, Pennsylvania State University, 2005

Love, A., "Some Problems of Geodynamics", Cambridge University Press, London, 1911.

McHale, G., "Generalized Concept of Acoustic Plate Mode and Love Wave Sensors", Meas. Sci. Technol., vol 14, pp. 1847-1853, 2003.

McHale, G., Newton, M.I., and Martin, F., "Layer Guided Shear Horizontally Polarized Acoustic Plate Modes", *J of App*

Phys, vol 91, no 9, pp. 5735-5744, 2001.

McHale, G., Newton, M.I., and Martin, F., "Resonant Conditions for Love Wave Guiding Layer Thickness", *App Phys. Lett*., vol 79, no 21, pp. 3542-3543, 2001.

McHale, G., Martin, F., and Newton, M.I., "Mass Sensitivity of Acoustic Wave Devices from Group and Phase Velocity Measurements", *J of App Phys*., vol 92, no 6, pp. 3368-3373, 2002.

McLean, J. and Degertekin, F., Directional Scholte Wave Generation and Detectino Using Interdigital Capacitive Micromachined Ultrasonic Transducer, *IEEE Trans. on Ultrason, Ferro, and Freq Control*, Vol 51 (6), pp. 756-764, 2003.

Morgan, D.P., "History of SAW Devices", Proceeds of *IEEE Intl. Frequency Control Symposium*, pp. 439-460, 1998.

Moser, F., Jacobs, L., and Qu, J., Modeling Elastic Wave Propagation in Waveguides with the Finite Element Method. *NDT and E International*, Vol 32 (4), pp. 225-234, 1999.

Newton, M.I., McHale, G., Martin, F., Gizeli, E., and Melzak, K.A., "Generalized Love Waves", *Europhysics Letters*, vol 58, no 6, pp. 818-822, 2002.

Nishimiya, N., Ueno, K., Noshiro, M., and Satou, M., Chemical Processes and Surface Hardening of Ion-Implanted Polyester Films, *Nucl Inst and Meth in Phys Res B*, Vol B59-60, pp. 1276-1280, 1991.

Ohta, Y., Nakamura, K., and Shimizu, H., "Piezoelectric Surface Shear Waves", *Proc. Ultrason. Committee Inst. Electron. Commun, Eng, and Japan*, 1969.

Pan, H., Zhu, H., and Feng, G., "The Love Wave Acoustic Sensor for Testing in Liquids", *Proc. SPIE*, vol 4414, pp. 250-253, 2001.

Panella, V., Carlotti, G., Socino, G., Giovannini, L., Eddrief, M., and Sebenne, C., Surface Acoustic Modes in InSe and GaSe Lamellar Films, *Proc. IEEE Ultrasonics Symposium*, Vol 1, 305-308, 1999.

Parker, T.E. and Wichansky, H., "Temperature-Compensated Surface Acoustic Wave Devices with SiO_2 Film Overlayers", *Journal of Applied Physics*, vol 50, no 3, pp. 1360-1369, 1979.

Petrillo, C., Sacchetti, F., Toker, O., and Rhodes, N.J., "Solid State Neutron Detectors", *Nucl Inst and Meth in Phys Res A*, vol 378, pp. 541-551, 1996.

Razan, F., Zimmermann, C., Rebiere, D., Dejous, C., Pistre, J., Destarac, M., and Pavageau, B., Radio Frequency Thin

Film Characterization with Polymer-Coated Love-Wave Sensor, *Sensors and Actuators B: Chemical*, Vol 108, pp. 917-924, 2005.

Rayleigh, L., "On Waves Propagated Along the Plane Surface of an Elastic Solid", *Proceeds of London Mathematical Society*, vol. 17, pp. 4-11, 1887.

Robertson, B.W., Adenwalla, S., Harken, A., Welsch, P., Brand, J.I., Dowben, P.A., and Claassen, J.P., "A Class of Boron-Rich Solid State Neutron Detectors", *Appl Phys Lett*, vol 80, no 19, pp. 3644-3646, 2002.

Rouif, S., Radiation Cross-Linked Polymers: Recent Developments and New Applications, Nuc. Inst. and Meth. B, Vol 236, pp. 68-72, 2005.

Rose, J., et al., Contaminant Detection System, *Patent # 5,932,806*, Aug 3, 1999.

Rose, J., "Ultrasonic Waves in Solid Media", Cambridge University Press, New York, 1999.

Rose, J.L. Ultrasonic Guided Waves in Structural Health Monitoring. *Key Engineering Materials: Advance in Nondestructive Evaluation*, Vol 270-273 (1), 14-21, 2004.

Sanderson, R., and Smith, S., The Application of Finite Element Modeling to Guided Ultrasonic Waves in Rails, *Insight: Non Destructive Testing and Condition Monitoring*, Vol 44 (6), pp. 359-363, 2002.

Schlensog, M.D., Gronewold, T.M.A., Tewes, M., Famulok, M., Quandt, E., "A Love-Wave Biosensor using Nucleic Acids as Ligands", *Sensors and Actuators B: Chemical*, vol 101, pp. 308-315, 2004.

Shalaby, S., Radiative Degredation of Synthetic Polymers: Chemical, Physical, Environmental, and Technological Considerations, *J. of Poly. Sci., Macromolecular Rev*., Vol 14, pp. 419-458, 1979.

Sias, U., Sanchez, G., Kaschny, J., Amaral, L., Behar, M., and Fink, D., Polymer Thermal Stability Enhancement by High Energy Ion Bombardment, *Nuc. Inst. and Meth. in Phys Res. B*, Vol 141 (1-4), pp. 187-192, 1998.

Sosman, R., "The Properties of Silica", Chemical Catalog Co., New York, 1927.

Staples, E., "Electronic Nose Simulation of Olfactory Response Containing 500 Orthogonal Sensors in 10 Seconds", *Proc. IEEE Ultrasonics Symp*, vol 1, pp. 417-423, 1999.

Sterling, L.H., "Introduction to Physical Polymer Science", John Wiley and Sons, New York, 1992.

Strashilov, V.L. and Yantchev, V.M., "Surface Transverse Waves: Properties, Devices, and Analysis", *IEEE Trans on*

Ultrason., Ferro., and Freq. Control, vol 52, no 5, pp. 812-821, 2005.

Tamarin, O., Dejous, C., Rebiere, D., Pistre, J., Comeau, S., Moynet, D., and Bezian, J., "Study of Acoustic Love Wave Devices for Real Time Bacteriophage Detection", *Sensors and Actuators B: Chemical*, vol 91, no 1-3, pp. 275-284, 2003.

Thompson, M., and Stone, D., "Surface Launched Acoustic Wave Sensors: Chemical Sensing and Thin Film Applications", John Wiley and Sons, New York, 1997.

Tittmann, B., Recent Results and Trends in Health Monitoring with Surface Acoustic Waves (SAWs), *Proc. SPIE*, vol 5045, pp. 37-46, 2003.

Tittmann, B., Yen, E., and Moose, C., Sensors for Material Process Monitoring and Control, *Proc SPIE,* vol 2643, pp.263-266, 1995.

Vellekoop, M.J., Jacoby, B., Batemeijer, J., A Love-Wave Ice Detector, *Proc. IEEE Ultrasonics Symposium*, Vol 1, pp. 453-456, 1999.

Victorov, I., "Rayleigh and Lamb Waves", Plenum Press, New York, 1969.

Wandracsek, K, Adams, J., and Fuhrmann, J., Effect of Thermal Degradation on Glass Transition Temperature of PMMA, *J. of Macromol. Chem. Phys*., Vol 205, 1858-1862, 2004.

Wang, Z., Cheeke, J.D.N., and Jen, C.K., "Perturbation Method for Analyzing Mass Sensitivity of Planar Multilayer Acoustic Sensors", *IEEE Trans. on Ultrason., Ferro., and Freq Control*, vol 43, no 5, pp. 844-851, 1996.

Wang, S.Y., Chu, P.K., Yang, B.Y., Zeng, X.C., and Wang, X.F., "Improvement of the Corrosion Property of Cr4Mo4V Bearing Steel Using Plasma Immersion Ion Implantation", *Nucl. Instr. and Meth. in Phys. Res. B*, vol 127-8, pp. 1000, 1997.

Weiss, M., Welsch, W., Schikfus, M., and Hunklinger, S., "Viscoelastic Behavior of Antibody Films on a Shear Horizontal Acoustic Wave Sensor", *Analyitcal Chem*, vol 70, no 14, pp. 2881-2887, 1998.

White, R.M. and Voltmer, F.W., "Direct Piezoelectric Coupling to Surface Elastic Waves", *Applied Physics Letter*, vol 7, pp. 314-316, 1965.

Wigner, E., Theoretical Physics in Metallurgical Laboratory of Chicago, *J. of App Phys*, Vol 17 (11), pp. 857-863, 1946.

Yang, Y., Yang, P., and Yang, X., “Electronic Nose Bases on SAWs Array and its Odor Identification Capability, *Sensors and Actuators B: Chemical*, vol 66(1), pp. 167-170, 2000.

Zhu, W., A Finite Element Analysis of the Time-Delay Periodic Ring Arrays for Guided Wave Generation and Reception in Hollow Cylinders, *IEEE Trans on Ultras., Ferro, and Freq Control*, Vol 52 (5), pp. 892-903, 2005.

Zimmerman, C., Rebiere, D., Dejous, C, Pistre, J, and Planade, R., “Love-Waves to Improve Chemical Sensors Sensitivity: Theoretical and Experimental Comparison of Acoustic Modes”, *Proc. IEEE Frequency Control Symp*., pp. 281-288, 2002.

Michael K. Pedrick

Education

The Pennsylvania State University, University Park, PA 2002-2007
PhD in Engineering Science and Mechanics
Advisor: Dr. Bernhard Tittmann, Schell Professor of Engineering

Lebanon Valley College, Annville, PA 1998-2002
BS, Physics

Research Areas

- Modeling, fabrication, and characterization of Layered Surface Acoustic Wave devices
- Analytical and Numerical modeling of wave propagation in various materials
- Ultrasonic sensors based on Guided waves in thin wires
- Ultrasonic transducer modeling, fabrication, and characterization for elevated temperature environments
- Ultrasonic sensors for differential pressure monitoring
- Signal processing and Automation algorithms for Ultrasonic sensor applications

Awards

- Leadership Award – Lebanon Valley College Academic Scholarship, 1998-2001
- NCAA Letter Winner: Lebanon Valley College Varsity Basketball, 1998-1999
- Sabih and Gueler Hayek Academic Scholarship, 2004-2005
- Chancellor's List (Who's Who among American Graduate Students), 2005
- Best Student Paper in Structural Acoustics and Vibration at the 151st Meeting of the Acoustical Society of America, 2006

Selected Publications

Pedrick, M.; Heckman, M; Tittmann, B.R. A Novel Technique with a Magnetostrictive Transducer for *In Situ* Length Monitoring of a Distant Specimen. *Proceeds: ASME PVP, Ultrasonic Nondestructive Evaluation for Materials Science and Industries* , Vol 456, 73-78, 2003

Pedrick, M.; Seliga, J; Tittmann, B.R.; Design and Performance of a 10 MHz Broadband Transducer for Elevated Temperature Applications. *Proceeds: ASME PVP, Recent Advances in Nondestructive Evaluation for Materials Science and Industries*, Vol 484, 111-116, 2004

Pedrick, M. and B.R. Tittmann; Precision Ultrasonic Micrometer Position Indication System with Temperature Compensation. *Proceeds: Ultrasonics Symposium, IEEE-UFFC 50th Anniv. Joint Symp.* Vol 2, 1199-1202, 2004

Pedrick, M., and Tittmann, B.R. Charged Particle Detection: Potential of Love Wave Acoustic Devices. *Quantitative Nondestructive Evaluation. AIP Conference Proceedings*, Volume 820, pp. 1476-1483, 2006.

Kropf, M., **Pedrick, M**., Wang, X., and Tittmann, B.R. Advancement of Wave Generation and Signal Transmission in Wire Waveguides for Structural Health Monitoring Applications. *Proc. SPIE-Advanced Sensor Technologies for Non Destructive Evaluation and Structural Health Monitoring.* Vol 5770, 135-141, 2005

Jayaraman, S., **Pedrick, M.,** and Tittmann, B.R. Measurement of Absolute Strain by Non-Contact Technique. *Quantitative Nondestructive Evaluation. AIP Conference Proceedings*, Volume 820, pp. 1469-1475, 2006.

K. Joseph, B. R. Tittmann, **M. Pedrick**, and M. Kropf, Low Attenuation Waveguide for Leaky Surface Waves, *Proc. SPIE* Vol. 6179, 61790E, 2006